A Study of Dissolved Gaseous Oxygen and Nitrogen Fluxes in the Upper Ocean

by

Craig Logan McNeil
B.Sc., Heriot-Watt University, Edinburgh, Scotland, 1989

A Dissertation Submitted in Partial Fulfiiiment of the
Requirements for the Degree of

DOCTOR OF PHILOSOPHY

in the Department of Physics and Astronomy

We accept this dissertation as conforming
to the required standard

Dr. D.M. Farmer, Supervisor (Institute of Ocean Sciences, Sidney, B.C.)

Dr. C.J.R. Garrett, Department Member (Department of Physics and Astronomy)

Dr. R.W. Stewart, Department Member (Department of Physics and Astronomy)

Dr. M.J. Whiticar, Outside Member (School of Earth and Ocean Sciences)

Dr. D.W.R. Wallace, External Examiner (Brookhaven National Laboratory, Upton, N.Y.)

University of Victoria

Supervisor: Dr. David M. Farmer

ABSTRACT

The air-sea interface and the upper ocean mixed layer have globally significant roles in the redistribution and recycling of dissolved atmospheric gases and their organic and inorganic derivatives. However, the detailed mechanisms by which the redistribution and recycling processes occur and the magnitude of the resultant fluxes are known poorly. This motivated a study to measure simultaneously dissolved oxygen and nitrogen concentrations under a wide range of oceanographic and meteorological conditions. The chief advantages of studying oxygen and nitrogen are two-fold. First, the dissolved concentrations of these two primary atmospheric gases significantly determine bubble mediated air-sea gas exchange rates, an important contribution to gas flux at higher wind speed. Second, as dissolved nitrogen, unlike dissolved oxygen, has a low biological activity, simultaneous measurements of these two gases provide a differential indicator of the magnitude of biological *versus* non-biological processes affecting these gases. To this end, novel dissolved nitrogen-oxygen-gas tension devices were developed. Operating *in situ*, the devices can be moored or placed on a freely floating array to obtain extended time series measurements. Recent measurements obtained in a fresh water lake validate the robustness of the instrument performance and nitrogen separation technique. Two other data sets were collected and used to study the interactions between air-sea gas transfer, physical oceanographic processes and biological oceanographic processes. First, air-sea gas transfer was observed in a coastal strait during a storm. The dominant physical oceanographic processes were mixed layer deepening and Langmuir circulation. A dissolved gas budget analysis of the storm period requires previously published gas transfer coefficients to be enhanced by a factor of up to four. Further, the enhancement

factor is correlated with bubble penetration depth, providing evidence for the role of bubbles in enhancing air-sea gas exchange of weakly soluble gases. Second, dissolved gas concentrations obtained in the open ocean during early spring are investigated. Measurements obtained with neutrally buoyant floats indicate a strong diurnal cycle in mixing layer depth associated with day time solar heating and nocturnal convective mixing. Dissolved nitrogen measurements are used to infer that air-sea gas transfer is of secondary importance to the interpretation of simultaneous oxygen time series which also show a strong diurnal cycle. The oxygen measurements are interpreted in terms of the interaction between primary production, respiration and convectively driven mixing. It is concluded that, if diurnal oceanographic processes are neglected, primary production estimates by the oxygen production method can be overestimated by a factor which depends primarily on the ratio between the maximum nocturnal mixed layer depth to the oxygen measurement depth.

Examiners:

Dr. D.M. Farmer, Supervisor (Institute of Ocean Sciences, Sidney, B.C.)

Dr. C.J.R. Garrett, Department Member (Department of Physics and Astronomy)

Dr. R.W. Stewart, Department Member (Department of Physics and Astronomy)

Dr. M.J. Whiticar, Outside Member (School of Earth and Ocean Sciences)

Dr. D.W.R. Wallace, External Examiner (Brookhaven National Laboratory, Upton, N.Y.)

TABLE OF CONTENTS

LIST OF TABLES

LIST OF FIGURES

GLOSSARY OF NOTATION

Variables

A_V - vertical eddy diffusivity [$m^2\ s^{-1}$].

c - dissolved gas concentration in the well mixed layer [mol m^{-3}].

c_{sat} - 'saturated' dissolved gas concentration when the partial pressure of the overlying gas is one standard atmosphere [mol m^{-3}].

c^* - dissolved gas concentration right at the very water interface, assumed to be in equilibrium with the atmospheric gases [mol m^{-3}].

c_d - dissolved gas concentration in stratified water below the mixed layer [mol m^{-3}]

c_p - phase speed of an internal wave [$m\ s^{-1}$].

c_s - equilibrium oversaturated (bubble induced) mixed layer dissolved gas concentration [mol m^{-3}].

C_d - drag coefficient over the ocean surface.

D - molecular diffusivity of gas in water [$m^2\ s^{-1}$].

f - Coriolis parameter [s^{-1}].

f_o - resonant frequency of a bubble [s^{-1}].

F - fraction of the daily averaged oxygen production that is respired.

g - gravitational acceleration [$m\ s^{-2}$].

h - mixed layer depth [m].

h_m - the mean depth of the mixed layer in the presence of internal waves [m].

h_{max} - seasonal thermocline depth [m].

h_w - the amplitude of internal waves at the base of the mixed layer [m].

i - subscript for a particular gas, *e.g.*, N_2, O_2, Ar, H_2O, ...

I - solar radiation intensity time dependence [W m^{-2}].

k - vertical diffuse solar radiation attenuation coefficient or, where specified, a wavenumber [m^{-1}].

K_T - gas transfer coefficient or "piston velocity" [m s^{-1}].

M_o - empirically derived constant used in the Thorpe (1984*b*) model [m^{-1}].

n - number of moles of gas [mol].

N - Brunt-Väisälä frequency [rad s^{-1}].

$N(r)dr$ - bubble size distribution, N bubbles of radius r in a one micron bin [m^{-3} μm^{-1}]

p_{air} - air pressure [Pa].

p_i - partial pressure of gas i [Pa].

P - source of gas in the water column [mol m^{-3} s^{-1}].

P_a - atmospheric pressure of a particular gas [Pa].

P_b - total pressure inside the bubble [Pa].

P_{avg} - daily averaged, vertically integrated production of oxygen over the depth of the seasonal thermocline [molO_2 m^{-2} day^{-1}].

q - average gas flux associated with one bubble of radius r. Calculated from an average Nu, bubble lifetime, penetration depth, *etc.* [mol m^{-2} s^{-1}].

Q - total surface gas flux [mol m^{-2} s^{-1}].

Q_b - bubble mediated surface gas flux [mol m^{-2} s^{-1}].

r - bubble radius [m].

R - sink of gas in the water column [mol m^{-3} s^{-1}].

s - dissolved gas solubility coefficient, function of T,S [mol m^{-3} atm^{-1}].

S - water salinity [ppt].

S_o - Stokes drift velocity scale [m s^{-1}].

S_s - non-dimensionalised bubble induced equilibrium supersaturated level [mol m^{-3}]

T - water temperature [°C].

T_w - internal wave period [s].

U - horizontal current speed [m s^{-1}].

$U*$, $u*$ - friction velocity [m s^{-1}].

U_{10} - wind speed at 10 m height [m s^{-1}].

U_i - a coefficient used in the Woolf and Thorpe (1991) model [m s^{-1}].

w_e - entrainment velocity at the base of the mixed layer [m s^{-1}].

w_L - Langmuir circulation vertical velocity scale [m s^{-1}].

x - horizontal dimension [m].

z - depth from water surface [m].

z_s - e-folding depth scale of the Stokes drift [m].

Greek Symbols

α - time dependent multiplication factor used to enhance K_T.

β - inverse time scale for mixed layer equilibration by surface gas exchange [s^{-1}].

γ - coefficient of surface tension [kg s^{-2}].

γ' - the ratio of the specific heat capacity of water at constant pressure to that at constant volume.

δ - oxygen production efficiency [mol O_2. J^{-1}].

Δ_i - bubble induced supersaturation of mixed layer from the Woolf and Thorpe (1991) model.

ε - the ratio of wave height to wave length, or wave steepness.

θ - phase lag.

Θ - time and depth dependence of solar radiation intensity [W m^{-2}].

λ - internal wavelength [m].

ν - kinematic viscosity of water [m^2 s^{-1}].

ξ - dimensionless time scale.

ρ_a - air density [kg m^{-3}].

ρ_w - water density [kg m^{-3}].

τ - time scale.

χ - normalisation coefficient of the piston velocity by a *Sc* dependence.

ω - frequency [s^{-1}].

Dimensionless Numbers

Nu - Nusselt number, non-dimensional number parameterising the enhancement of gas transfer associated with fluid flow around the bubble. It is parameterised in terms of the *Pe* and *Re*.

Pe - Peclet number, [rU/D].

Re - Reynolds number, [$2rU/\nu$].

Sc - Schmidt number, [ν/D].

We - Weber number, [$2\rho U^2 r/\gamma$].

ACKNOWLEDGMENTS

At the top of the list of many people I would like to thank for contributing 'in various sizes, shapes and forms' to this thesis work, and to the enjoyment of my time spent in Canada, is David Farmer. Abounding in insight, support, enthusiasm, and plain fun, it has been a pleasure to study under his guidance.

I thank the help and support offered by my committee members at all stages of this work. In particular, I thank: Chris Garrett for providing generously his time, ideas and direction, Bob Stewart for his comments on improving the thesis, particularly the revision of Chapter 7 and the interpretation of the neutrally buoyant float data, and Micheal Whiticar, for providing the essential outside member's perspective through many discussions on various interdisciplinary aspects of this work.

Intimately linked to this work through close collaboration between David Farmer and myself and continued participation in field work is Bruce Johnson from Dalhousie University, Halifax. He built and generously provided the gas tension devices used in this work and instigated the idea of using dissolved oxygen and gas tension measurements to measure dissolved nitrogen concentration. Both of these contributions are key features of this work. His generosity and modesty with his scientific ideas have made it a pleasure to work with him.

At the Institute of Ocean Sciences I thank: Grace Kamitakahara and Willi Weichselbaumer for solving all my computing problems, and Grace, Marilee Andrews, Pip Sumsion and Netta Delacretaz collectively for solving all my everyday problems, Patricia Kimber for her continued help in the graphics division, particularly in preparing my poster

presentations; Reg Bigham, Tom Juhasz, Darren Tuele, Al Adrian, Reo Phillips, John Love and Les Spearing for superb technical support during my five or so experiments; Reg Bigham in particular is thanked for his unending concern that students get good data in copious amounts, Dario Stucchi for lending me his oxygen sensors which Neptune kept, Mark Trevorrow for his continued help with instrumentation development and processing of acoustic data, Johannes Gemmrich for providing breaking wave statistics, heat flux calculations and many helpful discussions, Donald Booth is thanked for helping to solve many mathematical problems. Rosaline Canessa is thanked in particular for reading carefully through the thesis, helping in its final preparation, and for being patient and supportive.

The following people are thanked for discussions. Kenneth Denman and Angélica Peña, on bio-physical interactions, Douglas Wallace, on using dissolved N_2 and O_2 measurements to obtain information on biological *versus* non-biological processes affecting dissolved O_2; Bill Asher, on bubble mediated gas transfer and associated asymmetry processes. Thanks goes to all my fellow students and colleagues for providing a stimulating environment in which to work. Bill Watterson is thanked for the laughs during my revisions. I thank the Royal Society of Edinburgh for providing financial support during the first two years of my studies. Saving the best for last, I thank Marie-Claude Bourque for providing support, encouragement and a 'life' during the write-up of my thesis.

I dedicate this thesis to my parents,
William and Margaret McNeil.

XXIV

CHAPTER 1.

INTRODUCTION

1.1. The Oceanographic Context

The surface microlayer of the world's oceans (within a few mm's from the surface), comprising approximately 70 % of the Earth's surface area, continually exchanges gases between the atmosphere and ocean. This exchange can be enhanced considerably by surface heat and momentum fluxes. The exchange of gases such as carbon-dioxide and oxygen is of critical importance to marine and terrestrial ecosystems Of equal importance to climate and climate change is the exchange of carbon-dioxide and water vapour [Stewart, 1992].

Below this surface microlayer, the oceanic mixed layer acts as a reservoir of these gases. The ability of the oceanic mixed layer to retain dissolved atmospheric gases is governed primarily by the water properties, the dissolved gas concentrations and air-sea transfer coefficients. These factors depend on the dynamical processes by which the surface microlayer can communicate with the well-mixed layer. These processes, which are of current interest across many disciplines [Denman, 1992; Denman & Gargett, 1994; Garrett, 1994], include. wind mixing, Langmuir circulation; diurnal convection; wave

breaking, which disrupts the surface microlayer and provides additional turbulence, and gas transfer through bubbles formed by breaking waves. The bubble surface can be considered an extension of the oceanic surface microlayer, albeit under increased pressure. Gas transfer of a particular gaseous species is coupled *via* the total internal pressure of the bubble to all other dissolved gas species [Thorpe, 1982]. As approximately 80 % of the total internal pressure of the bubble results from dissolved nitrogen, this gas plays an important role in the transfer of other atmospheric gases, like carbon-dioxide, between the atmosphere and ocean [Keeling, 1993; Woolf, 1993]. This is one of the reasons why it is important to measure dissolved gaseous nitrogen in the ocean.

Another reason for measuring dissolved gaseous nitrogen relates to the difference in biological activity between nitrogen and oxygen. In contrast to oxygen, dissolved gaseous nitrogen is essentially biologically inactive over periods of weeks to months, having less than 0.1 % of the effective biological activity of oxygen for typical oceanic conditions. Thus simultaneous measurements of oxygen and nitrogen will provide a differential measurement of biological activity [*e.g.*, Craig & Hayward, 1987]. Measured dissolved nitrogen variability over short time scales can be attributed only to physical processes, such as gas transfer. These physical processes, which also contribute to measured dissolved oxygen variability, then can be removed from the oxygen measurements so as to infer oxygen variability due to biological effects. From these measurements primary production can be estimated. Primary production estimates are relevant to address questions relating to 'greenhouse warming' and the role of the oceans in absorbing atmospheric carbon-dioxide. As will be discussed subsequently, the technology and instrumentation which was developed and tested in this thesis and in a larger and ongoing programme in collaboration with Dr B. Johnson (Dalhousie University) has resulted in the

possibility of new and more stable dissolved oxygen and carbon-dioxide sensors than are available presently.

The flux of dissolved oxygen, carbon-dioxide and, to a lesser extent, nitrogen across the air-sea interface and the resulting transformations within the mixed layer have significant roles in the Earth's bio-geochemical cycles. As mankind has the capability to disrupt these balances with uncertain consequences, it is essential to understand these processes separately and in the context of the oceanographic environment where they interact on various temporal and spatial scales. Perhaps most important to understand are any feedback mechanisms and nonlinearities in the processes and their interactions with the ocean dynamics. The motivation for this work is to contribute some insight into these diverse and interdisciplinary areas.

1.2. Project Definition and Thesis Plan

Diverse and extreme oceanographic and meteorological conditions encountered at sea provide an opportunity to study oceanographic processes separately, although it is rare for any one process to dominate to the exclusion of all others. For example, during stormy conditions, air-sea gas transfer is expected to determine mixed layer dissolved gas concentration changes [Watson *et al.*, 1991; Wallace & Wirick, 1992]. However, rapid changes in mixed layer properties can occur simultaneously as a result of entrainment and/or advection, obscuring the interpretation of dissolved gas measurements. This may lead to incorrect estimates of gas transfer coefficients and hence incorrect conclusions During fair-weather conditions, where dissolved oxygen changes are dominated by biological processes, namely primary production and respiration, very different and often

subtle processes can occur also, such as nocturnal convection and daytime restratification due to solar heating.

The separation of physical from biological processes affecting a biologically active gas can be aided by measuring simultaneously a biologically inactive gas This methodology has been applied to help interpret measurements and profiles in the ocean [Craig & Hayward, 1987; Emerson *et al.*, 1991] and the atmosphere [Keeling & Shertz, 1992] To date, however, oceanic observations have been limited by the methods required for analysis of biologically inactive gases (*e.g.*, N_2, Ar, He... *etc.*), such as the use of *in situ* bottle samples and gas chromatographic analysis of the samples. An important development of this thesis is the realisation of continuous *in situ* measurements of dissolved nitrogen to oxygen ratios in the ocean using newly developed instrumentation

A question then arises from the preceding discussions: *By combining observations obtained during diverse and extreme conditions with a coupled physical-chemical-biological oceanographic model, can we understand, and hence use, budgets of dissolved gaseous oxygen and nitrogen in the upper ocean to investigate the dominant bio-physical processes affecting the flux of these gases into and out of the oceanic mixed layer?* Addressing this question is the main objective of this research and was approached as follows.

When this work began, only dissolved oxygen could be measured routinely by *in situ* instruments. Thus new instrumentation and techniques had to be developed to measure total dissolved air content and hence dissolved gaseous nitrogen concentration *in situ* Observations were made under a wide range of conditions and complementary models were developed to interpret them. Analysis is focussed on gas exchange processes and bio-physical interactions. Budget type modelling of dissolved gas content of the upper water column is used to calculate air-sea gas exchange coefficients and, when air-sea gas

exchange is less important, primary production estimates of the water column. The influence of nocturnal convection and day time restratification processes on biophysical interactions is examined in more detail.

The thesis outline is as follows. Chapter 2 describes background theory and terminology used in studying gas transfer between the atmosphere and ocean, and presents a brief introduction to various biological processes affecting dissolved oxygen and nitrogen concentrations. Chapter 3 describes the development and testing of new *in situ* dissolved gas instrumentation capable of measuring total dissolved gas pressure in the water and dissolved nitrogen concentration. These developments represent a significant technological advance which has resulted from this thesis work in close collaboration with Dr. B.D. Johnson (Dalhousie University). Chapter 4 describes additional methods and techniques used in our observational programme. Chapter 5 sets up the modelling framework used to interpret our observations. Chapters 6 and 7 describe observations and modelling of two different experiments. Chapter 6 is a study of gas transfer during a storm, where changes in mixed layer depth resulting from wind mixing and air-sea gas transfer from bubble dissolution dominate the measured dissolved gas changes Chapter 7 is a study of the interaction between biological and physical processes in a convecting mixed layer. Measured changes in dissolved oxygen at two depths within the seasonal mixed layer are interpreted in terms of the interactions between primary production, respiration and diurnal convective mixing. Chapter 8 summarises the chief scientific findings of this work and indicates implications for other research areas. A discussion of ongoing work concludes the thesis.

CHAPTER 2.

BACKGROUND

2.1. Dissolved Gases

In this section, frequently used equations and terminology relating to dissolved gases are defined and explained.

2.1.1. Gas Tension

The component of the total pressure exerted by a particular gas in a multi-gas atmosphere is defined as the *partial pressure* of that particular gas. The sum of the partial pressures exerted by all dissolved gases in the water phase, including water vapour pressure is defined as the *gas tension* (*i.e.*, the water phase analog of barometric pressure in the air phase). The measurement and instrumentation will be described in Chapter 3 Previous to Anderson & Johnson [1992] and Farmer *et al.* [1993], the only reported use of this measurement was in water quality control. Gas tension was measured to indicate the degree of aeration of water flowing over a dam [D'Aoust *et al.*, 1975; D'Aoust & Clark, 1980]. High concentrations of dissolved air in natural water systems in fact can be lethal to fish [Fickeisen & Schneider, 1976].

As gas tension is a composite measurement, it provides no discrimination of the dissolved gases present in the water phase. The measurement is, however, important to the oceanographic community for two reasons. Firstly, as discussed previously, it is an analogue measurement of air pressure in the water phase. The driving force for transfer of gases between the atmosphere and ocean, excluding bubble dissolution, is the differential pressure between the water gas tension and the atmospheric pressure. This driving force can be measured directly with a gas tension device and an atmospheric pressure sensor, although, as stressed previously, with no gas discrimination. Secondly, gas transfer during storms is believed to be dominated by bubble mediated transfer. Total dissolution of bubbles will increase the air content of the water and hence the gas tension. Partial dissolution of bubbles (Section 2.5.2.) will result in transfer of atmospheric gases in molar ratios different to that of the atmosphere, a consequence of the differences in solubility and diffusivity coefficients of the different gases. These ideas, supported with measurements and modelling, form the basis of Chapter 6.

From simultaneous measurements of gas tension and dissolved oxygen, dissolved nitrogen concentration can be inferred. The significance of these measurements and a discussion of the technique is deferred until Section 3.3.1..

2.1.2. Henry's Law

William Henry (1775-1836) related the pressure, P_a [atm], of a dissolved gas in equilibrium with an overlying atmosphere to the *equilibrium saturation concentration*, c_{sat} [mol.m^{-3}], of that gas in the water by:

$$c_{sat} = s\ P_a \qquad (2.1)$$

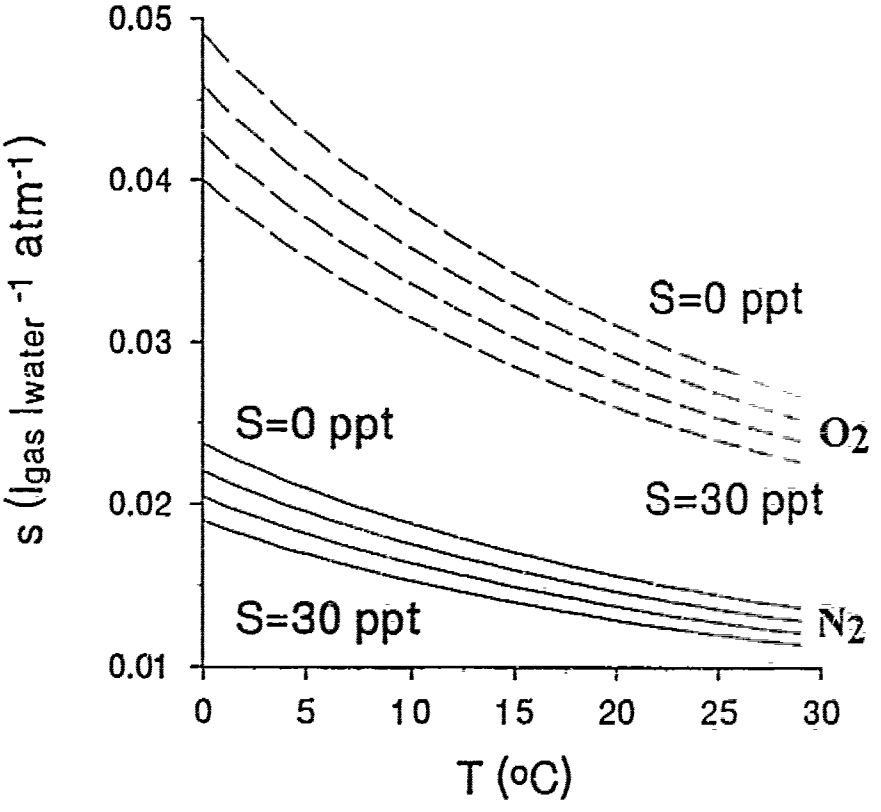

Figure 2.1 . Bunsen coefficient (s) *versus* temperature (T) over a range of salinity (S) for nitrogen (solid line) and oxygen (dashed line) [Weiss, 1970].

where $s = s(T,S)$ is the *Bunsen solubility coefficient* having dimensions of $l_{gas}.l_w^{-1}.atm^{-1}$ and is a function of temperature, T, and salinity, S [Weiss, 1970]. Figure 2.1 shows a plot of $s(T,S)$ for oxygen and nitrogen. This equation expresses a physical limit to the volume of a specific gas that can be dissolved by a given volume of water at a particular pressure.

The retention mechanism and strength of dissolution depend on two things. First, the chemical properties of the gas, namely its chemical bonding and polar nature, and its ability to react chemically with the water. Second, the water properties, namely its temperature and salinity. For the most abundant atmospheric gases, solubility decreases with increasing temperature. Salinity has a similar effect in that ions create an effective pressure that decreases the retentive capacity of water to dissolve a particular gas

2.1.3. Saturation Level

Oceanographers and marine chemists deal with an atmosphere, not of only pure gas and water vapour, but of air, which for the major gases has a stable and well known composition [Kennish, 1989]. It is then the partial pressure of the gas in the atmosphere which determines the *equilibrium concentration* in the water, c^* [mol.m^{-3}]. The ratio of a dissolved gas concentration, c, to the equilibrium concentration, is defined as the *saturation level*, (c/c^*), of the dissolved gas with respect to the atmosphere. For expressing long term time series measurements, c^* is usually defined with respect to one *standard atmosphere* (abbreviated to 1 *atm* - air at a total pressure of 101.325 kPa) of moist air. *Oversaturated* (also called *supersaturated*) water, for which c/c^* is defined to be greater than one, will then lose gas to the atmosphere, in the absence of bubble mediated gas transfer, if the air pressure is less than one standard atmosphere.

2.2. Chemical Properties

The equilibrium concentration of a particular dissolved gas depends on the water's properties, primarily temperature and salinity. Changes in temperature and salinity of a water mass affect the equilibrium concentration through the Bunsen coefficient, which is gas specific (see Section 2.1.2.). For most gases, including oxygen and nitrogen, raising the temperature or salinity of a water mass, with no gas exchange into or out of the water, will raise the degree of saturation. Seasonal heating cycles of oceanic mixed layers have important implications for mean annual fluxes of dissolved gases. Oversaturation can occur at the end of summer for both nitrogen and oxygen (notwithstanding the Spring bloom period), due to solar heating and low gas transfer rates over the summer period

The thin film effect, whereby the near surface (<1 mm) can be colder than the bulk water by up to ~0.6 °C (typically ~0.3 °C) due to heat loss from the surface, has implications for satellite observation of water temperature [Bernstein & Morris, 1983]. Due to the increased capacity of this near surface water to dissolve gases, the effect also has important implications for air-sea gas transfer. It has been estimated that an additional 0.7 Pg (1Pg = 1GT) of anthropogenic carbon (or ~ 25% of the net annual oceanic carbon uptake) is transferred to the ocean from the atmosphere due to this effect [Robertson & Watson, 1992].

2.3. Physical Processes

In this section the various physical processes that affect the saturation level of dissolved gases in the ocean will be identified and discussed.

Atmospheric Pressure Changes

Air pressure is the sum of the partial pressure of each gas in the atmosphere, and thus affects the equilibrium dissolved gas concentration, c^*, of a particular gas in the water phase according to Henry's Law (Equation 2.1). These changes then will affect the saturation level of the gas. Typically, atmospheric pressure variations are of the order of 3 kPa, equivalent to a saturation level change of ~ 3%.

Air-Sea Gas Exchange

Various processes and mechanisms exist whereby gas is transferred from the atmosphere to the ocean. On a microscale, however, all 'handover' processes are diffusive. The

important quantity describing the rate of transfer of gas between the atmosphere and ocean, other than the dissolved gas saturation levels, is the gas transfer coefficient K_T. It is important in determining the equilibration time scale of the mixed layer in response to saturation level changes. Due to the importance of air-sea gas transfer to this work, a description of various models and parameterisation of air-sea transfer rates is deferred to a more comprehensive discussion in Section 2.5..

Mixing and Entrainment

An important result of this thesis is the recognition that the role of mixing and entrainment in changing the saturation level of dissolved gases in the mixed layer previously had not been appreciated fully in budget studies of the ocean. Stratification of dissolved gases below the mixed layer can exist for many reasons, including: depth dependent biological production and respiration, previous mixing events; sinking of denser water which was either partially or completely equilibrated to different atmospheric pressures; frontogenesis and intrusions. If the mixed layer deepens and entrains this stratified water, changes in mixed layer concentrations of these gases will occur. Initial profiles of the dissolved gases have to be known in order to predict these changes from observed deepening rates

2.4. Biological Processes

In this section, various biological processes that affect the saturation level of dissolved oxygen and nitrogen will be discussed. Differences in the degree to which these processes affect oxygen and nitrogen independently are quantified.

2.4.1. Dissolved Oxygen

The discovery of oxygen is attributed to Joseph Priestley (1733-1804), who in 1774 prepared the element by heating mercuric oxide, although Antoine Lavoisier (1743-1794), the 'Father of Chemistry', named the element oxygen from the Greek meaning acidic as many element oxides are acidic in nature [Hutchinson, 1962]. The atmosphere is composed of ~21 % oxygen by volume. The equilibrium concentration of oxygen, c^*, in standard sea water (T = 15 °C, s = 35 ppt) at an air pressure of one standard atmosphere is 5.70 $ml.l^{-1}$ (247 $\mu mol.kg^{-1}$ or 7.92 $mg.kg^{-1}$) [Weiss, 1970].

Primary Production

Odum [1971] defines primary productivity of an ecological system, community, or any part thereof, "as the rate at which radiant energy is stored by photosynthetic and chemosynthetic activity of producer organisms (chiefly green plants) in the form of organic substances which can be used as food materials." In the ocean, it generally is expressed as grams of carbon produced in a column of water intersecting one square meter of sea surface per day ($gC.m^{-2}.day^{-1}$). By the process of photosynthesis, green plants utilise light energy to synthesis a carbohydrate with n carbons from carbon dioxide and water in the presence of chlorophyll with oxygen released as a by-product, or

$$nCO_2 + nH_2O + 0.5n\,MJ \rightarrow (CH_2O)_n + nO_2. \qquad (2.2)$$

This equation does not reflect the complicated multistage processes of photosynthesis An upper bound on the time scale, τ, for release of photosynthetically produced oxygen from the phytoplankton cell can be estimated using the diffusivity of oxygen in water, $D \sim O(10^{-9}$ $m^2.s^{-1})$ and the dimensions of the cell, $r \sim O(10^{-4}$ m) to be $\tau \sim r^2/D \sim O(10$ s). This calculation is an upper bound, as oxygen enrichment within the cell and electro-chemical

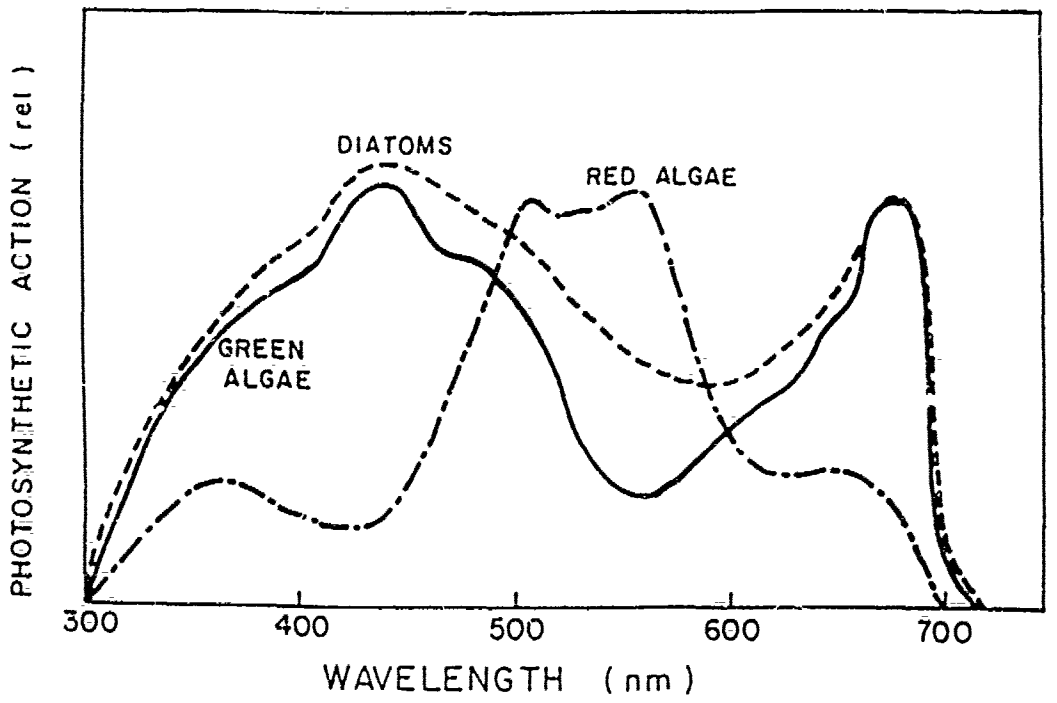

Figure 2.2 . Relative patterns of Action Spectra, or photosynthetic light utilisation efficiency, of three major algal groups in the sea. diatom, red algae, and green algae [Halldal, 1981].

transfer processes across the cell and cell membrane act to decrease this time response Thus, the net oxygen produced by the phytoplankton, *i.e.*, production minus respiration (see next Section), is released to the water almost instantaneously compared to the time scale of our measurements, $O(10^3$ s). The ratio of carbon dioxide fixed to oxygen released in this process is called the photosynthetic quotient (commonly called the PQ ratio). Equation 2.2 implies PQ = 1, however observed PQ ratios vary from 0.9-2.5, depending primarily on the plant species, the source of nutrient (*e.g.*, NH_4^+ or NO_2^-), the environment and the final product of carbon assimilation (*e.g.*, carbohydrates or proteins) Typically, however, values lie between 1.1 and 1.3 for natural oceanic distributions of phytoplankton species [Kennish, 1989, Parsons *et al.*, 1984]. The main physical and

chemical factors affecting primary production in the oceans are light availability (see Figure 2.2) and nutrient availability. The chief limiting nutrients are organic and inorganic forms of fixed nitrogen (nitrate NO_3^-, nitrite NO_2^- and ammonia NH_3) and phosphorus (PO_4^{3-}). In addition, iron, a micronutrient, has been identified as limiting production particularly in the N.E. subarctic Pacific [Miller *et al.*, 1991, Martin & Fitzwater, 1988].

Measurements of primary productivity in the ocean are difficult and involve two distinct approaches. (1) measuring the exchange of individual chemicals between marine plants and their environment; and (2) calculating the increase in biomass of a plant population. In the first approach, measurements of oxygen or carbon provide values of *in situ* photosynthesis. Somewhat less preferable is the second approach, in which increases in biomass are measured, at best yielding estimates of *in situ* growth. Net primary production in this context is defined as the rate of appearance of new algal biomass

For many years the light and dark bottle oxygen technique [Kennish, 1989] has been employed to measure primary productivity. In this method, variations in dissolved oxygen concentration of water samples cultured under light and dark conditions, *in vitro* incubations, yield a measure of the difference between production and use of oxygen by the phytoplankton. This method has been superseded by the ^{14}C (radioactive) method whereby radioactively labelled carbon can be traced throughout the photosynthetic process. However, the reliability and validity of this method have been questioned [Platt & Harrison, 1986]. Potential problems cited include. (1) methodological errors, (2) physiological problems, (3) containment deficiencies, and (4) sampling and incubation strategies. One major controversy centers on whether the ^{14}C method measures gross, net or some intermediate value of primary productivity [see Platt & Harrison, 1986 for a complete discussion]. An alternative approach which excludes some of these problems is the *in situ* oxygen production method, whereby dissolved oxygen changes in the water are

measured at specified depths with no containment of the water. At sea however, only net primary production can be measured by a moored instrument. Typically, simple budget studies are performed over several weeks as the observed changes are small compared to the absolute errors associated with the measurements. From such studies one obtains a time integrated net primary production estimate (*e.g.*, Emerson *et al.*, 1993).

Typically, primary productivity estimates in the ocean range from: 50 g $C.m^{-2}.yr^{-1}$ in nutrient depleted ocean gyres, to 100 g $C.m^{-2}.yr^{-1}$ in coastal zones to 300 g $C.m^{-2}.yr^{-1}$ in upwelling regions [preceding excerpt from Kennish, 1989; Parsons *et al.*, 1984].

Respiration

When plants or animals respire, oxidation of carbohydrate occurs yielding useful energy This process requires oxygen and releases carbon-dioxide. Plants (including phytoplankton), animals (including zooplankton) and bacteria all respire The standing stock of phytoplankton in the ocean is chiefly governed by micro and macro zooplankton grazing, where daily requirements of zooplankton generally approach 30 to 50% of their weight [Parsons *et al.*, 1984]. Sinking of organic matter, especially fecal pellets, from the euphotic zone occurs, resulting in a net carbon removal from the mixed layer. Other interesting possibilities exist for removal, and recycling of organic material in the water column. The rich (> 50%) organic film that collects around a dissolving bubble can form upon bubble collapse an aggregate of higher density, serving to enhance the vertical transport of carbon. The aggregates also act as enhanced sites for bacterial respiration and also serve as a concentrated food source for grazers. The importance of these processes, however, are not understood fully [Johnson & Cooke, 1980]. Physiological factors of respiration in the ocean include: vertical migration of zooplankton whereby they surface during the night time and go deeper during the daytime; acceleration of

zooplankton grazing at night time and subsidence during the daytime, phytoplankton and zooplankton patchiness, community changes in both phytoplankton and zooplankton often caused by selective feeding. All of these factors contribute to the spatial and temporal variability of respiration and hence production, as they are coupled closely A challenging task is to parameterise and model these processes [Kennish, 1989; Parsons *et al.*, 1984; Frost, 1991; Miller *et al.*, 1991; Mackas *et al.*, 1993].

2.4.2. Dissolved Nitrogen

Nitrogen gas was first isolated by Daniel Rutherford, an Edinburgh born physician, in 1772 while working on "dephlogisticated air" (to the fatal end of many mice, [Weast & Astle, 1981]). Di-nitrogen is a very stable, triple bonded molecule [Hutchinson, 19[illegible]] The equilibrium concentration of nitrogen, c^*, in standard sea water (T = 15 °C, s = 35 ppt) at an air pressure of one standard atmosphere is 10.4 $ml.l^{-1}$ (451 $\mu mol.kg^{-1}$ or 12.6 $mg.kg^{-1}$) [Weiss, 1970]. As the atmosphere is only 21 % oxygen, the ratio of nitrogen to oxygen solubility coefficients, or Bunsen coefficients, is approximately one half, *i.e.*, nitrogen is half as soluble in sea water as oxygen. Certain phytoplankton, particularly blue-green algae, and some bacteria species in the ocean photochemically can fix nitrogen, however a very complex energy storage cycle is involved whereby 6 ATP molecules (adenosine triphosphate, the major source of energy for cellular reactions) and the enzyme nitrogenese are required to dissociate the nitrogen molecule and chemically bond it with water to form fixed useable nitrogen. The nitrogenase enzyme is easily destroyed in the presence of oxygen, hence for the reaction to proceed, anaerobic conditions have to be maintained at the reaction site. This requires controlling the movement of oxygen radicals, formed during the synthesis process from the dissociation of water molecules, away from

the enzyme before the fixation takes place. A thorough description of this fascinating process is given in Carpenter [1983].

Once the di-nitrogen molecule has been fixed, it is available to enter the ecosystem, where it is recycled through various nitrification and denitrification processes. The loss of fixed nitrogen through denitrification of nitrate is thought to occur in anaerobic environments, such as sediments and, possibly, within detrital particles in the water column, this is probably due to the formation of anaerobic microzones of bacterial activity within the particles [Parsons *et al.*, 1934]. The predominance of nitrogen gas over nitrate, the thermodynamically stable form of nitrogen in the presence of oxygen, demonstrates the global importance of denitrification in controlling nitrogen speciation over geological time scales [Carpenter, 1983].

Nitrogen fixation rates in the ocean and laboratory are usually estimated using either (1) the Acetylene Reduction Method, where easily detected acetylene (C_2H_2) serves as a surrogate for di-nitrogen (N_2) and is reduced to ethane (C_2H_4) by a two electron transfer process; or by (2) the $^{15}N_2$ Incorporation Technique, where the rate of uptake of ^{15}N, which is added to the incubating sample, is measured by mass-spectrometry [Kennish, 1989]. The reduction of di-nitrogen (N_2) to ammonia ($2NH_3$) requires a six electron transfer process, implying a theoretical molar conversion ratio between acetylene reduction and di-nitrogen fixation of 3.1. This theoretical ratio, however, may vary in practice by a factor of 10 or more depending on the concentration of other nutrients in the sample [see Mague *et al.*, 1974 for a more complete discussion]. Measurements obtained using both techniques in the N. Pacific Ocean [Mague *et al.*, 1974] and the Atlantic Ocean [Goering *et al.*, 1966] yield average values of 2 $\mu gN.m^{-3}.hr^{-1}$, with maximum rates reported of 300 $\mu g.N.m^{-3}.hr^{-1}$ in a surface spring bloom of the blue-green algae species *Trichodesmium*. From these measurements we can estimate that over one day, nitrogen

fixation will change the oceanic mixed layer dissolved nitrogen saturation level by ~ 10^{-4} %. This change is very small, being typically 10^3 to 10^4 times smaller than dissolved oxygen changes over comparable time scales, and would certainly be indistinguishable from other physical and chemical processes affecting the saturation level.

We conclude that biological influences affecting dissolved nitrogen saturation levels in the ocean are very small and, over time scales of days to weeks, are insignificant in interpreting our time series measurements of dissolved nitrogen. Simultaneous measurements of dissolved nitrogen and oxygen then, allow one to obtain a differential measurement of biological *versus* non-biological (*i.e.*, chemical and physical) processes, as discussed in Section 1.2..

2.5. Air-Sea Gas Exchange

This section begins with an introduction to air-water gas transfer and the 'thin film' model for gas transfer. The key coefficients and dependencies, which allow various models to be generalised so as not to be gas specific, are identified. Other conceptual models, which attempt to understand in more detail the transfer of gas through the thin film or parameterise it for oceanic conditions, are discussed. Finally, various models which include other mechanisms of gas transfer, specifically gas transfer associated with bubbles, are discussed. These models are used throughout the thesis. The section concludes by discussing measurements of gas transfer coefficients in the laboratory, over lakes and in the ocean.

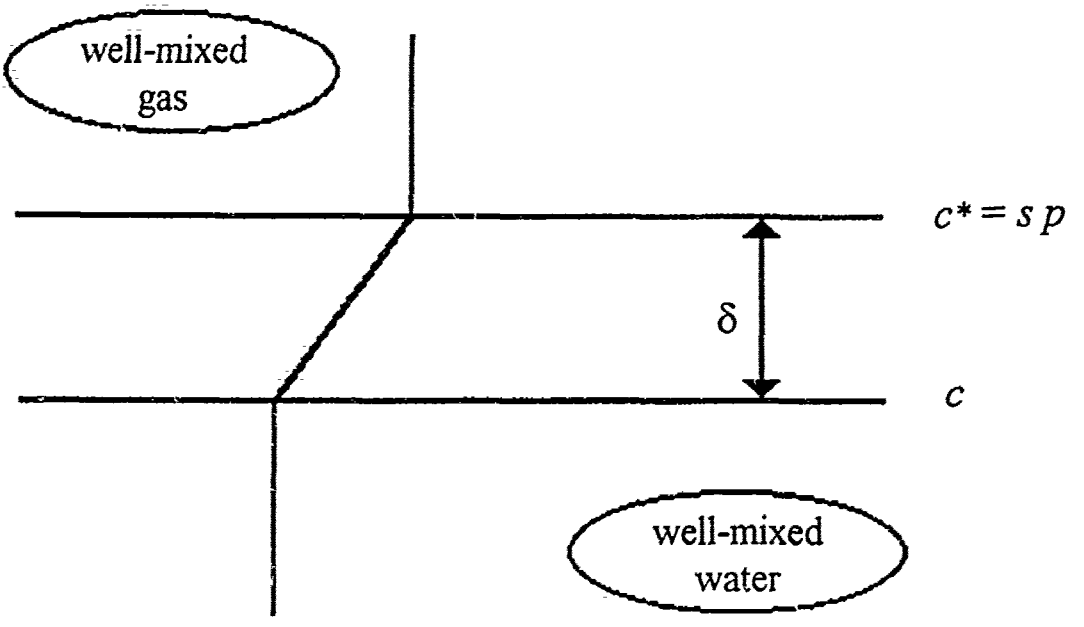

Figure 2.3 : Sketch of the thin film gas transfer model.

2.5.1. Introduction to Air-Water Gas Transfer

Thin film air-water gas exchange models were originally developed for chemical engineering applications, the founding work being acclaimed to Whitman [1923] or, less commonly cited, Nernst [1904]. In this model, a thin diffusive layer of constant thickness δ is envisioned at the surface of the water (see Figure 2.3.) for *water phase controlled* air-water gas transfer. (For very reactive and easily dissolved gases, a molecular boundary layer may develop in the air phase; if the resistance to air-water gas transfer is dominated by transfer through this layer the gas transfer is said to be *air-phase controlled*). The water below the film is well mixed. The diffusive flux of a particular gas across the film is given by:

$$Q = -K_T(c^* - c) \tag{2.3}$$

where. $K_T \equiv D/\delta$ is the *transfer velocity* or *piston velocity*, having dimensions of ms^{-1}, D is the molecular diffusivity of the gas in water, having dimensions of m^2s^{-1}; c^* is the equilibrium concentration of the gas in the water at the very air-water interface, given by Henry's Law (Equation 2.1), c is the dissolved gas concentration in the well-mixed layer of the water in the bulk fluid.

Let us now consider the transfer coefficient, K_T. The parameterisation of K_T is of primary importance in describing gas transfer. It is usual to describe K_T by a power law dependence on the Schmidt number $Sc \equiv \nu/D$, where ν is the kinematic viscosity of water having dimensions of m^2s^{-1}, or:

$$K_T(Sc) \propto Sc^{-n} \tag{2.4}$$

Note that for the Whitman model described above, n=1 in Equation 2.4. A more complex model by Deacon [1977] uses boundary layer theory developed in micrometeorology together with Reichardt's formulation for the velocity profile over a smooth rigid surface to predict an exchange rate with Sc dependence of n=2/3. This is the commonly used '2/3 power law' for a smooth water surface. For a free surface boundary condition, one obtains a dependency of n=1/2 [Brumley & Jirka, 1988, Csanady, 1990]. Surface renewal models (to be discussed in Section 2.5.2.) predict a Sc dependence of n=1/2 [additional references: Wilhelms & Gulliver, 1990].

2.5.2. Physical Transfer Mechanisms and Models

Stagnant Thin Film Model

Liss [1988] applied the stagnant thin film model of Whitman [1923] to the ocean, by expressing the flux of a specific gas across the air-sea interface as:

$$Q = -K_T(c^* - c) \tag{2.5}$$

where $K_T = K_T(U_{10},Sc)$ is parameterised in terms of wind speed at 10 m height, U_{10}. Discussions of the parameterisation of K_T in terms of wind speed is deferred to Section 2.5.3..

In this thin film model of gas exchange at the air-sea interface, the fluxes of different atmospheric gases are independent, *i.e.*, the dissolved oxygen saturation level, for example, does not affect the dissolved nitrogen flux. Also, as will be discussed subsequently, this model describes air-water gas exchange as a symmetric, 'down gradient', Fickian type diffusion process, *i.e.*, gas invasion or gas evasion occurs depending *only* on the saturation level of the water. This description will be seen to be *incorrect* when bubble mediated fluxes are considered.

Surface Renewal Processes

A variety of surface renewal models were developed and extended by Higbie [1935], Danckwerts [1951] and Dobbins [1956]. In this type of model the surface is renewed by the impingement of eddies at the surface which have associated with them a renewal time, being related to the residence time of the eddies at the surface. Dankwerts [1951] assumed a Gaussian probability distribution for the age of the eddies at the surface, and

derived an expression for the transfer velocity, $K_T=(D\tau)^{1/2}$ where τ is the mean surface renewal rate. This model predicts a Schmidt number dependence of $n=1/2$ (Equation 2.4).

Interestingly, the physical handover process underlying the surface renewal model was not appreciated fully until a later date. As eddy sizes decrease closer to the boundary, the eddies impinging on the surface do not have enough energy to overcome surface tension forces and deform the fluid surface (*i.e.*, comparing $\rho u^2 \sim \gamma k$, where u is the fluid velocity perpendicular to the interface, γ the coefficient of surface tension and k the eddy wave number). Although the mechanism of surface renewal is actually quite different, the same scaling applies. It is caused by the horizontal divergence created by the larger eddies impinging on the surface of the fluid. This results in a distortion of the surface thin film by stretching the film to make it thinner, hence allowing gas transfer to occur more rapidly [Csanady, 1990].

Surface Wave Processes

The effect of surface waves has been discussed in several papers [Csanady, 1990, Hasse, 1980, 1990]. The pertinent points are as follows:

- Waves slightly increase the surface area of the water available for exchange with the atmosphere. This increased surface area is of the order of ε^2, where ε is the ratio of wave height to wave length, or the wave steepness. For ocean surface waves, ε is typically 1/17, hence the increased surface area is only of the order of 1% [Hasse, 1980] Capillary waves however can increase the surface area significantly, with a theoretical limit of up to 50% as noted by Crapper in 1957. This limit is imposed by the breaking condition of the capillary waves.

- Surface waves allow thinning of the surface thin film by straining. This effect is of the same order of magnitude as the increased surface area (of the order of 1%), and hence is greater for the capillary waves [Hasse, 1980].
- Wave breaking has several important implications for gas transfer. First, it produces a site of high turbulence level and hence low resistance to gas transfer [Csanady, 1990] Second, it produces bubbles which can dissolve in the increased turbulence and also be carried down to depth, subsequently dissolving at increased pressure [Thorpe, 1982] From wind tunnel experiments, it is expected that these processes dominate gas transfer of weakly soluble gases at wind speeds greater than 12 ms^{-1} [*e.g.*, Broecker & Siems, 1984].

Bubble Mediated Transfer

Bubbles enhance air-sea gas transfer in several ways in addition to the effects of the increased surface area they present. Firstly, the boundary layer close to the bubble surface is renewed by the moving fluid and allows exchange of the gases to occur more rapidly This effect is incorporated in the Nusselt number (Equation A.7) and is a function of the rise velocity of the bubble. Secondly, the higher pressure inside the bubble due to surface tension effects (also called the *Laplacian* pressure) and hydrostatic compression (Equation A.3) allows an increased concentration right at the air/water interface of the bubble, according to Henry's law (Equation 2.1), thus enhancing the concentration gradient in the exterior fluid resulting in an increased diffusive flux. Bubble dissolution at increased hydrostatic and Laplacian pressure can result in supersaturation (relative to the air-sea interface) of dissolved gases in the mixed layer [Thorpe, 1984*b*].

Further factors influence the transfer of a particular gas from a bubble containing more than one gas. The total pressure inside the bubble, determining its size and hence rise

velocity and *lifetime* in the water, is given by the sum of the partial pressures of all the composite gases, including water vapour. Thus the total mass transfer of a particular gas from a bubble over its lifetime is coupled to the other gases in the bubble through their effect on the total pressure of the bubble. This is seen more clearly by considering the following extreme example. Consider bubbling pure nitrogen gas through a shallow water sample which is initially equilibrated with an atmosphere of air. The pure nitrogen bubbles maintain a low, initially zero, oxygen partial pressure environment in the liquid. As the bubbles rise, oxygen will diffuse into the bubbles (water vapour, contributing only 1% of the total internal pressure, can be assumed to equilibrate instantaneously compared with the other gases). Thus dissolved oxygen is stripped from the water when the bubbles burst at the surface. This process is dynamic and very complicated if one considers gas transfer from a bubble plume where not all the bubbles dissolve completely, as is the case in oceanic bubble plumes. Gas transfer from bubble plumes is much more complex than the single bubble gas transfer discussed thus far. To calculate the rate of transfer of a particular gas from a multi-gas bubble plume, one has to integrate the flux of that gas from individual bubbles over the depth and size distribution of the plume. The integration can be performed to provide an effective instantaneous gas flux estimate or a time averaged gas flux estimate over the life time of the bubbles in the plume (see Appendix A). The dominant processes and factors affecting bubble cloud size, temporal and spatial distributions include. wave-breaking, namely frequency of events, areal coverage and initial size distribution, Langmuir circulation, namely cell dimensions, downwelling velocities and persistence thereof, near surface turbulence, including the wave breaking process, wind mixing and all other sources of mixing, and water properties, including temperature, salinity, turbidity and dissolved gas saturation levels. With few measurements of oceanic bubble size distributions at sea, direct calculation of the bubble

mediated gas flux from bubble size measurements has not yet been possible. Fundamental advances have been made however by various modelling efforts and/or combined with whatever data is available; see the published work of Thorpe, Woolf, Asher, Emerson and their colleagues [see reference list], and dissolved gas budget studies such as that performed by Spitzer & Jenkins [1989].

Thorpe Model

Thorpe developed a semi-empirical gas exchange model based on bubble penetration depth [Thorpe, 1984*b*]. He expressed the bubble mediated component to gas transfer, Q_b, in the following form:

$$Q_b = -M_o c^* D(\frac{2g}{9D\nu})^{1/3} \exp(0.74U_{10}) s_1 (s_1 - \frac{c}{c^*}) \qquad (2.6)$$

where M_O = 1.7x10^{-8} m^{-1}, s_1=(1.5 ÷ 0.5 U_{10}) and the units are determined by the units of the solubility coefficient used. The coefficient s_1 encompasses his observations of bubble penetration depth from Loch Ness, Scotland. A surface 'thin film' component would have to be added to this bubble mediated component to obtain the total air-sea gas flux.

Woolf and Thorpe Model

Woolf and Thorpe [1991] developed a stochastic Lagrangian model of bubble dissolution in a bubble cloud to overcome the difficulties of solving the equations describing gas fluxes of different atmospheric gases from bubble clouds (Appendix A). Their model includes simplified representations of turbulence and Langmuir circulation. They constrain their model to match the observed bubble cloud distributions of Johnson and Cooke [1979] at 0.6 m depth. The model results do not include bubbles of sizes greater than 500

μm, thus they considered gas transfer associated with small bubbles. Qualitatively the model reproduces the key features of bubble mediated gas transfer previously discussed, *i.e.*, supersaturation of the mixed layer dissolved gas concentration at equilibrium with the atmosphere, and coupling of the atmospheric gases *via* the total pressure inside the bubbles. Additional insight was gained into the effects of variations in Langmuir circulation properties on bubble size distributions and bubble mediated gas transfer. However, due to the complexity of their model parameter space and, hence, solution space, for application purposes they had to compromise their findings describing gas transfer with the need for simplicity. They reported the following functional form expressing the flux of a particular gas by:

$$Q = -K_T(c^*(1+\Delta_i) - c) \tag{2.7}$$

where $\Delta_i = 0.01(U_{10}/U_i)^2$, is the fractional supersaturation of an equilibrated mixed layer induced by bubble dissolution for each dissolved gas constituent denoted by the subscript i and $U_{N2} = 7.2$ ms^{-1}, $U_{O2} = 9.0$ ms^{-1}, $U_{Ar} = 9.6$ ms^{-1} and $U_{CO2} = 49.0$ ms^{-1}. It is noted that this equation has no explicit coupling terms relating gas transfer coefficients of different gases, although they are implicit in the U_i coefficients.

Equation 2.7 describes the bubble mediated contribution to air-sea gas flux in terms of the air-sea partial pressure difference for that particular gas multiplied by a gross transfer coefficient, even though the actual flux of gas from any bubble will depend on the internal pressure of the bubble, which is, necessarily, higher than the atmospheric partial pressure Complications then result from determining what Schmidt number dependency one should use to describe the gross transfer coefficient. Further, for air-sea gas transfer of a specific atmospheric gas associated with a naturally occurring bubble cloud, the gross transfer coefficient will not be simply a function of the Schmidt number of the specific gas only,

but will depend also on the solubility and diffusivity of all the other gases present in the bubble. As oxygen and nitrogen are the two major atmospheric gases, maintaining ~ 98 % of the total dissolved gas pressure inside an air bubble, their saturation levels in the water and hence their individual gas flux are intimately coupled to the transfer of all other atmospheric gases *via* bubbles. For the limiting case of a bubble completely dissolving in water, the Schmidt number and gas transfer coefficient dependency (Equation 2.4) of a particular gas species is unimportant, as all the gas goes into solution. For the case of partial bubble dissolution, the solubility and diffusivity of all major gases (nitrogen and oxygen) have to be included in the parameterisation of the transfer coefficients. As oceanic bubble plumes are intrinsically complicated in nature, numerical models of the clouds provide a convenient way with which to study gas transfer by them. However, with few measurements of oceanic bubble size distributions at sea, this is still an open research topic.

These and other model results [Merlivat & Memery, 1983] indicate that the small (<150 μm) bubbles size distributions observed in the ocean contribute significantly to the transfer of weakly soluble gases, such as N_2 and O_2, but do not contribute significantly to the transfer of more soluble gases, such as CO_2. Other modelling studies [Woolf, 1993; Keeling, 1993] indicate that larger bubbles (of the order of 1 mm) formed during breaking waves can contribute significantly to the transfer of CO_2.

Other parameterisations of bubble mediated air-sea gas transfer have been developed by, for example, Spitzer & Jenkins [1989] (see Wallace & Wirick (1992) for a comparison of the performance of this model *versus* other models against data) and Erickson (1993)

2.5.3. Laboratory and Field Experiments

Because of the difficulty of making measurements at sea, especially at higher wind speeds, most gas exchange experiments have been conducted in laboratory facilities under different conditions and with different gases [Liss, 1973, Broecker *et al.*, 1978, Broecker & Siems, 1984; Merlivat and Memery, 1983; Jähne *et al.*, 1985]. Normalisation of transfer velocities are typically performed to a Schmidt number of 600 (that of CO_2 in fresh water at 20 °C) by the dominant theoretical Schmidt number dependency described in Section 2.5.2.. These experiments show a strong nonlinear dependence of gas transfer coefficients on wind speed, with perhaps three regimes and a rapid increase at the onset of wave breaking in the tanks [*e.g.*, Merlivat and Memery, 1983]. However, it is questionable whether laboratory results can be safely applied to the open ocean environment, where obvious differences in scales and transfer mechanisms exist. Langmuir circulation is a ubiquitous near surface oceanographic process yet is absent from wind tunnel studies due to fetch and depth limitations of wind-wave tunnels. Sea state and wave breaking properties (namely frequency and penetration depth) at higher simulated wind speeds are rather unrepresentative of the ocean, chiefly as a result of fetch limitations. These under-represented, or even absent, processes during laboratory studies do not permit the simulation of bubble mediated gas transfer of weakly soluble gases at higher wind speeds.

Again, to avoid the difficulties of oceanic conditions, many lake studies have been performed to measure gas transfer wind speed dependence [Wanninkhof *et al.*, 1985; Upstill-Goddard *et al.*, 1990]. These particular lake studies were performed by measuring the evasion rate of sulphur hexafluoride (SF_6), a deliberately introduced tracer, from the lakes. However, the processes studied by evasion experiments are intrinsically different to those which occur in nature during periods of high wind speed. Bubble injection transfers

gas from the atmosphere to the water, *i.e.*, an invasion process. Gas transfer associated with complete bubble dissolution cannot be measured by this technique. Further, partial dissolution of bubbles and stripping of the tracer from the water by rising bubbles will complicate further the interpretation of this measurement. The importance of this asymmetry in the transfer process has yet to be addressed fully in the literature; however, W.E. Asher (Battelle Marine Sciences Laboratory, Sequim, WA) currently is studying the topic. Other problems, which relate to previously published lake studies in general, is the apparent lack of appreciation of changing limnological conditions. For example, in Upstill-Goddard *et al.* [1992], SF_6 was added to a lake having the following properties: an area of 0.5 km^2; a mean depth of 6 m and a depth range of 2-16 m; extensive (10 %) marginal reed beds which were observed to damp surface wave growth and retain water of different properties, and 0.5-0.7 % throughput of fresh water *per* day. Tracer was added at mid-depth and the lake was left to 'mix' for 2 days. Measurements were then made at mid-depth, spatially averaged with up to 40 % horizontal heterogeneity. Solar heating of near surface waters by up to 0.3 °C was observed. Transfer coefficients were calculated from tracer concentration changes over 6 h to 70 h, using the mean water depth value. Under such a complicated environment, it is hard to imagine that transfer velocities can be estimated reliably. The exclusion of horizontal advection, restratification and particularly entrainment processes from such lake studies places additional constraints on their reliability and applicability to oceanic estimates.

Very few oceanic measurements of transfer coefficients have been made. Direct measurements include the Eddy Correlation Technique [Smith & Jones, 1983], although the results from this work still appear to be rather controversial [CJGOFS-93, 1993; *Fluxes*, 1993]. Some deliberate tracer experiments in shallow seas, where mixing is good, have been performed using a 'dual tracer' technique [Watson *et al.*, 1991; Wanninkhof *et*

al., 1993]. In this technique two tracers are added, usually SF_6 and ^3He. The difference between the apparent transfer velocities of the two gases is measured and related *via* an assumed Schmidt number dependency to a normalised, absolute, transfer velocity K_T (they used n~1/2 in Equation 2.4 based on other lake studies they performed using SF_6 and ^3He). Again, however, questions relating to solubility effects and asymmetry in the invasion/evasion process from bubble dissolution arise [Woolf, 1993]. Other tracer studies have been made in the open ocean using naturally occurring ^{222}Rn and pCO_2 distributions [*e.g.*, Smethie *et al.*, 1985].

General findings of field experiments are qualitatively consistent with laboratory data wind speed trends, particularly at moderate wind speeds ($7<U_{10}<14$ ms^{-1}), however there is still appreciable scatter with an uncertainty range of more than a factor of three. At higher wind speeds, measurements diverge. Those made by the direct Eddy Correlation Technique are typically a factor of ten times those measured in most laboratory tanks By far the most commonly used empirical fits to field and laboratory data are those of Liss and Merlivat [1986]. These relationships were based on experimental results of Wanninkhof *et al.* [1985], an SF_6 experiment in a lake with wind speeds not exceeding 8 ms^{-1}. The results were extrapolated to higher wind speeds using the shape of the wind speed dependence observed in wind-wave tank studies [Broecker *et al.*, 1978, Broecker & Siems, 1984]. Recent graphs taken from Wanninkhof [1992] comparing measurements and best fits of K_T *versus* wind speed over the open ocean and over some lakes near Lamont-Doherty Observatory are shown in Figures 2.4 and 2.5 respectively The non-linear dependency of K_T on wind speed can introduce significant bias to oceanic transfer coefficient estimates [Wanninkhof, 1992]. This bias will depend on the wind speed distribution and fetch.

To parameterise gas exchange across the air-sea interface, dominant processes have to be identified, understood and measured. This has contributed significantly to the motivation of this thesis. Normalisation of measurements by wind speed is inadequate as it fails to capture the essential physics. Researchers now have identified this issue and are seeking to establish a more fundamental correlation with other independent measurements like, for example, fractional white cap coverage [Monahan *et al.*, 1992; Asher *et al.*, 1992], radiation backscatter [Wanninkhof & Bliven, 1991], air-sea thermal stability [Erickson, 1993], significant wave height [Wallace & Wirick, 1992] and bubble and Langmuir cell distributions [*e.g.*, Thorpe, 1984*b*; Farmer *et al.*, 1993]. *In situ* measurements in the same locale are particularly useful for studying these kind of processes. Due to their short intrinsic time scale (*e.g.*, the persistence of Langmuir cells is typically less than 15 minutes) a high enough sampling rate is required to investigate each process in turn.

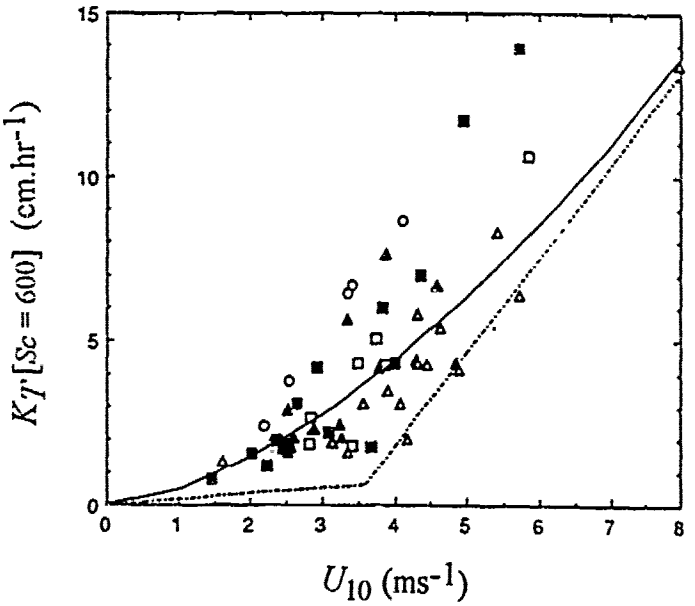

Figure 2.4 : Compilation from many experiments, using various techniques, measuring transfer coefficient, K_T, *versus* wind speed over the ocean. See Wanninkhof [1992] for a complete description of all the data points. Lines indicate empirical and theoretical fits. The most commonly used Liss & Merlivat [1986] parameterisation is indicated as a dash-dot line.

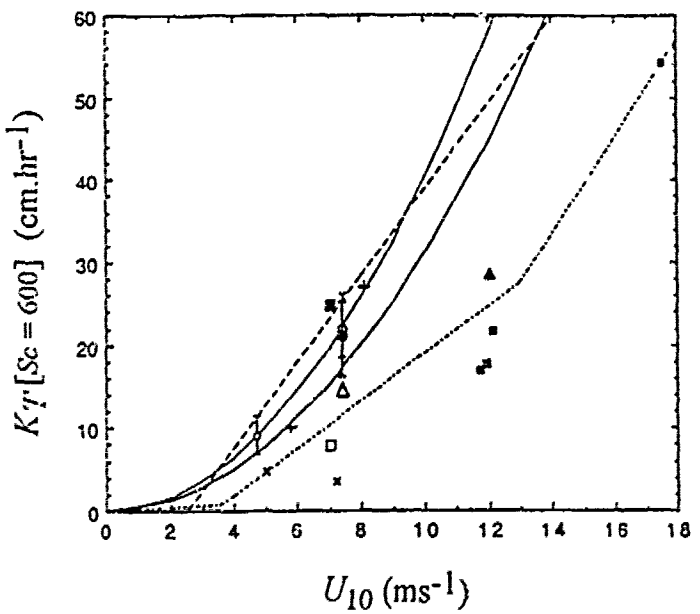

Figure 2.5 : Compilation from all deliberate tracer (SF_6) experiments measuring transfer coefficient, K_T, *versus* wind speed over lakes by Lamont Observatory. See Wanninkhof [1992] for a complete description of all the data points. Lines are as in Figure 2.4.

CHAPTER 3.

DEVELOPMENT OF IN SITU DISSOLVED GAS INSTRUMENTATION

"Nitrogen is so inert that Lavoisier named it *azote*, meaning without life, yet its compounds are so active as to be most important in foods, poisons, fertilizers, and explosives."

Weast [1981]

3.1. Motivation

Unlike dissolved oxygen there are as yet no commercially available dissolved nitrogen probes, due predominantly to the chemical inactivity of the di-nitrogen molecule (Section 2.4.2.). This has motivated development of the gas tension device and subsequent extension to a dissolved nitrogen measurement system. Dissolved nitrogen is biologically inactive compared to dissolved oxygen (Section 2.4.2.). Therefore, simultaneous measurements of both gases allow one to subtract the effects of biological processes from both physical and chemical processes affecting dissolved oxygen saturation level variations. Additionally, as oceanic bubbles are composed of more than 98 % nitrogen

and oxygen, these measurements allow one to measure bubble mediated air-sea gas exchange. The development of an autonomous instrument, capable of being deployed before a storm and recovered afterwards, provides the possibility of measuring gas exchange at high wind speed and sea state.

Our measurement of *in situ* dissolved nitrogen is made indirectly *via* a measurement of gas tension, defined in Section 2.1.1.. The following two sections form the basis of an instrumentation and methodology paper which has been accepted for publication in *Deep-Sea Research* [McNeil *et al.*, 1994].

3.2. The Gas Tension Device

3.2.1. Instrumentation

Anderson & Johnson [1992] developed a laboratory version of a gas tension device (GTD). This device was however, far from suitable for use in the field. In a continued collaboration with Dr. B. Johnson (Dalhousie University) a field version of the device was developed. Figure 3.1 illustrates the basic design. It consists of a rigid end plate with 0.018 inch pressure port drilled through it. A 0.004-inch-thick permeable spacer having 74% void volume is secured to the surface of the support. Over this entire surface is stretched a gas permeable membrane (of the type used in artificial lungs) consisting of a 0.005-inch-thick silicone elastomer product of Dow Corning secured by an annular mount O-rings enclose ~0.2 cm^3 of air behind the membrane. This space consists of the sensing volume of the pressure sensor and the void volume of the spacer. The purpose of the spacer is both to act as a distributed volume over which the gases behind the membrane can equilibrate with the dissolved gases in the water phase, and also to act as a rigid

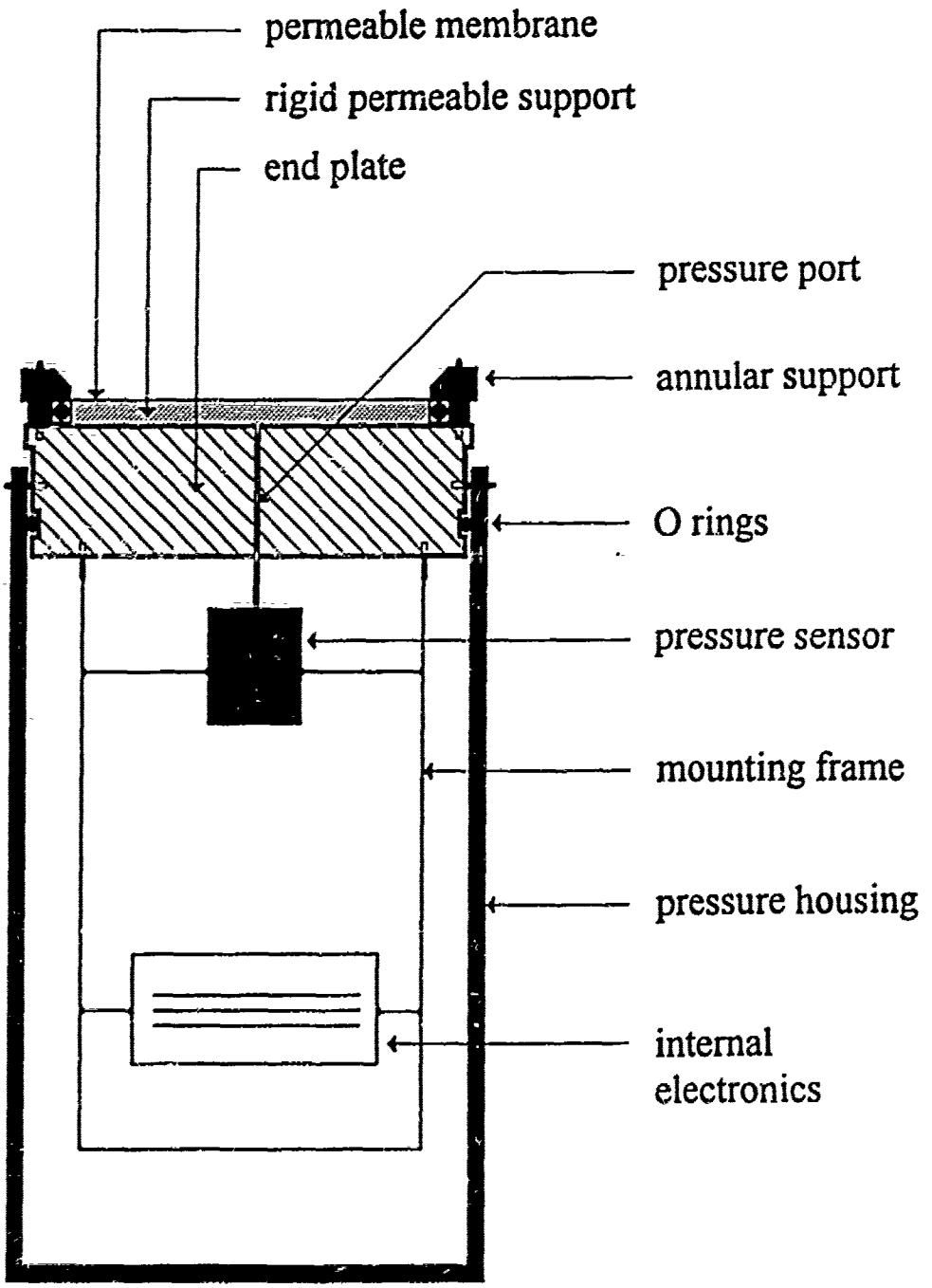

Figure 3.1 : Schematic of the gas tension device (not to scale). The instrument is approximately 20 cm high and 11 cm in diameter.

support against the hydrostatic pressure acting on the pressure port. Thus the permeable membrane serves to communicate the dissolved gases in the water with the pressure sensor, while the rigid, permeable spacer supports the membrane against the hydrostatic pressure which would otherwise deform the membrane, forcing it into the tube communicating with the pressure sensor. A pressure sensor measures the pressure of the sample volume enclosed behind the membrane at equilibrium. Equilibrium occurs when the partial pressure of each gas in the sample volume equals each dissolved gas partial pressure. The measured pressure is then the gas tension.

Upon deployment of the device, a transient pressure increase is measured by the pressure sensor, due to hydrostatic compression of air trapped between the membrane and the spacer. This transient signal is used to calculate the equilibration time of the device. As described in Anderson & Johnson [1992], there are three factors which control the equilibration time. These include the sample volume behind the membrane, the diffusivity of the membrane material, and the renewal rate of the diffusive water boundary layer adjacent to the membrane. For the various data sets reported in this thesis, the instrument had an e-folding equilibration time of 10-50 minutes. Once this initial pressure increase has relaxed by diffusion of air through the membrane, the device will only operate properly if the hydrostatic pressure is sufficient to keep the membrane pressed flat against the spacer surface. Thus the hydrostatic pressure must exceed the gas tension of the water This condition is easily satisfied with operating depths greater than a few meters An essential feature of the design is the rigidity of the spacer and supporting structure, which physically isolate the sample volume behind the membrane from hydrostatic pressure fluctuations. This physical isolation ensures that the gas tension measurement can have no hydrostatic component.

3.2.2. Developments

An important aspect of this thesis has been the continued development and testing of various field versions of the gas tension device in close collaboration with Dr. B.D. Johnson (Dalhousie University). The first successful field version of the device was used in a gas exchange study during a storm (Chapter 6). This instrument used a solid state differential pressure sensor (by Sensym, model # LX06001D). From this device evolved a second generation device using a much improved Digiquartz crystal oscillator pressure sensor (by Paroscientific, Seattle, USA) and more reliable electronics and internal recording system. This type of device was used in the open ocean measurements described in Chapter 7.

The final evolution of the device was used in Lake Biwa, Japan and the results are discussed in Section 3.4. of this chapter. For this application, designed for making long term measurements, we had a Sea-Bird Electronics CTDO modified to measure the outputs from the Paroscientific pressure sensor of the GTD. The data then are stored internally within the CTD and processed using software written for the application. This technological development was accomplished with the help of Dr. M. Trevorrow (IOS). The advantages of having the GTD data measured by a Seabird Electronics CTD are:

1. The CTD measurements of temperature, salinity and dissolved oxygen are necessary for the dissolved nitrogen calculation as described in Section 3.3.1.. These measurements are made at the same location in the water as the gas tension measurement. This avoids the problems encountered in Chapter 7 where the oxygen and gas tension measurements were made at separate depths.
2. The CTD technology (hardware and software) provided by Sea-Bird Electronics is perhaps the most reliable on the commercial market at this time. It easily can be customised to measure and record the gas tension device analogue voltage outputs,

hence possible timing errors between instruments are avoided and data processing is simplified considerably.

3. Long term moorings of the CTDO/GTD system are possible. Additional power requirements of the GTD are negligible, allowing moorings for up to 14 months.

3.3. Dissolved Gaseous Nitrogen Separation

3.3.1. Theory

The gas tension, P_T, of an equilibrated air-water system with N constituent gases is defined as the sum of the partial pressures, p_i, of each dissolved gas present in the water, or:

$$P_T = \sum_{i=1}^{N} p_i \tag{3.1}$$

where the notation i denotes each dissolved gas component. This is simply an expression of Dalton's Law of partial pressures. Henry's Law (Equation 2.1) relates the partial pressure of a particular gas in diffusive equilibrium with an overlying atmosphere to the concentration, c, of that gas in the water phase by:

$$c_i = s_i p_i \tag{3.2}$$

where $s_i = s_i(T,S)$ is the Bunsen solubility coefficient of that gas in water [Weiss, 1970] This expression then allows one to convert gas partial pressures to dissolved gas concentrations and *vice versa*. Combining Equations 3.1 and 3.2 we obtain an expression for the gas tension in terms of the dissolved gas concentrations:

$$P_T = \sum_{i=1}^{N} \left(\frac{c_i}{s_i(T,S)} \right) \tag{3.3}$$

To use Equation 3.3 to calculate dissolved nitrogen concentration, we need to know what gases make up the gas tension measurement and their relative importance.

Dissolved atmospheric gases in open ocean surface waters are typically within 10% of saturation with respect to one standard atmosphere of moist air. Thus, we would expect the equilibrated sample volume behind the membrane in the gas tension device to have, approximately, the same proportion of different constituents as air. The main components of dry air are nitrogen, oxygen and argon, with volume fractions of 0.7808, 0.2095 and 0.0093 respectively [Kennish, 1989]. These ratios remain relatively constant with observed annual variations in the global O_2/N_2 volume ratio of ~0.002 %; tropospheric mixing occurs over time scales of 30-60 days [Keeling & Shertz, 1992]. The next contributing gas is carbon dioxide with a negligible volume fraction of 3×10^{-4}. We also can expect the sample volume to be saturated in water vapour. The saturated vapour pressure of sea water is a function of temperature and salinity, being ~1 kPa for sea water at 10 °C and 32 S [Kennish, 1989], or approximately 30 times more significant than CO_2.

We can now use Equation 3.3 to calculate the concentration of dissolved nitrogen in the water as:

$$c_{N_2} = s_{N_2} \cdot \left[P_T - \left(\frac{c_{O_2}}{s_{O_2}} \right) - p_{H_2O} - p_r \right], \tag{3.4}$$

where p_r is the partial pressure of the remaining trace gases when nitrogen, oxygen and water vapour partial pressures are removed from the gas tension measurement As p_r is predominantly the partial pressure of argon, we use the following approximation: $p_r \approx$

c_{Ar}/s_{Ar}, where s_{Ar} is calculated at a mean mixed layer temperature and salinity (see the next section for a discussion of the errors associated with this assumption).

3.3.2. Accuracy and Resolution

The approximation of assuming that p_r in Equation 3.4 is the partial pressure of argon incurs an error in the nitrogen partial pressure measurement of ~0.05 % for typical oceanic conditions. The manufacturer's quoted accuracy for the Paroscientific pressure sensor is 0.01 % of one standard atmosphere, with a resolution of 10^{-8} of a standard atmosphere (here, and throughout the thesis, instrumentation *accuracy* is defined as the uncertainty in the absolute determination of a measurement and instrumentation *resolution* is defined as the minimum possible difference between two measurements that correctly indicates the sign and amplitude of the change in the measured property). The main contributing errors to the nitrogen measurement are from uncertainty in the determination of dissolved oxygen concentration and uncertainty in solubility coefficients. Winkler titrations performed at sea typically having an accuracy of ~0.5 %, although this can be much improved with the use of more sophisticated automated instrumentation These data are then used to calibrate the dissolved oxygen sensors. Solubility coefficient errors are estimated to be 0.25 % and 0.4 % for oxygen and nitrogen respectively [Weiss, 1970]. Thus a conservative estimate of the total error in the dissolved nitrogen concentration by this method is 0.7 %.

Some advantages and disadvantages of this unique *in situ* dissolved nitrogen measurement will be discussed now. The main measurements used to infer nitrogen concentration in sea water are gas tension, dissolved oxygen, temperature and salinity The gas tension measurement is an *absolute measurement*, *i.e.*, it depends only on the membrane equilibrating the sensing volume of air, unlike the oxygen probe (see Section

4.2.) where geometrical properties of the diffusion pathway and time dependent properties of the sensor electrolyte must be known. Pressure can be measured accurately to 0 01 kPa with a Paroscientific pressure sensor. Bio-fouling of the membrane can however, under prolonged exposure to biologically active conditions, lead to deterioration of the membrane diffusivity and hence decrease the instrument time response. Once the time response is greater than the environmental changes, aliasing of data will occur.

3.4. A Test of the Instrumentation and Nitrogen Separation Method

3.4.1. Introduction

A large international experiment was performed in Lake Biwa, Japan, during August 1993 The purpose of the experiment was to investigate bio-physical interactions and gas transfer in the lake. Our involvement in the experiment was related to testing a new instrument developed for the purpose of measuring time series of dissolved oxygen and nitrogen *in situ* at a specified depth. As the experiment was performed in fresh water, we also wanted to test the operation of the gas tension device under this new environment. Concerns relating to biofouling of the instrument under the severe biological activity anticipated in the lake were to be addressed.

3.4.2. Data Processing, Procedures and Calibrations

The calibration of the oxygen probe data was performed using a combination of Winkler titrated bottle samples and additional measurements of dissolved oxygen obtained by field

calibrated vertical profiling dissolved oxygen probes. Details of these procedures can be found in McNeil [1994]. The estimated accuracy for this procedure is ± 0.3 $ml.l^{-1}$.

3.4.3. Observations

The water temperature and dissolved gas measurements at 4-6 m depth are shown in Figure 3.2. Dissolved oxygen (Fig. 3.2*b*) and gas tension (Fig. 3.2*c*) are highly correlated. Figure 3.2*d* shows the results of the nitrogen subtraction process discussed in Section 3.3.1.. The time invariance of the dissolved nitrogen signal is quite remarkable, showing less than 0.5 % variability over time scales of a day. This is consistent with the discussions presented in Section 2.4.2. describing the biological inactivity of dissolved nitrogen gas

3.4.4. Discussion

The dissolved gas saturation levels in Lake Biwa at this time of year reflect the result of physical, chemical and biological processes in the water (see Chapter 2 for a discussion of these various processes). The oxygen measurements alone cannot determine which of these processes are dominant in determining the oxygen supersaturation (*e.g.*, Is the excess oxygen biologically produced or is it a result of warming over the summer months of the lake?). Use can be made of the unique nitrogen measurements to separate these processes. Gas exchange would equilibrate both oxygen and nitrogen over comparable time scales. As the dissolved nitrogen concentration is close to its equilibrium value with the atmosphere, we can conclude therefore that the oxygen supersaturation must be due primarily to biological processes, *not* physical processes, since nitrogen is expected to be biologically inactive over these time scales. Long term variability in the dissolved nitrogen signal is apparent however. The magnitude of this variability indicates the importance of physical processes on the oxygen variability. This interpretation illustrates the potential of

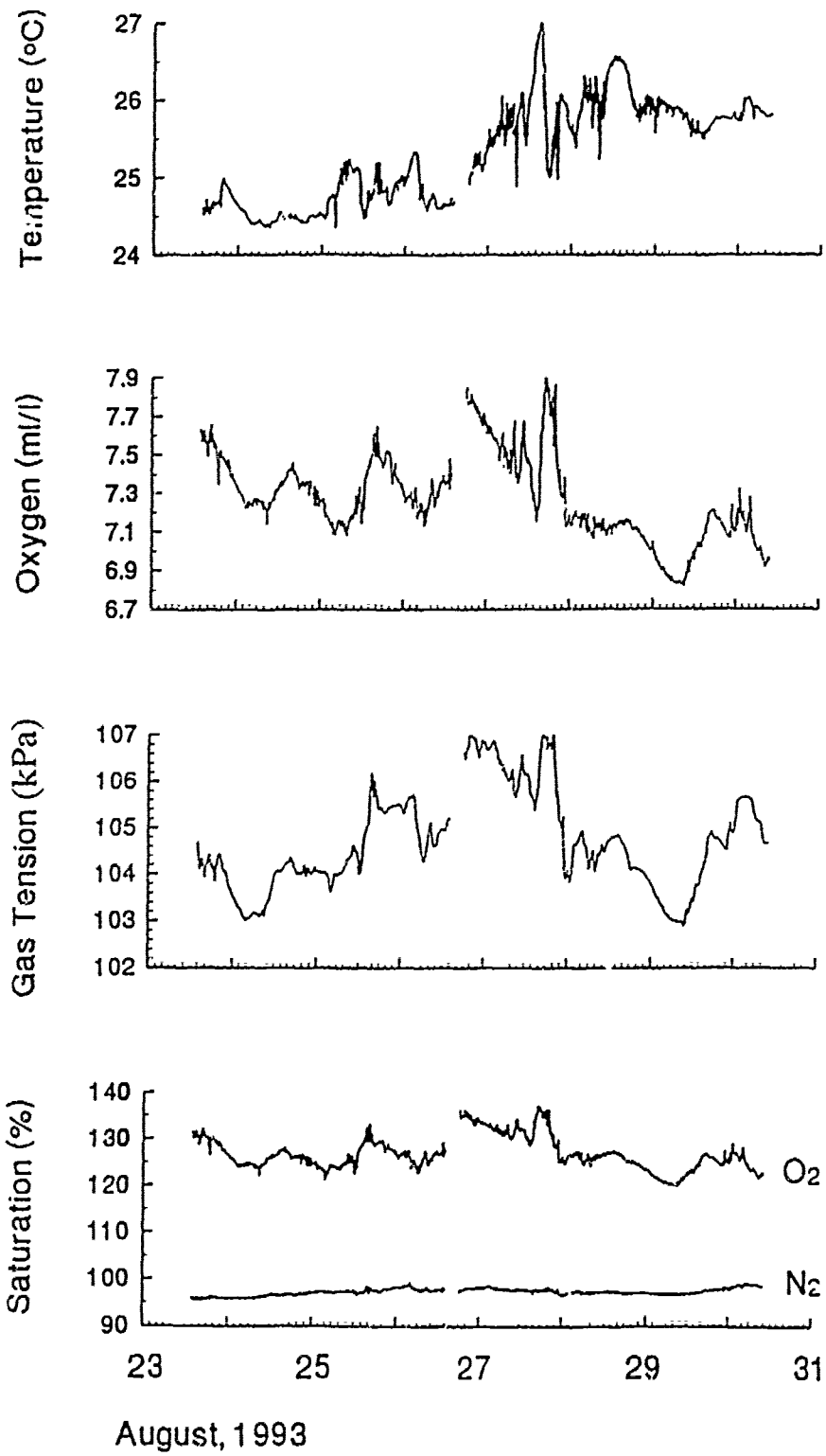

Figure 3.2 : Measurements made in Lake Biwa, Japan, at 4 to 6 m depth, showing: (*a*) water temperature, (*b*) dissolved oxygen concentration; (*c*) gas tension and (*d*) dissolved oxygen and nitrogen saturation level (w.r.t. 1 standard atmosphere of moist air).

simultaneous dissolved nitrogen measurements for interpreting short and long term time series observations of biologically active dissolved gases, like oxygen and carbon-dioxide.

Subsequent re-deployment of the instrument after 31 August, 1993, indicated that biofouling of the gas tension device was a problem. This became apparent from the data processing; the dissolved oxygen signal did not completely subtract out from the gas tension measurement. This was due most certainly to the drying of biological fouling on the membrane surface during the turn around of the instrument.

It is beyond the scope of this thesis to perform quantitative analysis of these dissolved gas measurements. This partly is due to the problems of performing a dissolved gas budget at the site of these data due to unmeasured advective effects. The purpose of this section is primarily to demonstrate the robustness of the instrumentation and nitrogen separation technique we have developed, and to indicate the potential of this system for interpreting dissolved oxygen measurements in terms of the biological and non-biological components.

CHAPTER 4.

ADDITIONAL MEASUREMENTS, METHODS AND TECHNIQUES

4.1. Introduction

Over the course of this investigation, the observational programme has been steered by scientific insight gleaned from concurrently collected data sets and advances in instrumentation development. The starting point for our observational programme is the strategy of developing freely drifting, internally recording, robust instrumentation. This avoids problems of acquiring data in heavy seas during which time conventional ship-board measurements are limited severely, if not impossible (see Watson *et al.* [1991]). This is particularly true for dissolved gas measurements in which bottle samples are required. A freely drifting array also can be designed in such a way to trace a common water mass. At any depth, relative movement between the instrument array and the local water mass at that depth will give rise to advective effects in the data (see Equation 5.4). The relative motion of the array will depend on the vertical profile of the horizontal current velocities and the vertical profile of the drag coefficient for the array. Our instrument arrays are designed to minimise relative movements between the array and the

water by using a drogue, this in some cases may be a large instrument package at depth. This technique, however, will minimise only differential movement between the array and the depth at which the drogue is set. Thus, even with the use of a drogue, the possibility exists for complicated advective trends entering the data through strong vertical shear, fronts or intrusions. As no direct measurements are made of the differential movement between the water column and the array, and typically sparse information is collected on the spatial variability in water properties due to practical limitations, advective trends cannot be removed reliably from our data. We rely then on the drogue system to minimise the importance of advective effects.

4.2. Dissolved Oxygen

Dissolved gaseous oxygen, unlike nitrogen, can be measured using commercially available probes. The most commonly used technology is a polarographic sensor. On applying a polarising voltage to sensor electrodes, oxygen molecules, in gaseous form, diffuse through a membrane to the working electrode (cathode). At the working electrode oxygen molecules are converted rapidly to hydroxyl ions (OH^-) in a series of reaction steps where the electrode supplies four electrons *per* molecule to complete the reaction, as summarised by the following equation:

$$O_2 + 2H_2O + 4e^- \rightarrow 4OH^- \qquad (4.1)$$

By measuring the current delivered to the electrodes and knowing the geometry of the diffusion pathway the dissolved oxygen concentration can be calculated At the other electrode (anode) silver chloride is formed and silver ions (Ag^+) are dissolved into the electrolyte. Consequently the chemistry of the sensor changes with use, producing a slow

but continuous change of the sensor calibration with time (the slope of the current *versus* oxygen concentration changes by a factor of about two in a few hundred hours of operation, Sea-Bird Electronics [1993]). After an initial factory calibration, it is necessary to make *in situ* field calibrations, which are performed typically on a daily basis. We use two different oxygen sensors in this study, a Sea-Bird Electronics YSI oxygen sensor on a pumped CTD system with a temperature dependent minimum sampling rate of 2-5 s and an ENDECO YSI (model 1024) sensor, operating in a modified way (to help improve stability) from the Sea-Bird Electronics YSI sensor, with a minimum sampling rate of 15 minutes. The resolution of these probes is 0.01 $ml.l^{-1}$.

The standard method of dissolved oxygen determination is the Winkler Titration Method [Kennish, 1989], and is used throughout this programme to calibrate the various O_2 sensors used. The technique is a wet chemistry method that requires analysis of water samples drawn from Niskin bottles triggered at specified depths. The accuracy of the Winkler method depends on the equipment and procedure used, but typically is stated as 0.05 $ml.l^{-1}$.

Post-processing of the oxygen probe data involves correcting the raw data with Winkler titration calibration points. The processed data then will have, at best, an accuracy of 0.05 $ml.l^{-1}$ and a resolution of 0.01 $ml.l^{-1}$.

4.3. The Meteorology

Meteorological measurements at sea are made by a Coastal Climate Company MINIMET buoy, freely floating in the vicinity (<5 km) of the experiment. Table 4.1 summarises the meteorological and oceanographic measurements made, and their specifications.

Quantity	Accuracy	Resolution
Wind Speed @ 3m	0.5 ms^{-1}	0.1 ms^{-1}
Direction	2 °C	1 °C
Air Pressure	0.05 kPa	0.01 kPa
Air/Water Temperature	0.3 °C	0.1 °C

Table 4.1 : Accuracy and resolution of MINIMET meteorological measurements.

For calibration of our GTD Paroscientific pressure sensors, and for making ship-board air pressure measurements, we use a Paroscientific Field Standard pressure sensor (model 760-15A), with the following manufacturer's specifications. accuracy 0.01 kPa (guaranteed for 3 years since the last calibration) and a maximum resolution of 10^{-6} kPa. This important measurement capability allows accurate air to sea pressure differences to be made. As discussed in Section 2.1.1., this differential measurement is the driving force for gas transfer when bubbles are absent.

Additional measurements of long and short wavelength solar radiation, humidity and cloud cover usually are taken to allow calculation of the *total* surface heat flux (*total* surface heat flux is comprised of sensible, latent, net infra-red long wavelength and short wavelength components, bulk formulations are applied to parameterise heat transfer rates). These measurements and calculations were performed by J. Gemmrich (IOS, UVic.).

Wind speed conversion from 3 m (height of MET buoy) to a standard height of 10 m was performed according to the procedure given by Smith [1981,*a*,*b*]. This work was carried out jointly with J. Gemmrich.

Quantity	Accuracy	Resolution
Conductivity	0.001 Sm^{-1} per month	0.0001 Sm^{-1}
Temperature	0.01 °C per 6 months	0.001 °C
Pressure	10 kPa	1 kPa
Oxygen	0.1 $ml.l^{-1}$ at calibration	0.01 $ml.l^{-1}$

Table 4.2 : Accuracy and resolution of CTD measurements.

4.4. The Oceanography

This section describes the basic instrumentation and measurement details used during our experiments to determine oceanographic variability.

4.4.1. CTD Measurements

We routinely use Sea-Bird Electronics 19 SEACAT profilers for CTD measurements, often taking two or three instruments on an experiment for intercalibration purposes This redundancy proved crucial on one experiment where a fault was discovered at sea with one of the CTDs, and was traced to a subtle pressure dependency of the conductivity cell (these data were rejected). Our CTD system also has a built-in dissolved oxygen sensor (see Section 4.2. for details). Additionally, a 25 cm path length Sea-Tech transmissometer was sometimes integrated onto the CTDO system. Pre- and post- calibrations of CTD instruments by Sea-Bird Electronics are performed routinely to maintain the integrity of the manufacturer's specifications as shown in Table 4.2. Salinity and density are calculated by the 1978 Practical Salinity Scale Equations [UNESCO, 1981].

4.4.2. Thermistor Chain Time Series

To measure the structure of the water column in the oceanic seasonal mixed layer, where typically salinity variations are small, vertical temperature structure time series proves a very useful measurement particularly for studying gross water column changes due to advection or frontogenisis. Thermistor chains are used for this purpose. We use internally recording Aanderaa Instruments thermistor chains of various lengths, 6 m, 20 m and 50 m with 11 thermistors on each chain. The thermistor chains are placed appropriately for better vertical resolution at the near surface and at the thermocline. The thermistor chains have a resolution of 10 m°C and an accuracy of 30 m°C. Damage to individual thermistors becomes apparent only after data processing. If the damage is minimal these data usually can be corrected by applying an offset. The magnetic tape recording technology provided with the chains is of antique design and can be rather inconsistent resulting in occasional corruption of the data by spurious spikes. Routines were written to remove these spikes while maintaining as much information from the raw data as possible This work was performed under my supervision by Mr. Tung Ho, a summer student from the University of Victoria Physics CO-OP programme.

4.4.3. Neutrally Buoyant Floats

Unique opportunities arose during our experiments to collaborate with E. D'Asaro and J Dairiki of the University of Washington. They deployed two neutrally buoyant floats, developed jointly with the Institute of Ocean Sciences, into the upper ocean The floats are ballasted to be very slightly positively buoyant, having a rise velocity of approximately 5-10 $m.hr^{-1}$ (E. D'Asaro, personal communication). They have a circular mesh of approximately one meter in diameter which provides a large drag with the water With this design, the floats tend to track larger scale water motions ($\sim 1 m^3$) within the seasonal

mixed layer. The floats internally record pressure and time, hence float velocities can be calculated.

During our coastal water experiment, where acoustically observed bubble distribution data indicated Langmuir circulation to be important, downwelling velocities within Langmuir circulation convergence zones were measured. During our open ocean experiment, corresponding vertical velocities associated with convection were measured. The floats, which cannot go deeper than the fluid parcels, indicate the depth of penetration of the convecting plumes. However, not all convecting plumes are expected to have the same kinetic and available potential energy. Furthermore, as there are at most only two such floats in the water column at any given time, in a statistical sense the water column is expected to be highly under-sampled. Notwithstanding these points, the float trajectories will be shown to provide, in the context of the data set, an indication of the depth of active mixing. This depth is difficult to assess from more conventional measurements, such as CTD profiles and thermistor chain data, which necessitate subjectively chosen criteria for data interpretation. This is particularly true in convective regimes, where density gradients within the diurnal mixed layer are close to the resolution of conventional instrumentation.

4.5. Bubble Distributions

The acoustical study of bubbles has been a long term project of the Ocean Acoustics group, led by Dr. D.M. Farmer, at the Institute of Ocean Sciences. The use of acoustics allows one to obtain bubble cloud depth and size distribution, two-dimensional images of the ocean surface bubble field, surface wave height and frequency spectrum, and potentially, directional wave spectra and estimates of turbulence [Farmer & Vagle, 1989; Zedel & Farmer, 1991; Vagle & Farmer, 1992].

Acoustical detection of bubbles is made possible by their resonant nature, having a quality factor 'Q' of up to 50 (a bubble may oscillate Q times before the amplitude of motion is $e^{-\pi}$, or ~4 %, of its initial value) [Urick, 1983]. The resonant frequency, f_o, of a bubble is inversely proportional to the bubble radius and is given by:

$$f_o = \frac{1}{2\pi r}\left(\frac{3\gamma' p}{\rho}\right)^{1/2} \tag{4.2}$$

where γ' is the ratio of specific heat capacities for constant pressure and volume respectively, p is the static pressure in the bubble and ρ is the density of water [Minneart, 1933]. The acoustical backscatter at a particular frequency from a bubble cloud will be attenuated by bubbles within that cloud having a resonant frequency close to the frequency of the insonifying field. Absorption of the incoming sound field by these bubbles and subsequent re-radiation and scattering of the absorbed sound will result in an attenuation of the total backscattered field from the cloud. Thus, from the attenuation of the backscattered sound field at a particular frequency, one can calculate the density of the resonant bubbles within the cloud. If one has various frequencies covering the bubble size range of interest, it is possible to infer the bubble size distribution of the bubble cloud by measuring the backscatter intensity at these various frequencies. This is the basic operation of the various acoustic packages used in our experiments.

The acoustic package is shown in Figure 4.1. The instrument sits at around 25 m depth, decoupled from the surface buoy by a large rubber bungy cord. It has six upward looking sonars, and four sweeping side scan sonars. Six upward looking sonars view the bubble clouds as they pass overhead the instrument. The multi-frequency upward looking sonars have a sampling frequency of typically 2 Hz and a frequency range of 28-400 kHz corresponding to resonant bubble radii of 116-8 μm. The azimuthially scanning sonar has

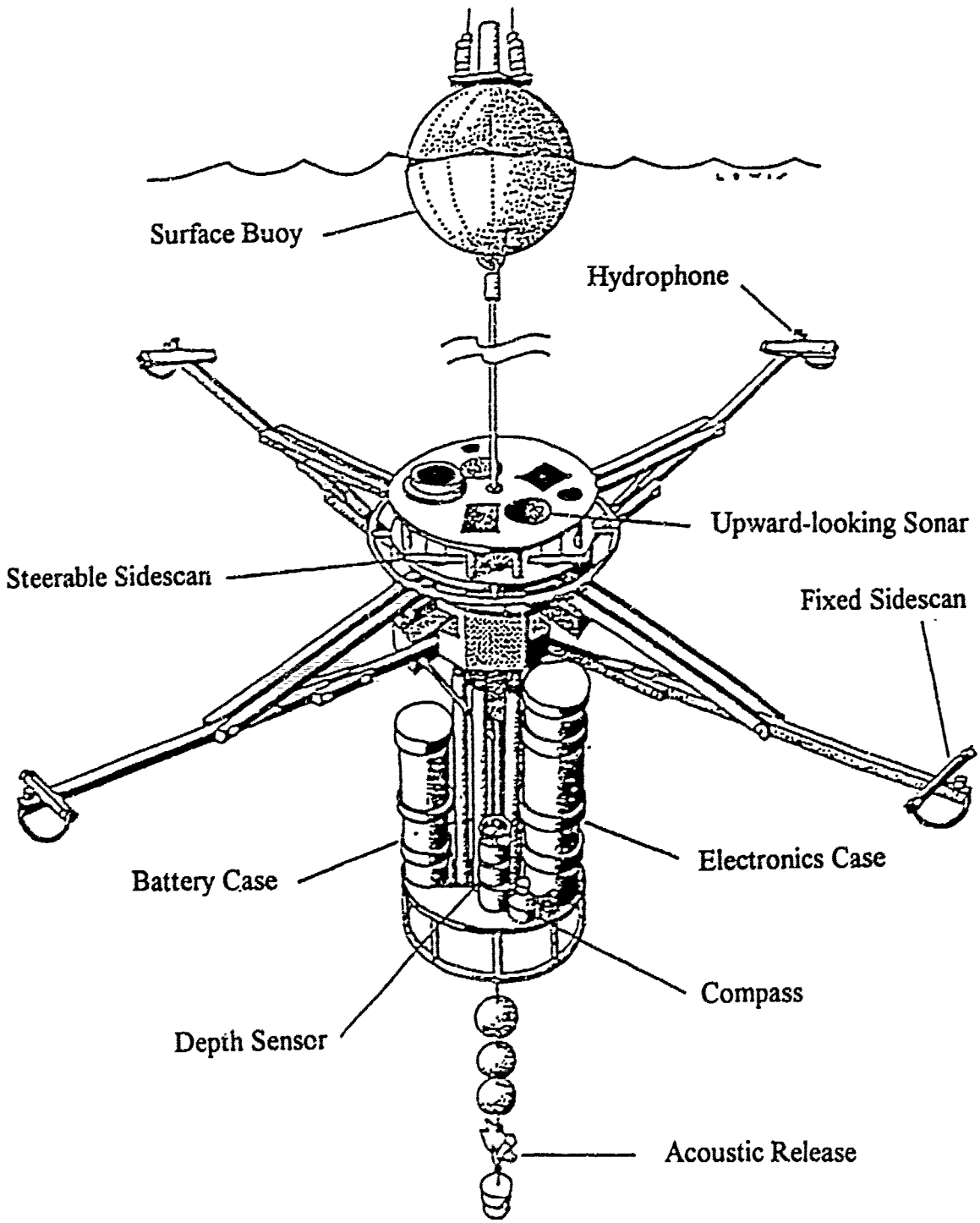

Figure 4.1 : Schematic of the acoustic package (SUSY) used for making bubble observations.

a steady sweep rate of 3^{o} s^{-1}, a frequency of 100 kHz and typically a horizontal radius detection range of 200-300 m. More technical details can be found in Vagle & Farmer [1992].

4.6. The Wave Field

The upward looking sonars on the acoustic platform discussed in Section 4.5. are used to measure wave properties. The air-sea interface provides a large back-scatter with which to calculate the distance from the instrument to the surface. After correction for the tilt and vertical motion of the instrument using acceleration sensors on the platform, it is possible to obtain an Eulerian time series measurement of the sea surface displacement. The logging of this data from raw acoustical data was performed by Dr. M. Trevorrow (IOS). A standard method is used to calculate the significant wave height from these measurements [see Longuet-Higgins, 1952, Kinsman, 1965] defined as four times the standard deviation of the surface wave field. The peak in the power spectrum of the surface height time series is used to measure the peak period of the waves. Programs were written to perform both of these calculations on the sea-surface displacement time series.

Wave breaking is an important variable in air-sea interaction. It has implications for heat, momentum and gas transfer. The mechanism is in fact the origin of the naturally occurring bubbles that we observe by our acoustic instrumentation. A novel device was developed and used in a study by Dr. D.M. Farmer and J. Gemmrich (UVic., IOS) to measure wave breaking frequency. The instrument detects breaking waves by an array of conductivity and thermistor sensors mounted onto a mechanical arm that rides the sea

surface. Four sensors are placed within ~70 cm from the surface. A video system for verification of the individual breaking wave events also is used.

CHAPTER 5.

MODELLING FRAMEWORK, A COUPLED PHYSICAL-CHEMICAL-BIOLOGICAL MODEL

"Do not unnecessarily multiply entities"

William of Occam (Medieval Philosopher)

5.1. Philosophy of Modelling

William of Occam's maxim is known metaphorically as Occam's razor. This principle, interpreted roughly as the simplest theory that fits the facts corresponds most closely to reality, has many applications throughout science. Such an approach is useful when trying to model a multi-process phenomenon, such as Nature often provides One is required first to identify, to the best of our knowledge of the phenomenon in general, the smallest set of independent processes which are assumed to describe the general features of the phenomenon to the level of complexity desired. Second, each process is parameterised using, at this stage, any necessary assumptions about the validity of the parameterisations ("Standing on the shoulders of giants" come to mind!). Third, the parameterised

processes are combined in a model, and model results are then compared to observations Models are particularly useful in that they allow one to perform sensitivity tests to each assumption in turn. The complexity of the model is only increased by necessity. Using this approach one then can be more confident that the phenomenon has been explained satisfactorily.

5.2. Formulation

In this section the modelling framework used to analyse data will be constructed The development of a simple coupled gas-exchange/biological/mixed-layer model with some specific solutions will be presented.

The model of choice is a horizontally homogeneous budget model, with a vertically integrated, slab type mixed layer with vertical resolution of scalars below the mixed layer The chief advantage of this modelling approach is that we can include oceanographic observations of mixed layer depth, temperature and salinity directly in the model This alleviates the need to fine tune a mixed layer model to match the oceanographic observations [*e.g.*, Thomas *et al.*,1993]. Also, as temperature and salinity are used in the determination of the mixed layer dissolved nitrogen concentration (Section 3 3 1), model-observation mismatches are not an added uncertainty as observations are used Questions relating to advection are always an issue and will be discussed throughout the thesis

A one-dimensional (in the vertical), slab type mixed layer ocean model is shown schematically in Figure 5.1. It consists of a mixed layer of depth h where all properties, including temperature, salinity and dissolved gas concentrations c are uniform both vertically and horizontally. Below the mixed layer is stratified water with a dissolved gas stratification given by $c_d(z)$. The surface gas flux, Q, is defined to be positive for evasion

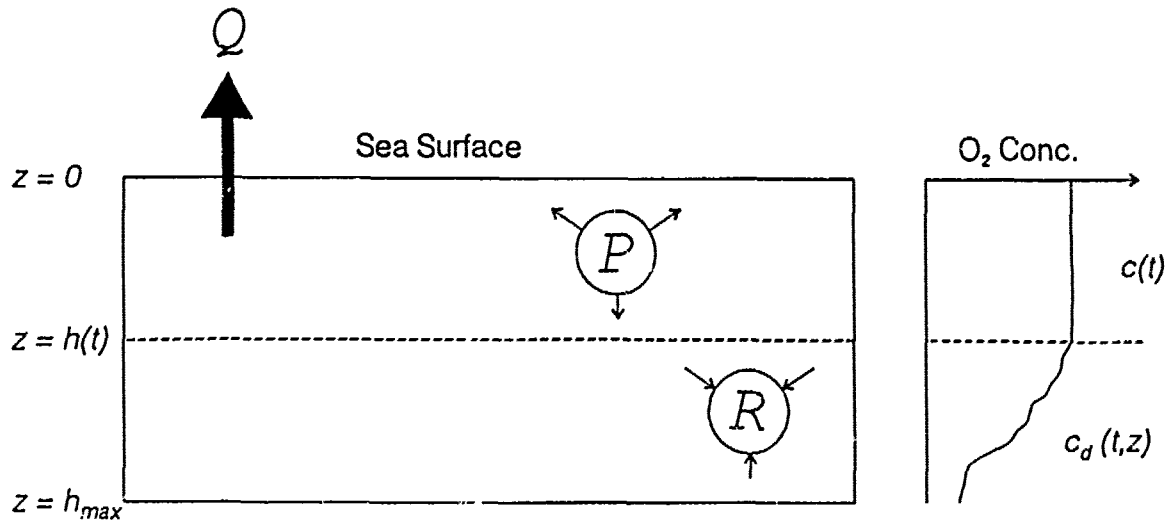

Figure 5.1 : Two dimensional slab layer model of the upper ocean.

This balance can be expressed by the following equation:

$$h\frac{dc}{dt} = -Q - w_e(c - c_{z=h}) + \int_{z=0}^{h}(P - R)dz \tag{5.1}$$

where the entrainment velocity, w_e, is described by:

$$w_e = \begin{cases} \dfrac{dh}{dt} & if \ \dfrac{dh}{dt} > 0 \\ 0 & otherwise \end{cases}, \tag{5.2}$$

and P and R denote production (source) and removal (sink) terms respectively

In the stratified layer of water below the actively mixed layer ($z>h$) between depth z_o-$\Delta z/2$ and $z_o+\Delta z/2$ (where $\Delta z<<h$), the dissolved gas concentration change is described by

$$c_d(t_o + \Delta t, z_o) = c_d(t_o, z_o) + \frac{\Delta t}{\Delta z}\int_{z_o-\Delta z/2}^{z_o+\Delta z/2}\{P(t_o, z_o) - R(t_o, z_o)\}dz. \tag{5.3}$$

In this formulation advective effects have been left out. They can be included by using the following operator change:

$$\frac{d}{dt} = \frac{\partial}{\partial t} + U\frac{\partial}{\partial x} \tag{5.4}$$

where U is the horizontally vector averaged water speed in the direction x. The concentration changes then would be those at a fixed point in space relative to the water movement, or an Eulerian measurement. Local water mass convergence or divergence by internal waves or Ekman pumping, also can be included in the above formulation. For example, internal waves can be incorporated by considering the mixed layer depth as $h(x,t) = h_m(t) \pm h_w\cos(\omega t - kx - \theta)$, where h_w is the maximum vertical displacement of the mixed layer due to an internal wave from the time averaged mean mixed layer depth, h_m. Continuity of mass will provide the currents, $U(x,t)$, associated with the internal waves (for a two layer system the currents can be considered barotropic within each layer). Unless the internal waves break, no new water will be entrained into the mixed layer (*i.e.*, $w_e(h=h_m)$). Local horizontal variations in $c(x,t)$ will occur with a time scale ω^{-1} and over a horizontal length scale comparable to the horizontal internal wavelength, λ. This horizontal variability will be of the order of h_w/h_m (typically <10 %) times the change in the mean mixed layer concentration (this will depend for gas exchange on the time scale ω^{-1} *versus* Q/hc, but typically < 0.2 %). These changes are small, and considered insignificant in our studies. In practice, lateral mixing will homogenise these variations. Variations in $c_d(z(t),t)$ may arise from the P and R terms. For example, individual phytoplankton will be exposed to varying light intensity which is sinusoidally varying in time and exponentially concentrated at the surface. The phytoplankton's instantaneous photosynthetic production will depend on its instantaneous photosynthetic response, time

scales intrinsic to production and the history of the light exposure [Denman & Marra, 1986]. These effects, which are expected to change the average production by less than 10 % [Denman & Marra, 1986], are neglected for simplicity.

5.3. Example Solutions, Coupling Air-Sea Gas Exchange with Mixed Layer Models

We will consider gas exchange into a mixed layer, the time evolution of which is described by various theoretical models. No biological processes will be considered at this stage. The motivation for this section is to gain insight into the effect of mixed layer development on air-sea gas exchange during high wind speed conditions, and to understand equilibration time scales relevant to the problem.

5.3.1. Niiler-Kraus, An Analytical Solution

Consider a vertical water column with density stratification denoted by the Brunt-Väisälä frequency N. When a step wind speed increase ($u*=0$ for $t<0$, $u*=U*$ for $t\geq 0$) is applied at the water surface, the resulting deepening can be described by a one-dimensional mixed layer model. Niiler and Kraus [1977] derive the mixed layer depth as a function of time prior to the dominance of rotation effects to be:

$$h(t) = U_* N^{-1} (12mNt)^{1/3} \tag{5.5}$$

where empirically $m=1.25$. The solution to Equation (5.1) with $P=R=0$, $h(t)$ specified by Equation (5.5) and the surface gas flux given by the Woolf and Thorpe model (see Equation 2.7) for a single gas is derived in Appendix B:

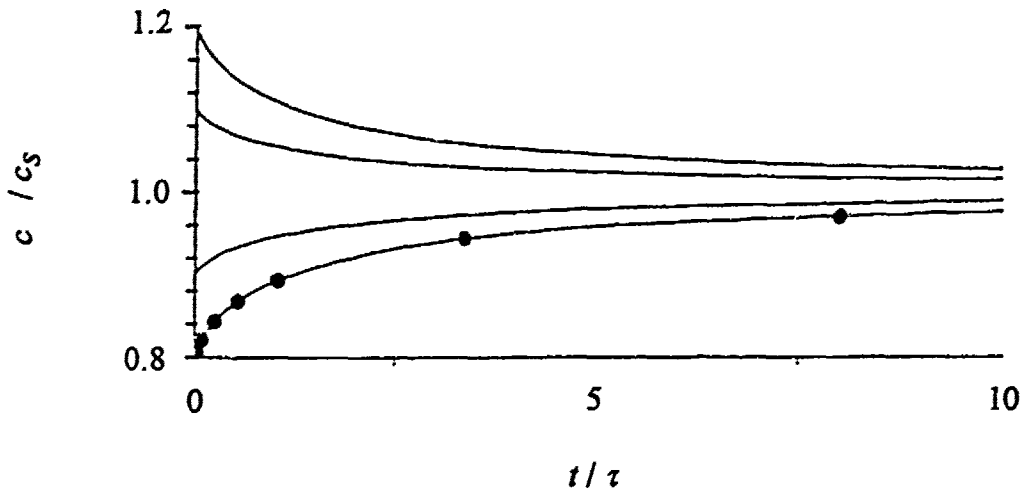

Figure 5.2 : Numerical solutions (——) and analytical solution (•) of mixed layer oxygen concentration for Niiler-Kraus mixed layer deepening.

$$c(\xi) = c_s + i(\frac{\pi}{4})^{1/4}(c_s - c_d)\xi^{-1/2}erf(i\xi^{1/2})e^{-\xi} \tag{5.6}$$

where $c_S = c^*(1+\Delta_i)$, $\xi = (t/\tau)^{2/3}$ and $\tau = (32m/9)^{1/2}(U*/K_T)^{3/2}N^{-1}$.

Figure 5.2 shows the numerical solution of the above model, with $c_d/c^* = 0.8$ and $c = c_d$ at $t = 0$, illustrating the rise or fall in concentration depending on initial conditions, asymptotically approaching the super-saturation level $\Delta_i(U_{10})$. It should be noted that this solution has only physical significance for a time period $t<\pi/f$. The dots overlying the numerical solution are a direct evaluation of the analytical solution using tabulated values of the error function from Abramowitz & Stegun [1970], giving independent verification of the numerical scheme used.

5.3.2. Pollard-Rhines-Thompson, A Numerical Solution

Consider now a two layer, slab type representation of the ocean with a mixed layer of depth h and a uniform wind stress $\tau=\rho_a C_d U_{10}^2$ acting on the ocean surface at time $t=0$,

where the drag coefficient is defined as $C_d=(a+b.U_{10})$ and a,b are constants. Below the mixed layer is a uniform density gradient with depth. Pollard *et al.* [1973] give the depth of the mixed layer as a function of time:

$$h(t) = (\tau/\rho_w fN)^{1/2}[4(1-\cos ft)]^{1/4} \tag{5.7}$$

where ρ_W is a mean (depth integrated) water column density.

The surface gas flux is parameterised by the formulation given by Woolf & Thorpe [1991], see Equation 2.7. Following Liss and Merlivat [1986] for moderate to high wind speeds, we use:

$$K_T = \chi(d.U_{10} - e) \tag{5.8}$$

where $\chi\equiv(600/Sc)^{-1/2}$ and d and e are empirically derived constants, obtained from the dashed-dot line on Figure 2.4. The supersaturating tendency of bubble dissolution at depth is expressed by the term $\Delta_i = 0.01*(U_{10}/U_{10}^{i})^2$ which is gas specific (denoted by superscript/superscript i), and is the fractional supersaturation of the mixed layer when equilibrated at a constant wind speed U_{10}.

Only entrainment processes are considered in this modelling. Re-stratification below the mixed layer is not considered.

Scaling of Equations and Asymptotic Solution

There are two time scales inherent to this problem. First, we have a time scale associated with the mixed layer deepening, $t\sim 1/f$ (physically, this is the time associated with the development of an Ekman spiral). Second, there is a time scale associated with the equilibration of the mixed layer after deepening has been arrested at a depth, $h_{o.}$, by rotation. This time scale is $t\sim h_O/K_T$ and is a function of the wind speed.

The above equations can be non-dimensionalised by either of the two time scales discussed. By combining Equations 2.7 and 5.7 with P=R=0 in Equation 5.1, and choosing to non-dimensionalise the above equations by the following parameters:

$$S_s = \frac{c}{c^*(1+\Delta)},\quad H = \frac{h}{h_o},\quad \Omega = ft,\quad S_d = \frac{c_d}{c^*(1+\Delta)} \tag{5.9}$$

where $h_O(U_{10}) = U_{10}\cdot[2\rho_a(a+bU_{10})/\rho_w fN]^{1/2}$, with f constant and U_{10} a variable, we obtain:

$$H\frac{dS_s}{d\Omega} = \beta[1-S_s] - \frac{dH}{d\Omega}(S_s - S_d) \tag{5.10}$$

where $\beta(U_{10}) = K_T/h_O f$. The variable S_s denotes the saturation of the mixed layer with respect to the equilibrium mixed layer supersaturation (*i.e.*, $\Omega\rightarrow\infty$). When entrainment has stopped after a time $t>\pi/f$, then we simply have:

$$\frac{dS_s}{d\Omega} = \beta(1-S_s)\ ,\ \text{B.C.: } S_s(\Omega=0)=S_O,\ S_s(\Omega\rightarrow\infty)=1 \tag{5.11}$$

with solution:

$$S_s(\Omega) = 1+(S_o-1)\exp(-\beta\Omega) \tag{5.12}$$

Thus the mixed layer concentration asymptotically approaches the supersaturation concentration with a dimensionless time scale $\tau = \beta^{-1} = h_O/fK_T$.

Numerical Solution

Solution of Equation 5.10 by a fourth-order Runge-Kutta method was performed for nitrogen and oxygen over a range of wind speeds. The following constants, perhaps indicative of a coastal environment, have been used:

- $a = 4.9\times10^{-4}$ $m^{-1}s$, $b = 6.5\times10^{-5}$ $m^{-1}s$ for neutral stability and $11<U_{10}<25$ ms^{-1} [Large *et al.*, 1981],
- $d = 5.9$, $e = 0.49$ mhr^{-1} for $U_{10} > 13$ ms^{-1} [Liss & Merlivat, 1986],
- $f = 10^{-4}$ s^{-1},
- $i = 1$ (oxygen) : $\chi = 818$, $c_d = 0.9$, $U_{10} = 9.0$,
- $i = 2$ (nitrogen) : $\chi = 772$, $c_d = 0.9$, $U_{10} = 7.2$, [Woolf & Thorpe, 1991].

For the time period $t<\pi/f$, it is best to normalise time by the inertial time scale, f^{-1} Shown in Figures 5.3 and 5.4 are the numerical solutions of Equation 5.10 for nitrogen and oxygen respectively.

The mixed layer concentration has been normalised by the equilibrium mixed layer concentration, c^*, not the supersaturation mixed layer concentration, c_s Due to the nonlinear dependence of wind stress and Δ on wind speed, the solutions for oxygen and nitrogen differ more significantly at higher wind speeds.

The change in saturation level is, for both gases at $U_{10} = 20$ ms^{-1}, of the order of 0 5 % over the inertial time period. An important conclusion of this modelling effort is that the modelled changes in dissolved oxygen can be measured by dissolved oxygen sensors of the type discussed in Section 4.2. and the gas tension instrumentation, and hence dissolved nitrogen sensors, discussed in Chapter 3. Using the above parameters the e-folding time scale ($\beta^{-1}(U_{10}) = h_O/K_T$) for equilibration of the mixed layer when further deepening has

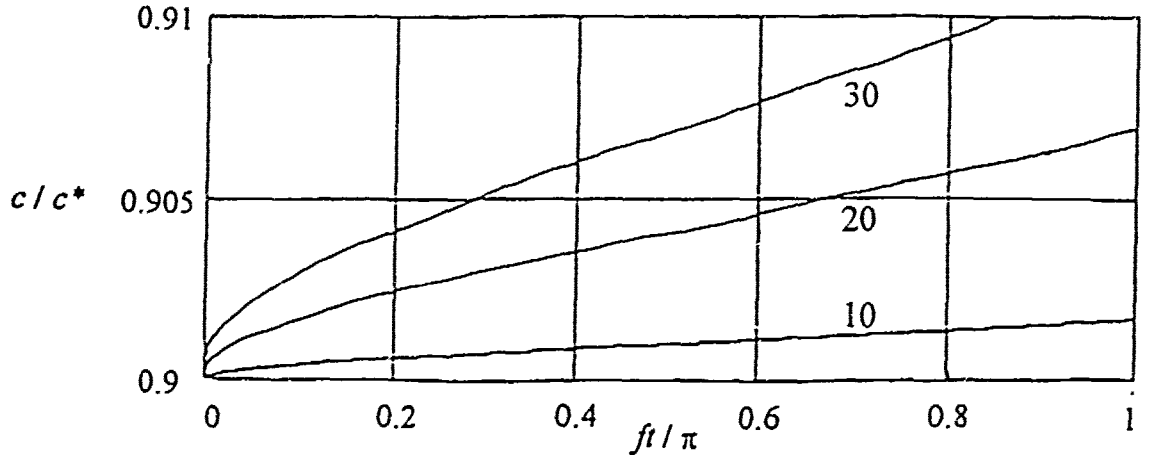

Figure 5.3 . Nitrogen mixed layer concentration for PRT mixed layer deepening. Wind speed (U_{10}) is indicated beside each curve in units of m s^{-1}.

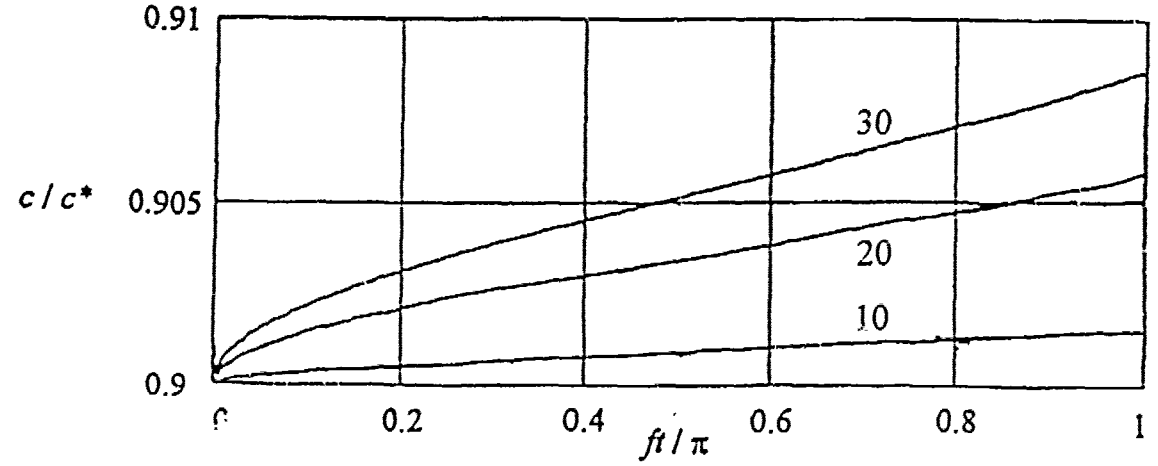

Figure 5.4 . Oxygen mixed layer concentration for PRT mixed layer deepening. Wind speed, (U_{10}), is indicated beside each curve in units of m s^{-1}.

U_{10} [m s^{-1}]	K_T [cm hr^{-1}]	Time Scale, β^{-1} [days]
10	19	11.0
15	39	5.3
20	69	3.0
25	98	2.1
30	128	1.6

Table 5.1 : Equilibration time scale for a 50 m depth mixed layer using K_T from Liss & Merlivat [1986].

stopped is shown in Table 5.1 for various wind speeds and for a gas with Sc=600. Thus, for typical wind speeds and mixed layer depths, the equilibration of a mixed layer with respect to dissolved gases can occur on time scales of days to weeks at high wind speeds, and weeks to months at low wind speeds. Knowing equilibration time scales of the mixed layer, one can address questions as to whether, for example, seasonal heating can result in seasonal changes in dissolved gas saturation levels. As seen from Table 5.1 the answer depends not only on the seasonal temperature changes but also on the wind speed history. These time scales are important for interpreting long term time series measurements

5.4. Summary

Having formulated our model framework, we have been able to consider both analytically and numerically the time scales relevant to equilibration of an oceanic mixed layer by air-sea gas exchange for particular cases involving no biological processes We have seen that storm events should provide measurable dissolved oxygen and nitrogen changes in the mixed layer due to gas exchange alone.

CHAPTER 6.

A STUDY OF THE INFLUENCE OF LANGMUIR CIRCULATION AND MIXED LAYER ENTRAINMENT ON AIR-SEA GAS EXCHANGE DURING A STORM

"In many senses, bubbles ... are the chemical engineer's elementary particles."

Clift *et al.* [1978].

6.1. An Introduction

This experiment took place in the Strait of Georgia, B.C., during November 1991 with the research vessel *C.S.S. Parizeau*. The location of the experiment is shown in Figure 6.1. The water depth was 100-200 m. The wind fetch for the data reported here was ~50 km.

The overall theme of the experiment was that of air-sea interaction and near-surface process study. Acoustical data were collected on bubble cloud size distribution and spatial patterns of bubble distribution at the near surface (Section 4.5.). These data have proven to be necessary in understanding the gas exchange and determining dominant oceanographic processes at the air-sea interface. Other instrumentation used on the

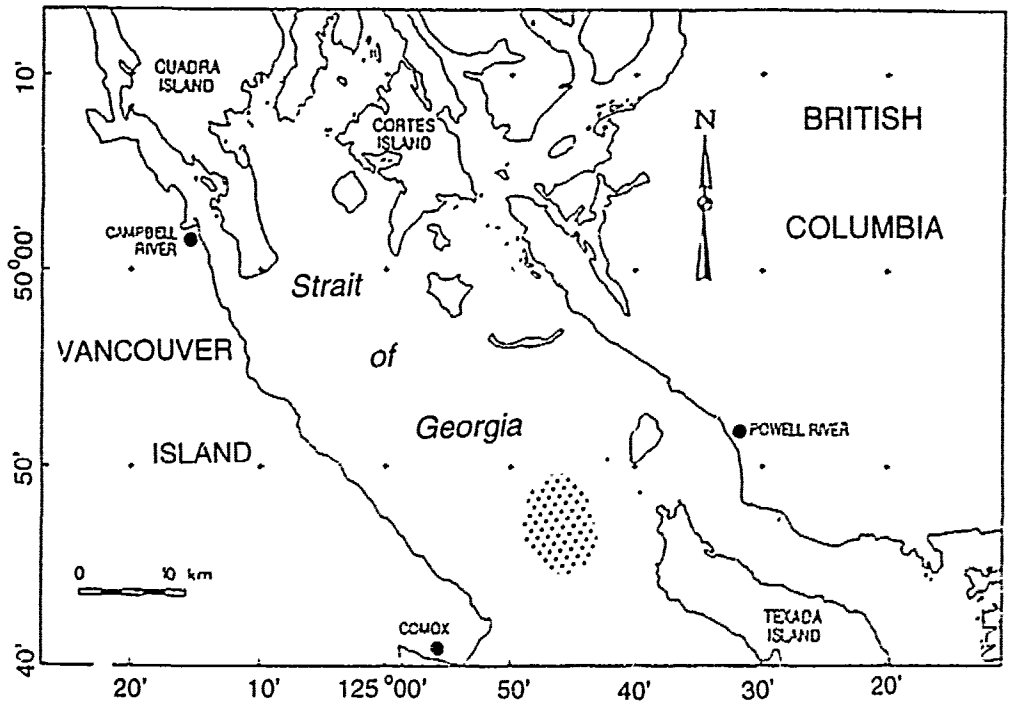

Figure 6.1 : Location of the November 1991 experiment in the Strait of Georgia.

experiment included a new wave breaking detector (Section 4.6.). From these observations wave breaking statistics were calculated. Complementary measurements were made by a high resolution video system to detect fractional whitecap coverage. These measurements were provided by Dr. Edward Monahan (University of Connecticut).

The principal measurements of the gas transfer aspect of the experiment were gas tension and dissolved oxygen. This was the first cruise where the GTDs were used in the ocean. There was, however, only one deployment when all the instruments were in the water and working. The data and discussion presented here focus on that particular deployment.

6.2. Technical Details of the Experiment

6.2.1. Instrumentation Overview

Below is a list of the instrumentation used for the deployment we shall consider:

- gas tension devices at 5.1, 9.9, 15.1 and 19.7 m, each with thermistors. The devices were separate packages, each internally recording using Sensym pressure sensors for gas tension pressure measurement (Section 3.2.).
- the acoustic package SUSY (a surface upward looking sonar instrument), shown in Figure 4.1. See Section 4.5. for details.
- a second acoustic package SEASCAN similar to SUSY.
- an instrument for detecting wave breaking, FLEX (see Section 4.6.).
- a high resolution video system measuring white cap coverage mounted on the ship bridge.
- a MET buoy (see Section 4.3.).
- three Sea Bird Electronics Seacat CTD profilers (Section 4.4.1.). Two instruments were used for profiling on the ship, one instrument also measuring dissolved oxygen was moored on the dissolved gas array at 15 m depth.
- bottle samples, taken for analysis of dissolved oxygen by the Winkler titration method (Section 4.2.).
- neutrally buoyant floats to track Langmuir circulation (Section 4.4.3.).

The dissolved gas array is shown in Figure 6.2. Attached to this array by a 50 m line was another array which supported the acoustic platform SUSY at a depth of approximately 25 m. A very large drag is provided by this instrument package, hence the whole system is

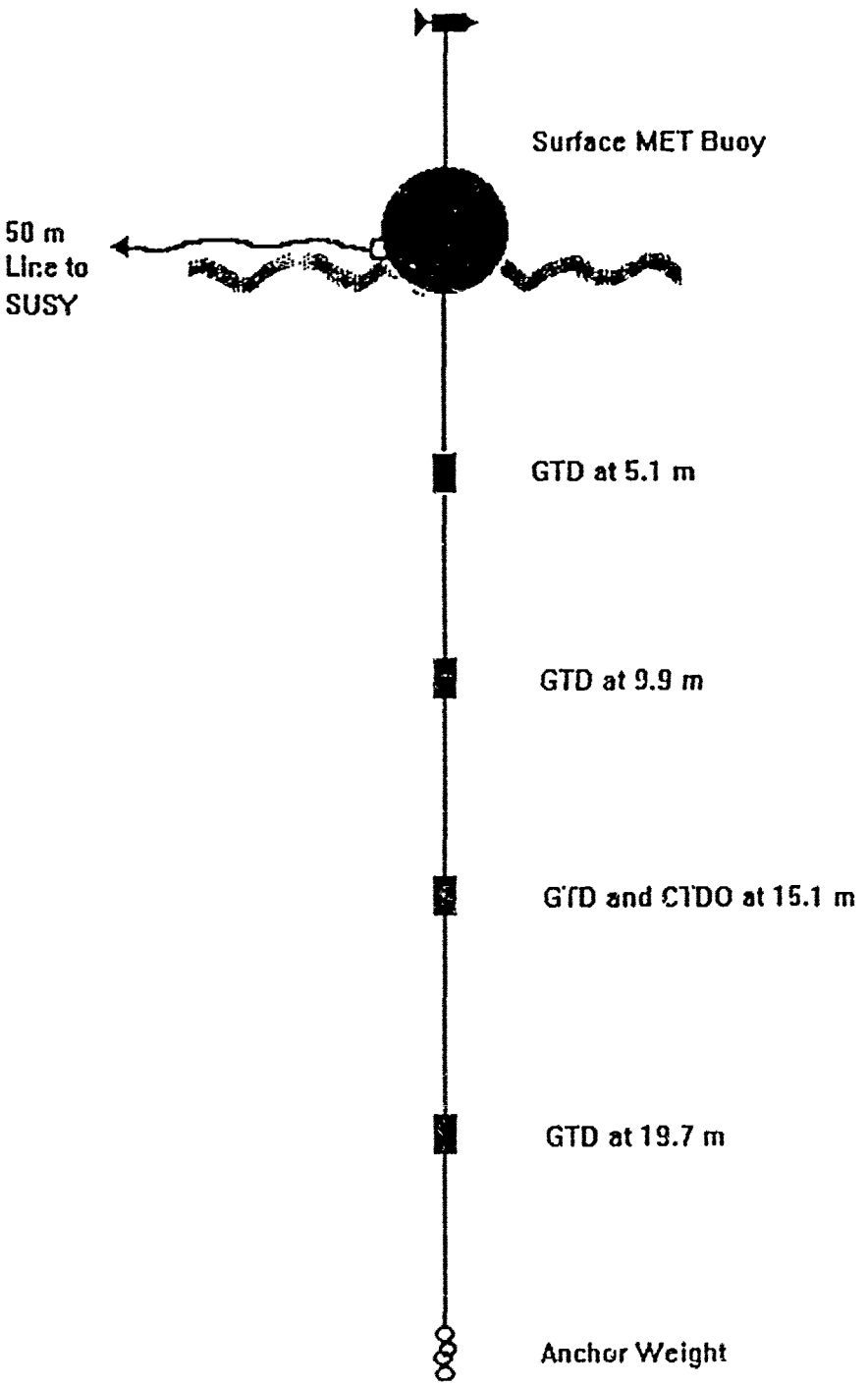

Figure 6.2 . Sketch of the instrument array used in the November 1991 experiment

expected to move with the local near surface currents (see the discussion of advective effects in Section 4.2.). Evidence that this was indeed so will be presented subsequently. The platforms SEASCAN and FLEX were deployed separately in the same vicinity.

During the experiment numerous inter-calibrations were carried out among the three CTD profilers. *In situ* bottle samples were taken and analysed by the Winkler titration technique for dissolved oxygen content. These measurements were used to calibrate the readings from the dissolved oxygen probe on the CTD. One limitation of the data set is that only a few bottle casts were taken and analysed by this method.

6.2.2. Data Processing, Procedures and Calibrations

Offsets were applied to match the gas tension and temperature measurements at each depth at 1800h on 24 November, 1991. This time period was chosen to correspond to a well-defined mixed layer, as seen from CTD measurements. This procedure proved necessary after calibrations [Johnson, 1992] were applied to the raw data. Maximum offsets of 0.4 kPa (0.4%) were applied to the gas tension sensors. The exact cause of the offsets is unknown, however drift during transportation of the instruments from Halifax is a possible explanation.

Heat flux calculations were made by using the recorded MET buoy wind speed and air/sea temperature difference, supplemented by meteorological data (*i.e.*, cloud cover and dew point) from Comox Airport MET station (see Figure 6.1). This work was carried out primarily by J. Gemmrich (IOS/UVic.).

6.3. Observations

Meteorological, oceanographic and dissolved gas measurements are shown in Figure 6 3 Water temperature and gas tension measurements are shown in Figure 6 4. Wave field measurements are shown in Figure 6.5. Bubble field measurements are shown in Figure 6.6.

6.3.1. Overview of Data Set

The wind, Figure 6.3*a*, was from the southeast, beginning at 0400h, 24 November, and rising to 15 ms^{-1}. Prior to the storm weak restratification occurred, appearing as a decrease in mixed layer depth, Figure 6.3*c*. The depth then stabilised or only slightly increased during the period of rising wind, followed by more rapid increase at 0700h. This initial slow deepening of the mixed layer is attributed to strong surface density stratification. This stratification is seen as a shallow surface layer of fresher, cold water overlying warmer, more saline water (see Figure 6.8 showing a CTD cast taken at 2325h on November 23, 1991). Bubble cloud penetration initially may have been inhibited by stratification also (Fig. 6.6*a*). At 0530h, coincident with the wind speed increase, the 5 m gas tension rose sharply until 0930h, thereafter declining steadily until 1700h Deeper sensors initially show little change until they are progressively incorporated in the mixed layer, first rising to, and later falling in step with the 5 m sensor. Following the storm, fresher surface water appeared in the form of a sharp front, leading to rapid restratification of temperature, salinity and gas tension.

Figure 6.5 shows observations of the processes responsible for bubble generation and distribution. The significant wave height (Fig. 6.5*b*) reaches 1.7 m at 1500h on 24 November with period 6.5 s. Wave breaking frequencies (Fig. 6.5*c*) are comparable to previous observations at the same wind speed [Lamarre *et al.*, 1992; Thorpe, 1984] when

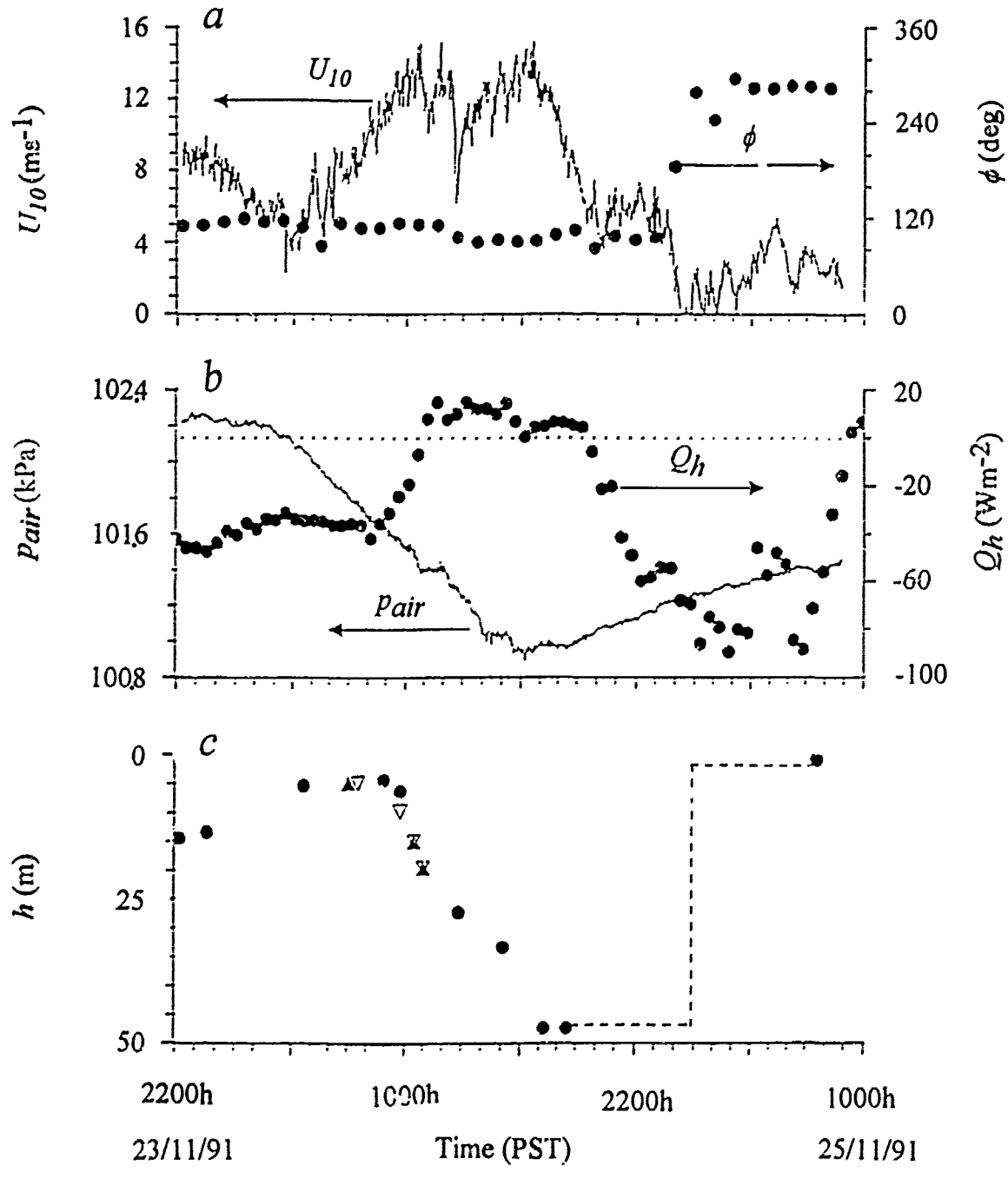

Figure 6.3 : Time series of observations in Georgia Strait (23-25 November 1991, 49° 46' N, 124° 45' W) showing. (*a*) wind speed U_{10} (*left*) adjusted to 10 m and (*right*) wind direction ϕ, (*b*) air pressure p_{air} (*left*) and total air-sea surface heat flux Q_h (*right*), (*c*) mixed layer depth inferred from salinity/temperature profiles (•), moored thermistors (Δ) and gas tension sensors (∇). Wind speed and mixed layer depth are estimated to have an uncertainty of ±10%;

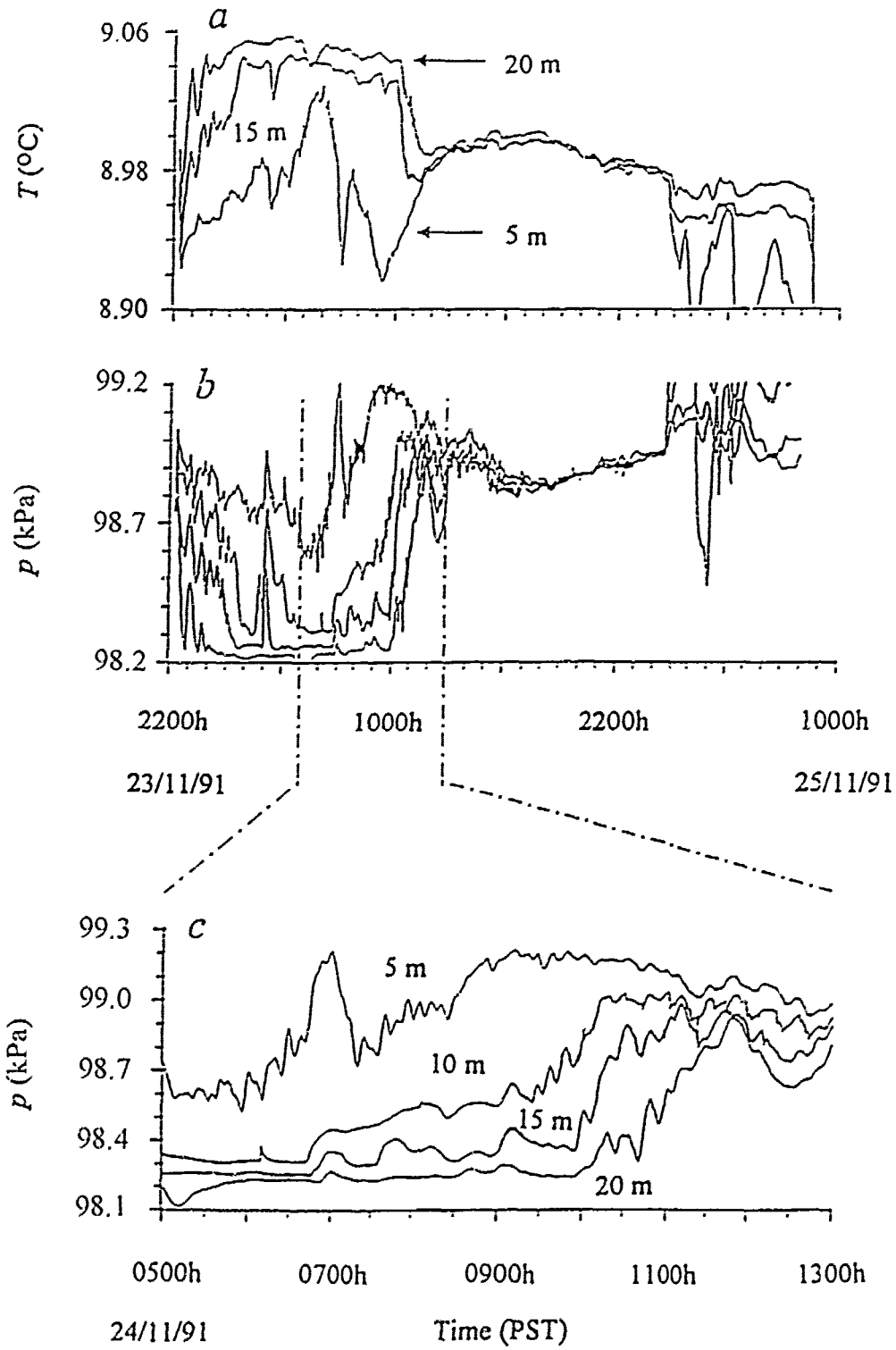

Figure 6.4 . Showing. (*a*) water temperature at 5,15 and 20 m; (*b*) gas tension at 5,10,15 and 20 m, (*c*) an expansion of (*b*) showing progressive incorporation of sensors into the deepening mixed layer. A temperature sensitivity of 0.02 kPa over the observed temperature range was also found. Water temperature is accurate to 0.02 °C.

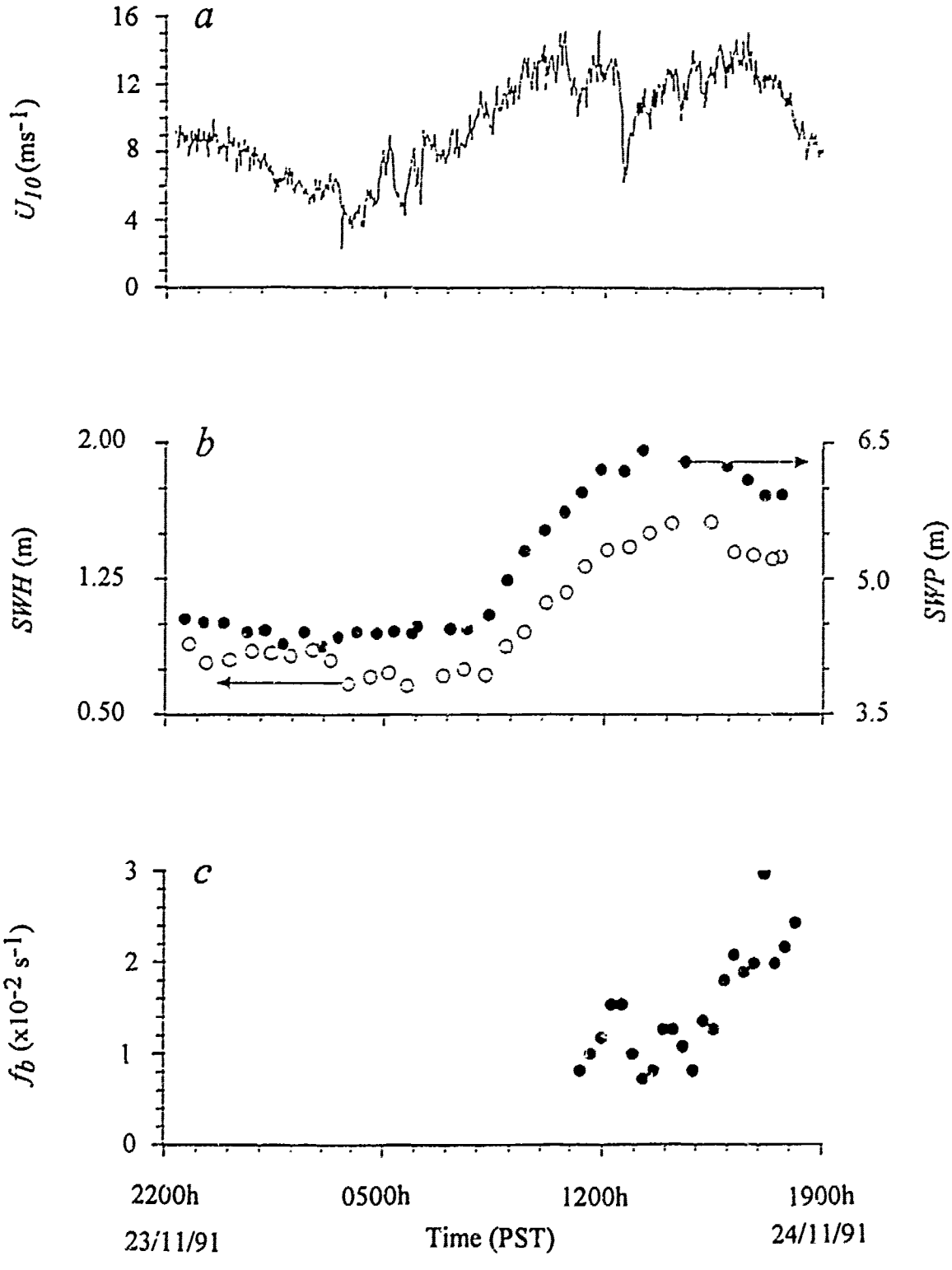

Figure 6.5 . Observations of wave conditions and bubble distribution. (*a*) wind speed U_{10}, (*b*) significant wave height (*left*) and significant wave period (*right*) measured with a vertical sonar, (*c*) wave breaking frequency (limited data set), measured by J Gemmrich (IOS/UVic.) with conductivity sensors.

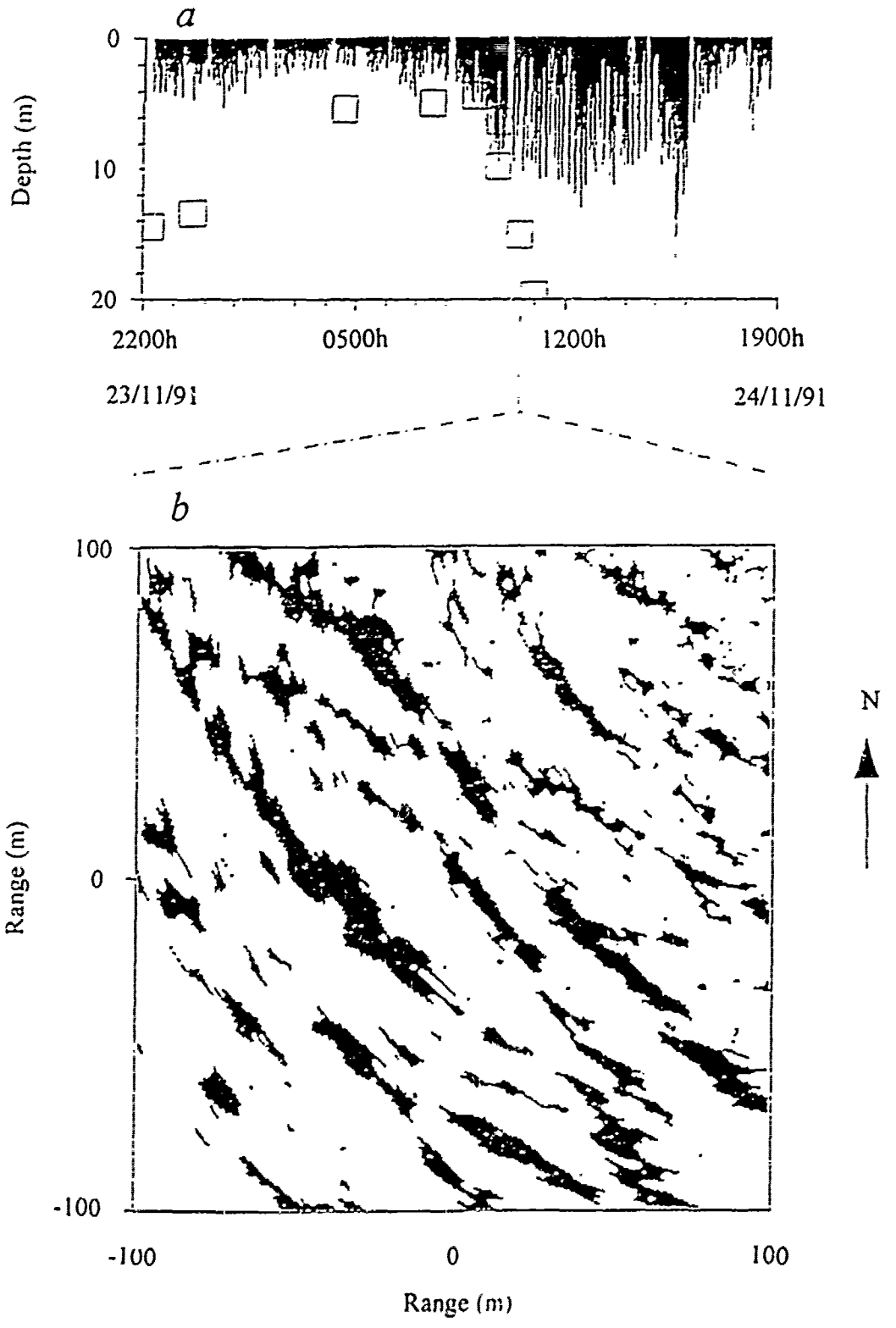

Figure 6.6 . Showing. (*a*) bubble cloud penetration depth determined from sonars, and mixed layer depth (□). (*b*) a segment of an image recorded by a scanning sonar at 1030h on 24/11/91, showing a two dimensional view of bubble clouds organised by Langmuir circulation.

normalised by the dominant wave period [J. Gemmrich, personal communication]. Bubble cloud penetration depth (Fig. 6.6*a*) shows a progressive increase with wind speed to 10 m. Figure 6.6*b* shows an azimuthally scanned sonar image with clear evidence of bubble clouds organised by Langmuir circulation into rows aligned with the wind. Neutrally buoyant float trajectories extended throughout the mixed layer with peak vertical velocities of 12 $cm.s^{-1}$ and r.m.s. values of 3-4 $cm.s^{-1}$ [E. D'Asaro, personal co mmunication].

These observations confirm that wave-breaking, bubble injection and Langmuir circulation, which are the essential ingredients of bubble enhanced gas transfer (see Section 2.5.2.), all occurred during the storm.

6.3.2. Dissolved Nitrogen Concentration

The dissolved nitrogen concentration can be calculated from measurements of dissolved oxygen, gas tension, temperature and salinity by the theory described in Section 3.3.1. A deployment on November 21, 1991 at 0200h of a gas tension instrument simultaneously with bottle samples, analysed for dissolved oxygen by the Winkler titration method, gave the following results:

- depth = 15 m , gas tension = 98.72 kPa, dissolved oxygen = 5.36 $ml.l^{-1}$

We use a mean T = 9.0 °C and S = 29.1 ppt for the water column to calculate the dissolved argon concentration, which is assumed saturated (see Section 3.3.2 for a discussion of the errors involved). The dissolved nitrogen concentration level can now be calculated by Equation 3.4 to be 12.33 $ml.l^{-1}$. The saturation levels of the constituent gases with respect to one standard atmosphere of moist air for nitrogen, oxygen and argon

are. 102.0 %, 80.1 % and 100.0 % respectively. The dissolved oxygen concentration is not atypical of Georgia Strait in winter [Crean & Ages, 1968].

6.3.3. Comparison of Dissolved Oxygen Measurements, Measured and Inferred

A Sea-Bird Electronics oxygen probe was mounted on the gas tension line at 15 m depth Because of the severity of the storm this instrument unfortunately was damaged during the deployment, and the dissolved oxygen data were corrupted after 1200h on 24 November, 1991. However, the data that were recorded have proven to be extremely interesting

Shown in Figure 6.7 is a time series of raw dissolved oxygen concentration measured by the CTD. Using the dissolved nitrogen and argon concentrations stated in Section 6.3.2., and assuming they are constant in time, an *inferred* dissolved oxygen concentration can be calculated using the following measurements. (1) gas tension from the 15 m GTD, and (2) water temperature and salinity from the CTD at 15 m depth. The results (Fig. 6 7) show remarkable qualitative consistence with the measured dissolved oxygen concentration, implying that the assumption of a constant dissolved nitrogen concentration over this time period is good. The absolute dissolved nitrogen concentration will not affect the inferred dissolved oxygen concentration calculation other than to change the d c level of the dissolved oxygen concentration. Although not published in the journal literature due to better and more recent measurements, these are the first measurements of dissolved oxygen, and hence dissolved nitrogen, made by the gas tension method

6.3.4. Additional Measurements

Fractional whitecap coverage measurements made by E. Monahan (University of Connecticut) during the storm period did not prove to be very interesting and hence the

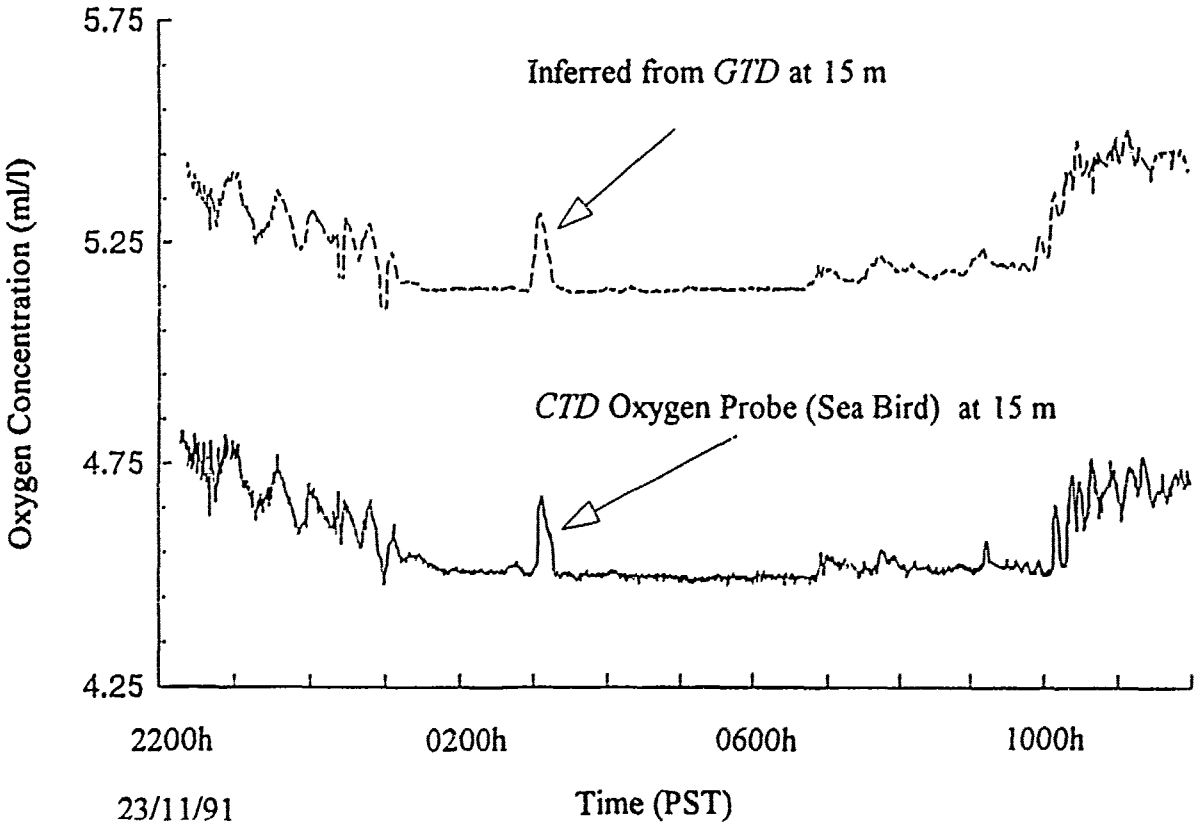

Figure 6.7 . Comparison of oxygen as measured from a CTD at 15 m depth and the inferred oxygen concentration calculated from the gas tension at 15 m depth using constant dissolved nitrogen and argon concentrations.

results are not reproduced here. This measurement is subject to many difficulties; severe limitation is imposed by requiring sunlit conditions. The data collected over our three week experiment are, however, consistent with previous measurements [Monahan *et al.*, 1992].

6.4. The Oceanography

The oceanography of Georgia Strait during the experiment was dominated by near surface temperature and salinity stratification. This is most probably the result of river runoff

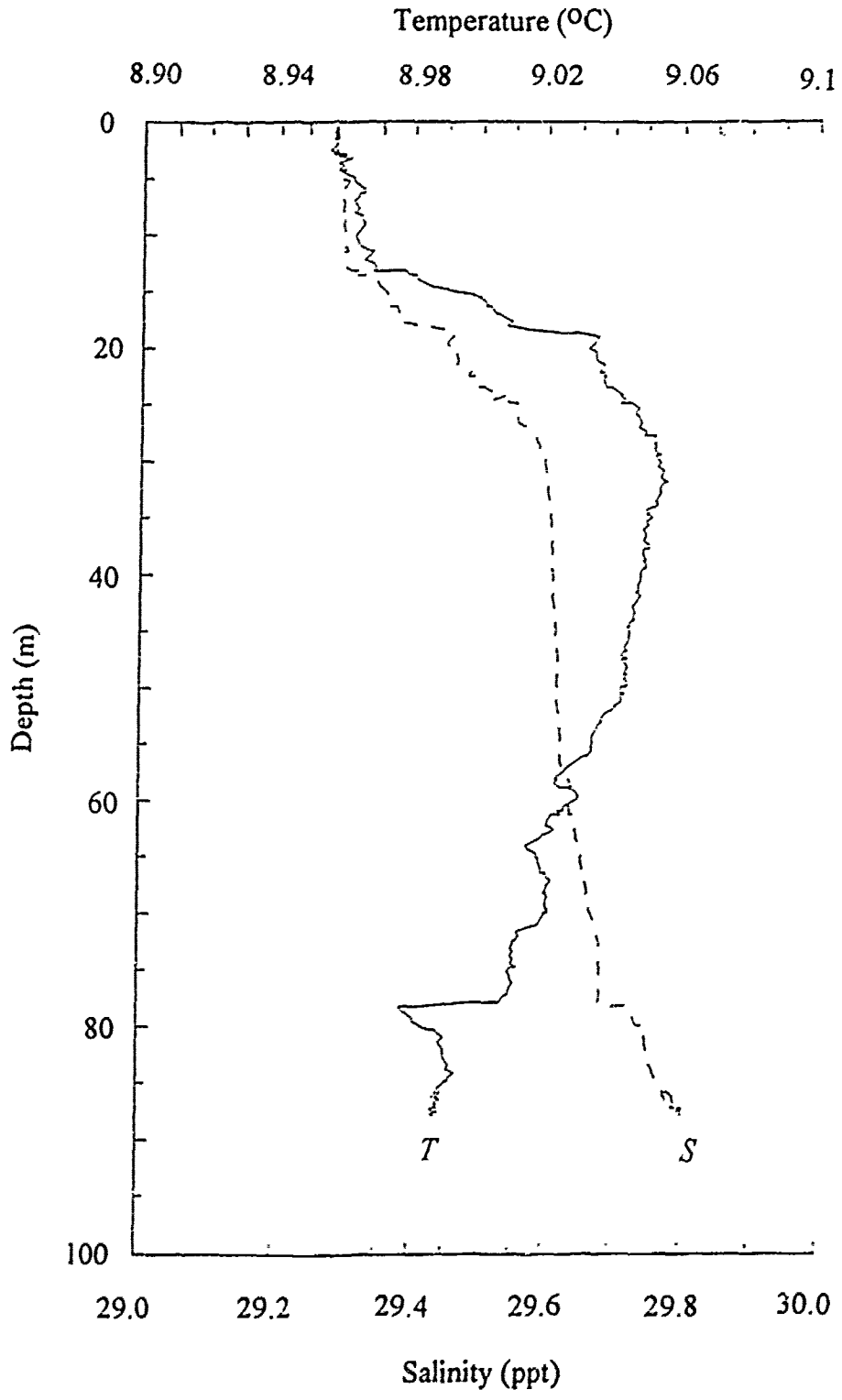

Figure 6.8 : CTD cast at 2335h on 23 November, 1991.

The surface waters were colder and fresher than the deeper waters (see Figure 6.8 of a CTD cast done at 2335h on 23 November, 1991). This is not atypical of Georgia Strait in winter time. The Brunt-Väisälä frequency can be calculated from Figure 6.8 to be N=0.0112 rad.s^{-1} (or a period of 14 minutes). It will be shown that what is presumed to be internal waves were observed in the gas tension time series, having a frequency of 0.0011-0.0021 s^{-1} (or a period of 8-15 minutes). Both these observations are compatible with internal wave theory which predicts internal waves to have a frequency range $f < \omega < N$ [Lighthill, 1978]. It is observed that the intensity of the internal waves decreases as the stratification is eroded and the mixing layer passes by each of the sensors Some mixed layer models describe the entrainment rate at the base of the mixed layer as a result of the breaking of internal waves (see review of mixed layer models given in Garrett [1994])

Internal waves will result in an uncertainty in our observed mixed layer depth and rate of change of mixed layer depth (see discussions in Sec. 5.2.). The amplitude of the internal waves, h_w, will depend on the rate at which energy is supplied to them and the rate at which the waves can transport this energy away and/or lose it to mixing processes For a simple two layer system with density difference between the layers of $\Delta\rho$ and the depth of the upper layer h_m, an upper bound on the internal wave amplitude can be estimated by comparing the kinetic and available potential energy, giving $h_w = (\rho U^2 h_m / g\Delta\rho)^{1/2}$, where U is the current speed resulting from the passage of the internal wave and h_m the mean mixed layer depth. For an idealised two layer system in which the interface wave has a wavelength much greater than the depth of the upper layer (*i.e.*, $kh_m << 1$, the *shallow water* or *long wavelength* approximation) and the lower layer is infinitely deep, the wavelength, λ, is given by $\lambda^2 = gh_m\Delta\rho/\rho T_w^2$, where T_w is the interfacial wave period [Lighthill, 1978]. For our measurements in the Strait of Georgia, $\Delta\rho$ (between 10 m and 20 m) = 0.3 kg.m^{-3}, $H \sim 15$ m, U is assumed to be of the order of 0.1 ms^{-1} (of the same

order as the phase speed, $c_p = (gh_m\Delta\rho/\rho)^{1/2}$, of the wave), $T \sim 15$ minutes (Fig. 6.4*c*), giving $\lambda \sim 200$ m and hence $h_w \sim 7$ m. It is stressed that this estimate is an upper bound for an idealised two layer system. It is expected that the internal wave amplitude will be significantly less than this value. A more representative estimate of the amplitude of the internal waves can be gained by the following argument. It is estimated that in the open ocean the flux of energy entering the internal wave field is between 0.5-5 % [Olbers, 1983] of the total surface energy flux input associated with the wind, $c_{in}\rho u^{*2}$, where $c_{in} \sim 0.8$ ms^{-1} [Gemmrich *et al.*, 1994]. Assuming a comparable efficiency for exchange of energy in our observations, we can estimate the amplitude of the internal waves by equating this energy fraction to the potential energy flux of the waves, $g\Delta\rho h_w^2/T$ giving h_w = 0.4-2.2 m. These amplitudes are more appropriate to use than the previous estimate This estimate agrees well with mixed layer depth variability between successive CTD casts taken within a couple of hours of each other. In summary then, it will be considered that the uncertainty in determining mixed layer depth due to internal wave motion is of the order of 10 %. The local maximum rate of change of mixed layer depth associated with such an internal wave (*i.e.*, 1 m *per* 15 minutes) is comparable in magnitude to the wind driven change in mixed layer depth during the deepening period of the storm However, the time scale of variability associated with the internal waves is much smaller than the time period we will model (*i.e.*, 15 minutes compared to 8 hours during the initial deepening period of the storm). Thus, by using average values of dissolved gas variability over the period of the internal waves, we can neglect justifiably the effect of internal waves modifying the mixed layer depth and its rate of change with time by water mass convergence and divergence.

As there are no time series of salinity above 15 m and no time series of temperature above 5 m, mixed layer development of salinity and temperature is modelled This is

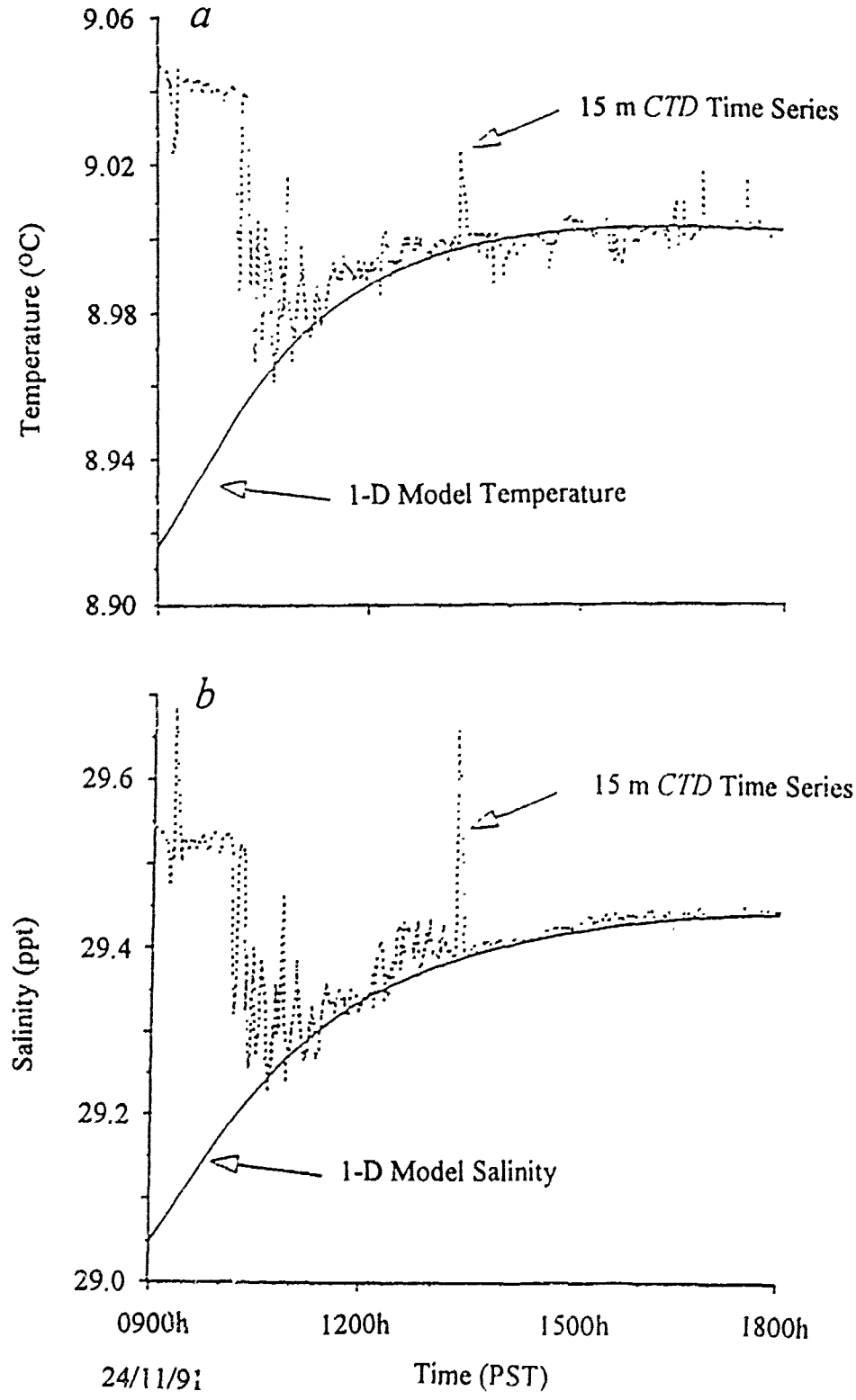

Figure 6.9 . Modelled mixed layer temperature and salinity time series and CTD observations at 15 m depth. Note that the mixed layer passes the depth of the CTD at approximately 1030h.

performed using depth integrated budget equations similar to Equation 5.1 Surface heat fluxes, calculated from meteorological parameters, are used as model input Salinity fluxes are assumed negligible. An initial CTD cast taken at 0435h on November 24, is used as an initial depth profile of salinity and temperature. This profile is very similar to that shown in Figure 6.8. Observed mixed layer depth and its time derivative are also used in the model. The use of the initial CTD profile to provide initial conditions throughout the water column in the model, is based on the assumption that no advection of water masses occurred during the deepening period. Alternatively, if the observations at 5, 10, 15 and 20 m agree with these modelled results one can then be justified in assuming that the use of a one-dimensional model is adequate, and that lateral advection was not dominating the observed signals.

The comparison of the modelled and observed temperature and salinity time series is shown in Figure 6.9. The model accurately reproduces the observed changes in temperature and salinity once the sensors are incorporated into the mixed layer. A small offset in salinity $S = 0.05$ ppt was applied to match the final mixed layer salinity This small offset can be incorporated easily into the uncertainty of S in the surface 5 m of water This comparison holds only for the deepening period illustrated.

It is important to note that the instruments are freely drifting and hence tend to track a common water mass. Hence, even if lateral advection of water did occur, the above modelling seems to show that, at least locally, the one-dimensional budget type modelling is applicable to this data set for the period indicated in the model. This conclusion allows us then to proceed, having confidence in our understanding of the oceanography, to model the dissolved gas budget during the same period.

6.5. A Model Study

In this section, we will use the modelling framework developed in Chapter 5 to investigate the data set. Biological processes affecting dissolved gas concentrations over the duration of the storm are assumed to be negligible. This will be justified by the short time scale of the storm event and the expected large fluxes due to gas transfer. The rate of change of dissolved gases within the mixed layer is then a result of gas exchange across the sea surface and entrainment from below the mixed layer. We will investigate this interaction by some preliminary modelling. Then, using observations to describe the time evolution of the mixed layer depth and water properties, we will derive a modelled mixed layer gas tension for direct comparison with the observations.

6.5.1. Introduction

Wallace & Wirick [1992] made observations of dissolved oxygen in a surface mixing layer over a period of four months. They observed rapid increases in dissolved oxygen during periods of increased wave breaking activity. Our measurements complement their observations by analysing dissolved gas concentration changes during a particular storm event, having a time scale of a day, but with sufficient vertical resolution to calculate gas exchange coefficients. During storm periods, they observed (subject to caveats of advection) large surface oxygen fluxes of the order of 10^{-5} $molO_2.m^{-2}.s^{-1}$ (it will be apparent from our data that we observe comparable fluxes). Using a typical winter primary production rate in coastal waters of 40 $gC.m^{-2}.yr^{-1}$ [Kennish, 1989] and converting to units of oxygen (Section 2.4.1.) gives a biologically produced oxygen flux that is an order of magnitude less than that observed by Wallace & Wirick [1992] This represents an upper bound for net biological production of oxygen as respiration will occur also. We can conclude that biological effects influencing dissolved oxygen, and

nitrogen (Section 2.4.2.), concentrations are of secondary importance in determining budgets of these gases during short time scale winter storm events, the dominant processes will be surface gas transfer and mixed layer entrainment. The preliminary experimental results and analysis presented here have been published as a letter to *Nature* [Farmer *et al.*, 199?].

6.5.2. Preliminary Investigations

In our observations, stronger near-surface density stratification and linearly increasing wind speed significantly reduce the initial entrainment rate (see Figure 6.3*c*) over the various models discussed in Sections 5.3.1. and 5.3.2. describing theoretical entrainment rates based on a step increase in wind speed. Thus, to gain insight into the observations of gas tension during the initial period of rapid entrainment, a more representative result for the data is obtained by solving Equation 5.1 for a linear increase in wind speed and a quadratic deepening rate as a function of time. Biological sources and sinks over the short period of entrainment are assumed negligible in the balance of Equation 5.1 (*i.e.*, P=R=0) The gas of particular interest is oxygen. The initial conditions, chosen to be depth independent, were c/c_S=0.8, *i.e.*, oxygen being 20% undersaturated. The gas transfer at the surface is given by the Woolf and Thorpe model (Equation 2.7). The model results are shown in Figure 6.10.

The modelled oxygen concentration first rises due to the dominance of bubble induced gas transfer as the water is undersaturated in oxygen. It then drops as entrainment dominates. This is in qualitative agreement with the observations of gas tension (Fig 6.4*b*), although the two are not directly comparable as this model result is for a single gas The maximum in the mixed layer concentration is given from Equation 5.1 when dc/dt = 0, *i.e.*, when the entrained gas flux equals the surface gas flux.

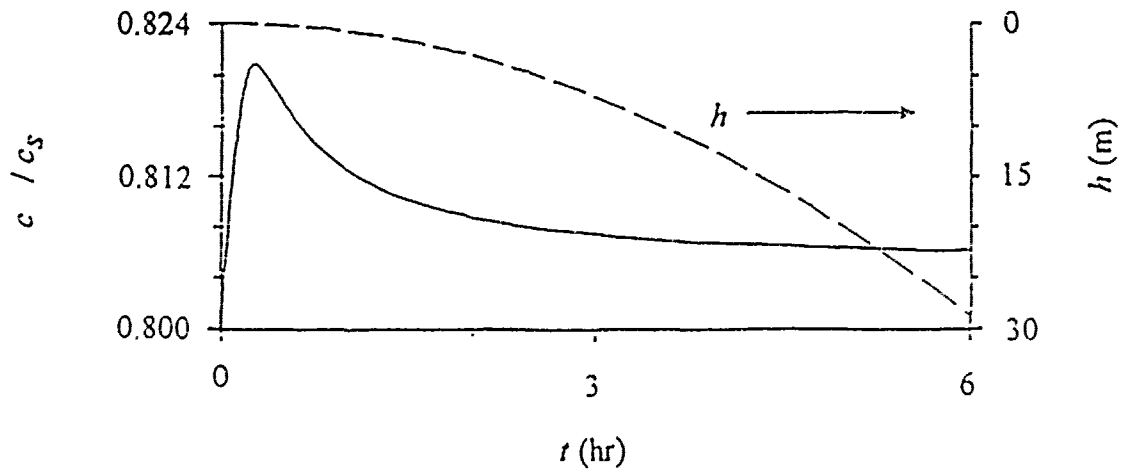

Figure 6.10 : Investigative model of the data set. Solution of mixed layer oxygen concentration (——) for a linearly increasing wind speed and a quadratic mixed layer depth (----) as a function of time.

6.5.3. Methodology

The dissolved gas budget model described by Equation 5.1 is solved separately for oxygen and nitrogen, allowing for changes in solubility [Weiss, 1970] due to water temperature, water salinity and atmospheric pressure. As discussed previously, biological sources and sinks of both oxygen and nitrogen are assumed negligible in determining the dissolved gas budgets (*i.e.*, P=R=0 in Equation 5.1). The surface gas flux is parameterised by wind speed and Schmidt number according to various models available for gas transfer (see Section 2.5.2.). Observed wind forcing and observed mixed layer depth are used in the model. The modelled oxygen and nitrogen dissolved gas concentrations are then combined (by Henry's Law, Equation 2.1) with water vapour pressure and argon partial pressure using Dalton's Law (Equation 3.1) to obtain a modelled gas tension. The modelled gas tension is then compared to the observed gas tension. The numerical scheme used is a 4th order Runge-Kutta [Press *et al.*, 1988].

6.5.4. Model Inputs

Wind speed and mixed layer depths are represented by functional approximations for ease of modelling. In the absence of observations above 5 m, calculations begin when the 5 m sensor is incorporated into the surface layer. The modelled mixed layer salinity of Section 6.4. was used during the deepening stage of 5 m to 15 m where no measured salinity variations within the mixed layer are available.

As no other water samples were taken for analysis after this time period, we assume that the nitrogen and argon concentrations do not change during the two days between the above measurements and the start of the storm period on 24 November 1991. This assumption can be justified from several perspectives. Firstly, there were no excessively strong wind events during this time period and hence low transfer velocities would be expected. Secondly, nitrogen is relatively inert as far as biological consumption and production in the ocean are concerned (see Section 2.4.2.), but biological demand of oxygen, especially in coastal environments like Georgia Strait and in winter months, is not insignificant. For this reason it was decided to proceed with analysis of the data set during the storm period by assuming that nitrogen and argon concentration levels did not change significantly. Evidence that this assumption is indeed correct is supported by the following comparison of oxygen measurements by quite independent means.

By assuming nitrogen and argon concentration independent of depth and equal to the values reported in Section 6.3.2., the gas tension at each sensor prior to the storm (0500h, 24 November) allows calculation of the initial oxygen profile to 20 m. The initial stratification of dissolved oxygen concentration is: 5.30, 5.19, 5.16, 5.15 $ml.l^{-1}$ at 5, 10, 15, 20 m depth respectively. Once the mixed layer has penetrated beneath 20 m. we have only the deeper observations of dissolved oxygen obtained two days before the storm, so the calculations are less certain.

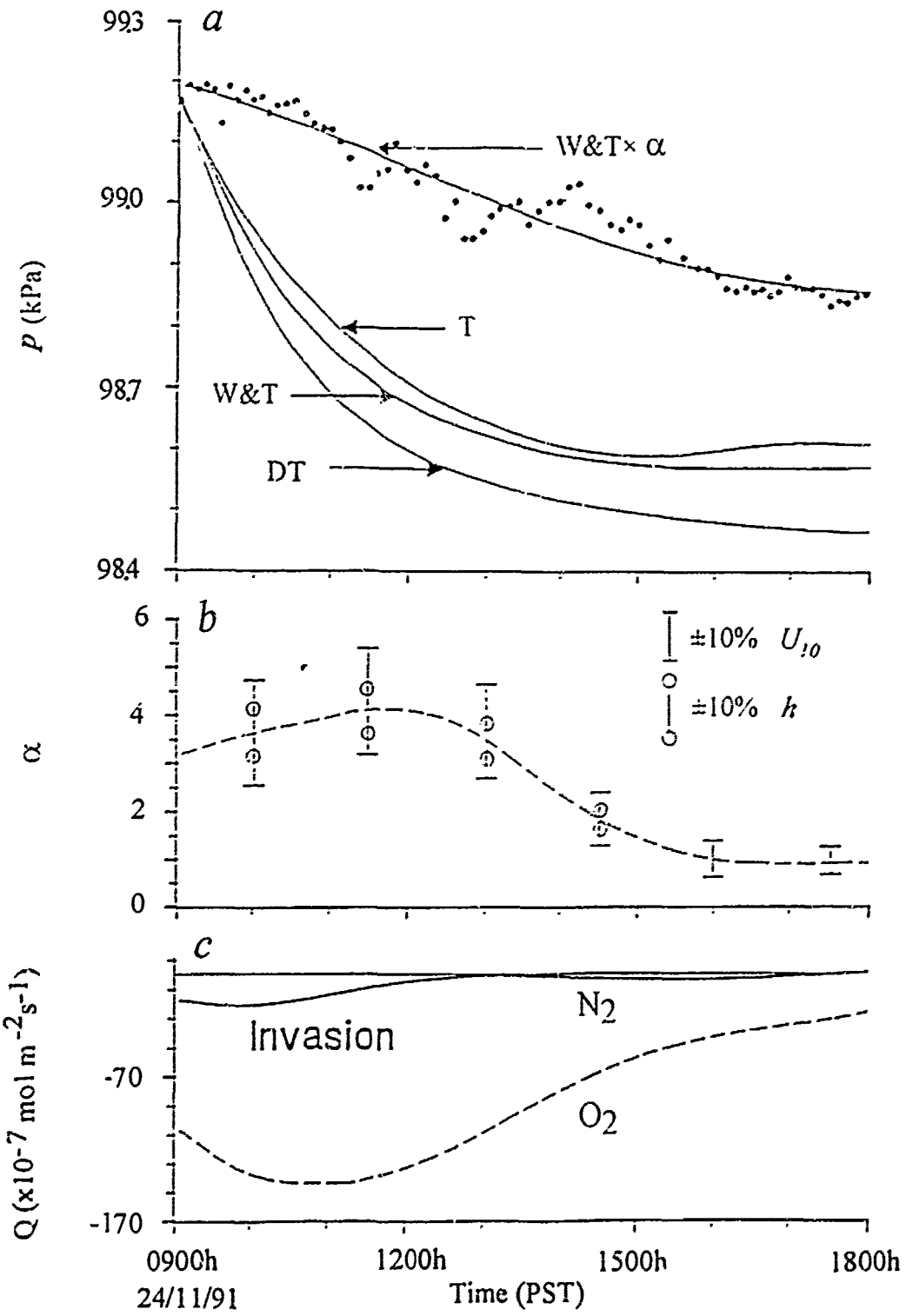

Figure 6.11 . Model results. (*a*) observations (•) and model predictions of surface layer gas tension, models include direct transfer (DT) [see Liss, 1988, Woolf and Thorpe, 1991], Woolf & Thorpe [1991] (W&T), Thorpe [1984b] (T). The quartic fit in (*a*) corresponds to W&T×α where α(*t*) is given in (*b*). Error bars indicate ±10% uncertainty in U_{10} and *h*; (*c*) inferred N_2 (solid) and O_2 (dashed) fluxes using W&T×[α(*t*)]

6.5.5. Model Results

Both the Woolf & Thorpe (W&T) and direct (or thin film) transfer models (DT) (see Figure 6.11*a*) under-predict the observations of air-sea gas transfer during the modelled period. The Thorpe model (T in Figure 6.11*a*) gives similar fluxes to the W&T model. There is great scatter in published values of K_T [see Section 2.5.3.]. We therefore choose to fit W&T to the observations by multiplying K_T by a factor $\alpha(t)$ as a function of time (Fig. 6.11*b*). The apparent enhancement is greatest ($\alpha \approx 4$) when the bubble clouds penetrate most deeply (Fig. 6.6*a*). The modelled surface fluxes corresponding to the observations are shown in Figure 6.11*c*.

6.5.6. Discussion

Calculated surface fluxes of oxygen (Fig. 6.11*c*) are comparable to previous observations by Wallace & Wirick [1992] during storm periods. This strengthens considerably the *a priori* assumption that biological processes were not dominant in affecting the dissolved gas budgets during the storm period (see discussions in Sec. 6.5.1.). The nitrogen flux is less than oxygen since nitrogen is close to saturation and oxygen is significantly undersaturated. Both gases are invasive during strong winds, but there is slight nitrogen evasion at low winds. Nitrogen evasion can occur when the nitrogen is oversaturated and the bubble injection is not strong enough to support a supersaturation level as large as that observed.

6.6. Discussion

There are several reasons for expecting significant departures from previously published values of the gas transfer coefficient, K_T (see Section 2.5.3.). Aside from limitations of

estimates based only on gas evasion, the influence of wind speed averaging period (K_l is a nonlinear function of wind speed) and fetch can introduce significant bias [Wanninkhof, 1992]. Fetch dependence of K_T arises primarily from the sea surface requiring time to develop. Hasselmann *et al.* [1973] report that wave fields 'grow' over distances of hundreds of kilometers offshore. Results from lake studies, such as those shown in Figure 2.5, which have areas ranging from 0.13-500 km^2, may be significantly affected. Note that these lake studies were used in the determination of the Liss & Merlivat $K_l(U_{10})$ relationship (Section 2.5.3.). The mechanism and magnitude by which lake study measurements may differ from open ocean measurements is unclear. Is $K_l(U_{10})$ overestimated or underestimated? One can argue that, in fetch limited environments, waves can be steeper and therefore can break more readily and may even plunge deeper, providing greater turbulence and bubble densities for increased gas transfer. However the Stokes drift, which helps drive Langmuir circulation, can be greater in the open ocean, possibly increasing the depth to which bubbles can penetrate and dissolve. Li & Garrett [1993] have estimated dependency of the maximum downwelling velocity of Langmuir circulation, w_L, on dominant forcing parameters to be $w_L \propto S_o^{1/6} z_s^{1/2} u*^{1/3} A_v^{-1/2}$ where the Stokes drift velocity is described by $S_o \exp(-z/z_s)$ and A_v is the vertical eddy viscosity Such relationships, combined with observations, are essential for investigating the role of Langmuir circulation on gas transfer processes. Other related issues affecting K_l are wave breaking intensity, bubble injection depth and initial bubble size distribution There are at present no data for direct comparison between wave breaking frequencies in lakes and the open ocean under similar conditions. The air entrainment depth under open ocean breaking waves may be shallower than that in lakes. Sea water tends to produce greater bubble densities with proportionately more small bubbles, which will affect the total amount of gas transferred. All these processes could contribute to observed variability in

estimates of K_T. Also, some previous field studies do not take into account entrainment processes, restratification processes and advective effects which, as shown here, can dominate gas concentration time dependence leading to incorrect transfer coefficients, especially in stratified coastal environments where vertical dissolved gas stratifications tend to be large.

The Woolf & Thorpe parameterisation of bubble mediated gas flux is approximate, as stated in their paper [Woolf & Thorpe, 1991]. The pertinent question is, how well is it approximated? If the parameterisation is not very good, we cannot say from our results whether the observed enhancement of surface gas fluxes is due to a direct enhancement of K_T or whether it is just a poor representation of the bubble mediated gas flux in the Woolf & Thorpe model. From Equation 2.7 one can see, upon multiplying out the brackets, that their equation reduces to a thin film flux plus an additional contribution to the total flux from bubble dissolution. This bubble mediated flux produces a supersaturation of the mixed layer at equilibrium. They have, however, not separated the bubble injection contribution inherent in the observed K_T relationship of Liss and Merlivat [1986]. This concerned us when using their model. What is required is a model of gas transfer that separates the contributing physical processes, *i.e.*, dissolution, partial dissolution, thin film transfer depending on the sea state, turbulent transfer at the breaking site, *etc*. As each process has a different *Sc* dependence, clever field and laboratory studies will need to be designed to address each process separately. Laboratory [Asher *et al.*, 1992] and theoretical work [L. Merlivat, personal communication] is underway to address these outstanding problems.

In view then of the large uncertainty in previous published values of K_T at higher wind speeds and the rather poor parameterisations of bubble mediated gas transfer in terms of the mechanisms that exist, the magnitude of the enhancement of K_T in the W&T model

and the correlation of this enhancement with bubble penetration depth is not surprising. For the limited period of data during the storm, when gas transfer is expected to be dominated by bubble injection and wave breaking processes, the observed enhancement of K_T in the W&T model by up to a factor of four at wind speeds of 14-15 ms^{-1} implies that the surface gas flux is approximately 15 times that at 7 ms^{-1} and 30-80 times that at 4 ms^{-1} (see the dash-dot line of Liss & Merlivat [1986] on Figure 2.4). Thus, we can conclude from these data that during the storm period the surface gas fluxes are enhanced considerably, in quantitative agreement with the observations of Wallace & Wirick [1992]. We *cannot* conclude, however, the exact cause or mechanism for the enhancement, except to say that the magnitude of the enhancement was found to be correlated with bubble penetration depth. This observed correlation, complemented by more recent modelling studies of Woolf [1993] and Keeling [1993] showing gas transfer from larger and shorter lived near surface bubbles to be less important in the transfer of weakly soluble gases, indicates that bubble dissolution at increased hydrostatic pressure is an important process in air-sea gas transfer of weakly soluble gases.

We anticipate that analysis of the bubble size distributions, Langmuir circulation and related phenomena (Fig. 6.6) during the storm will give insight to the observed correlation, and perhaps pave the way to a much better parameterisation of bubble mediated gas transfer. However tempting, this has proved beyond the scope of this thesis Work on the distribution of Langmuir circulation for this data set is currently being pursued [Farmer & Li, 1994]. Application of photographic measurements [Johnson & Cooke, 1979] of bubble size distributions in the W&T model could lead to an underestimate of the bubble induced gas transfer. These optical measurements have a smallest detectable bubble size of approximately 50 μm. For the data they reported, a peak in bubble size distribution at approximately 60 μm was observed. However,

acoustical measurements [Vagle & Farmer, 1992] suggest a spectral peak in bubble radius of less than 20 μm, which is less than the resolution of the optical system. Inclusion of these bubbles in the W&T model could lead to an increased modelled bubble induced gas transfer rate.

These initial results, however, indicating significant enhancement of air-sea gas fluxes during periods of strong bubble penetration, provide support for the role of bubble injection in the transfer of weakly soluble gases, and emphasise the relevance of near-surface oceanography to the estimation and parameterisation of transfer coefficients

CHAPTER 7.

A STUDY OF BIO-PHYSICAL INTERACTIONS IN A MIXING LAYER DRIVEN BY NOCTURNAL CONVECTION AND DAYTIME SOLAR HEATING

7.1. An Introduction

Our observations were obtained in open ocean conditions in the vicinity of 48°40' N and 127°30' W during 15 February to 2 March, 1993. The location of the experiment is shown in Figure 7.1. The research vessel was the *C.S.S. John P Tully.* The water depth was ~2800 m.

In this experiment we were interested in obtaining relatively long time series measurements of dissolved oxygen and nitrogen in contrast to the short time scale, coastal measurements we obtained in the Strait of Georgia Experiment (Chapter 6) As such, we deployed our instruments for more extended periods. The data and an earlier version of the modelling described in this chapter have been published in *Journal of Marine Research* [McNeil & Farmer, 1995].

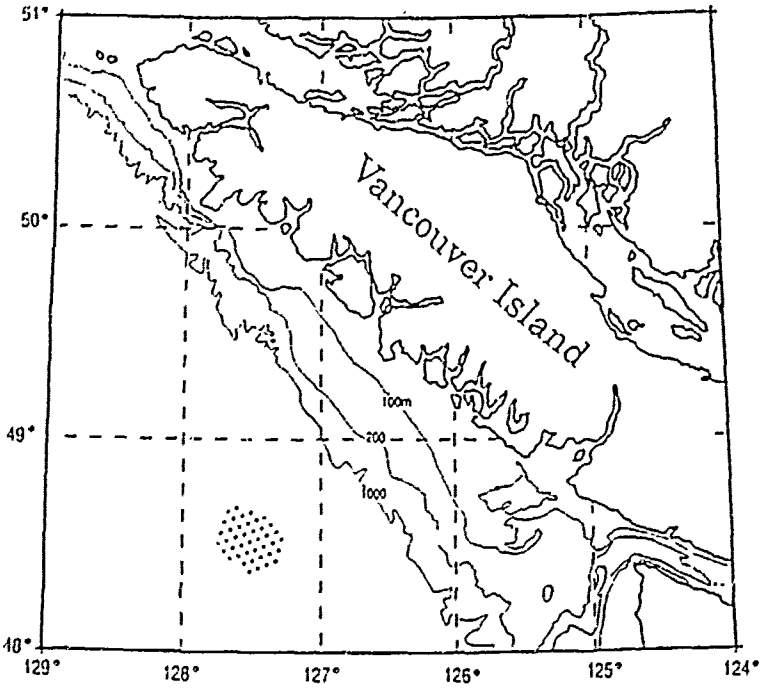

Figure 7.1 . Location of the February 1993 experiment in the N.E. subarctic Pacific

7.2. Technical Details of the Experiment

7.2.1. Instrumentation Overview

The instrument array, shown in Figure 7.2, consisted of a freely floating surface meteorological buoy (Section 4.3.) and a dissolved gas sensor array with surface buoy tethered 50 m down wind. From the MET buoy were suspended thermistor chains from 10 m to 120 m with vertical resolution of 5 m, and a 20 m chain extending from 80 m to 100 m straddled the thermocline with a vertical resolution of 2 m. The dissolved gas sensor array consisted of two ENDECO 1184 O_2 sensors at 21 m and 30 m depth, each with a sampling period of 15 minutes and a GTD using a Paroscientific pressure sensor (Section 3.3.2.) at 40 m depth, having a sampling period of 5 minutes. The GTD had an e-folding equilibration time of ~50 minutes. Frequent CTD casts were made

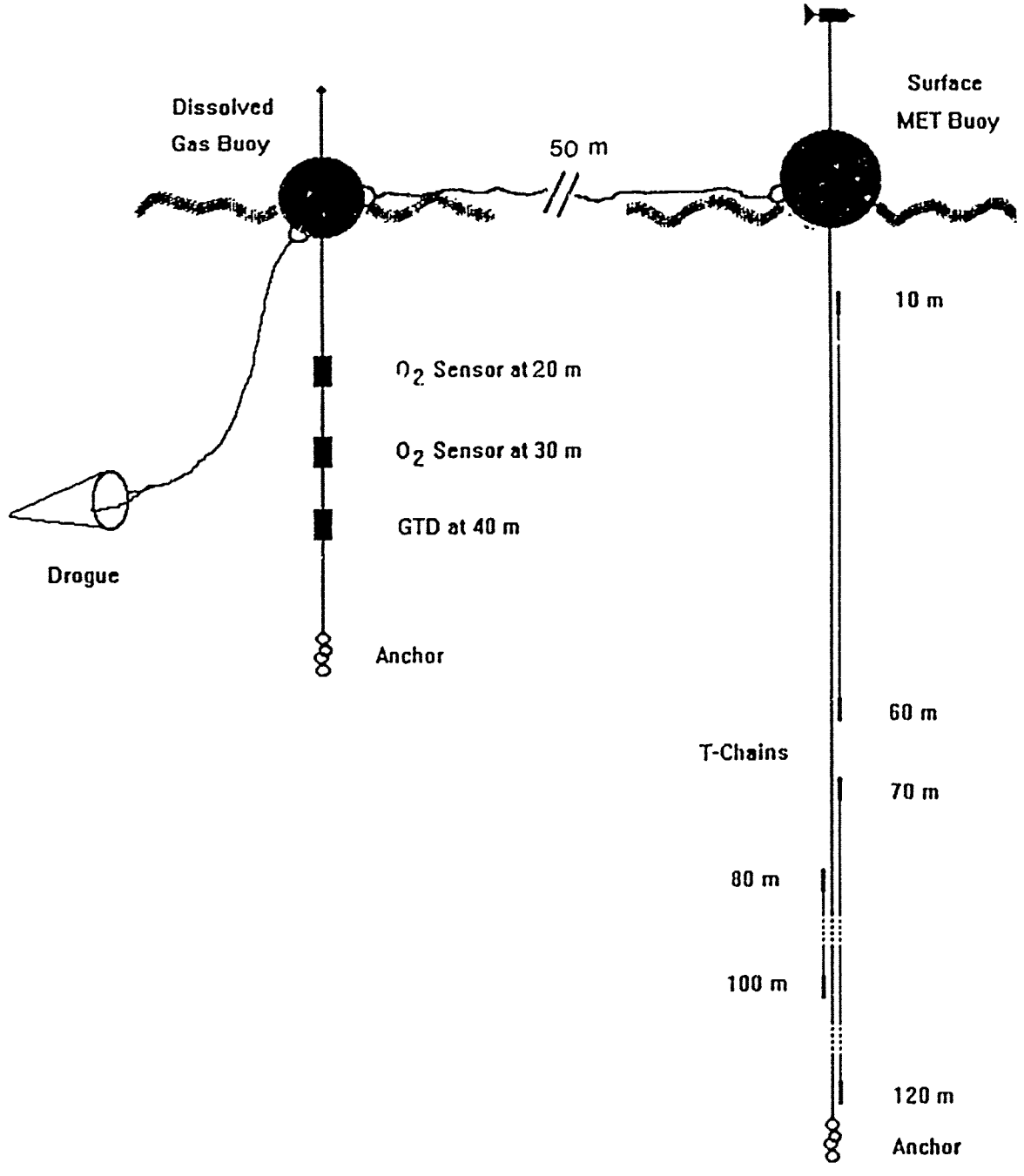

Figure 7.2 . A sketch of the instrument array used in the February 1993 open ocean experiment.

(approximately every 3 hr) in the vicinity of the instrument array (<13 km away) and Winkler casts were made at the instrument array daily. Periodically the acoustic instrument SUSY (Section 4.5.) was deployed in the vicinity at a depth of 30-40 m.

Spatial variability is a complicating factor in nearly all such open ocean experiments Dissolved gases in the water column, particularly dissolved oxygen, are patchy on the length scales of interest, of the order of 10 km [Denman, 1992]. It is normally unrealistic to plan measurements of the horizontal variability in water properties with this resolution, particularly before and after storms. As described in Section 4.1., rather than try to measure advective effects, we designed the array to minimise these effects by using a drogue (Fig. 7.2). During the experiment, the instrument array was observed to drift approximately 4 km per day ($\approx$ 5 cm s^{-1}) to the North West. This drift speed is comparable to historical records of near surface currents for this area at this time of year [Freeland *et al.*, 1984]. This provides confidence that the array did indeed drift with these currents, hence advective effects within the data set are expected to be small. However, as will be apparent from the data, strong advective trends were observed for a limited period during a storm event. These data will be discussed in detail.

7.2.2. Data Processing, Procedures and Calibrations

Winkler titrated bottle samples were used to correct the oxygen signals measured by the ENDECO 1184 oxygen sensors. A linear fit of: -0.01503 $ml.l^{-1}.day^{-1}$ + 0.451 $ml.l^{-1}$ was applied to the raw oxygen probe measurements at 30 m. An offset was applied to the 21 m data to match them to the corrected 30 m data (see the discussion of oxygen sensor drift in Section 4.2).

7.3. Observations: an Overview

7.3.1. Meteorology and Oceanography

Wind speed and direction at 3 m height is shown in Figure 7.3*a*. A storm occurred at the end of the experiment (28 February to 1 March). The air pressure and air/sea temperature difference are shown in Figure 7.3*b* and solar radiation intensity in Figure 7.3*c*. Each evening during the period 20-25 February, large air-sea temperature differences of between -3 °C and -6 °C were observed, giving rise to a convectively unstable atmosphere and upper ocean. No precipitation measurements were made.

A contour plot of the thermistor chain data (Fig. 7.4) shows a seasonal thermocline at around 80 m to 90 m depth during the period 20 to 27 March. The CTD measurements indicate that this depth also corresponds with the halocline. During the storm (27 February to 1 March) large changes in the upper ocean properties occurred, with the depth of the thermocline decreasing to approximately 60 m. This portion of the data will be discussed subsequently.

Very limited information on bubble penetration depth was recorded due to instrumentation problems. Of the data that were recorded, bubble plumes were not observed to penetrate deeper than 5 m during the period 20 to 27 February, indicating weak Langmuir circulation effects. Bubble penetration increased to more than 8 m depth during the evening of 27 February, at the onset of the storm, indicating that Langmuir circulation became a more dominant process as the wind speed increased.

7.3.2. Dissolved Gases

The measured gas tension (Fig. 7.5*a*) and water temperature (Fig. 7.5*b*) at 40 m depth are shown. The dissolved oxygen concentration at 30 m depth (Fig. 7.5*c*) is expressed as a

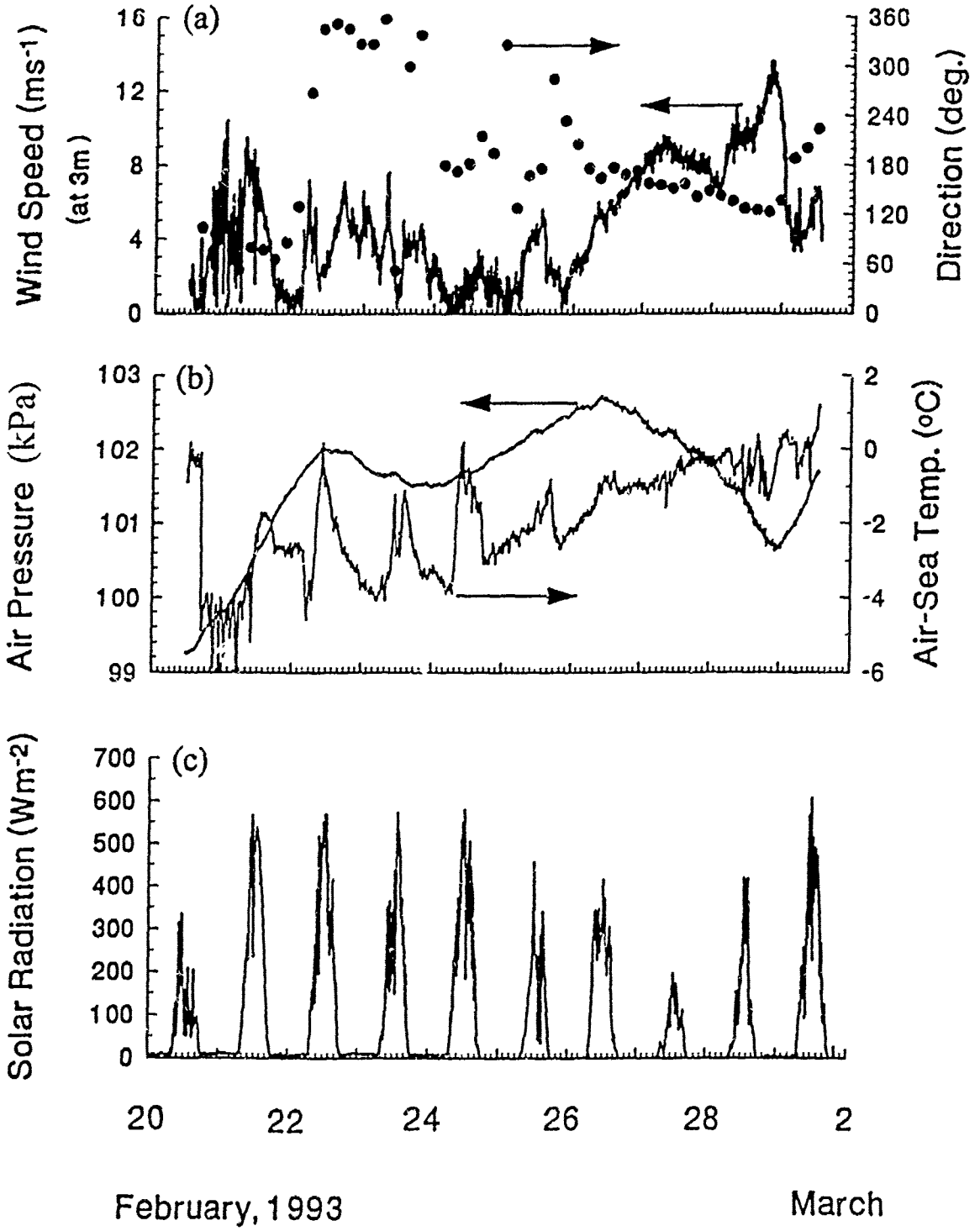

Figure 7.3 : Meteorological measurements, showing: (*a*) wind speed (*left*) and direction (*right*) at 3 m height; (*b*) atmospheric air pressure (*left*) and air minus sea temperature difference (*right*); (*c*) solar radiation intensity.

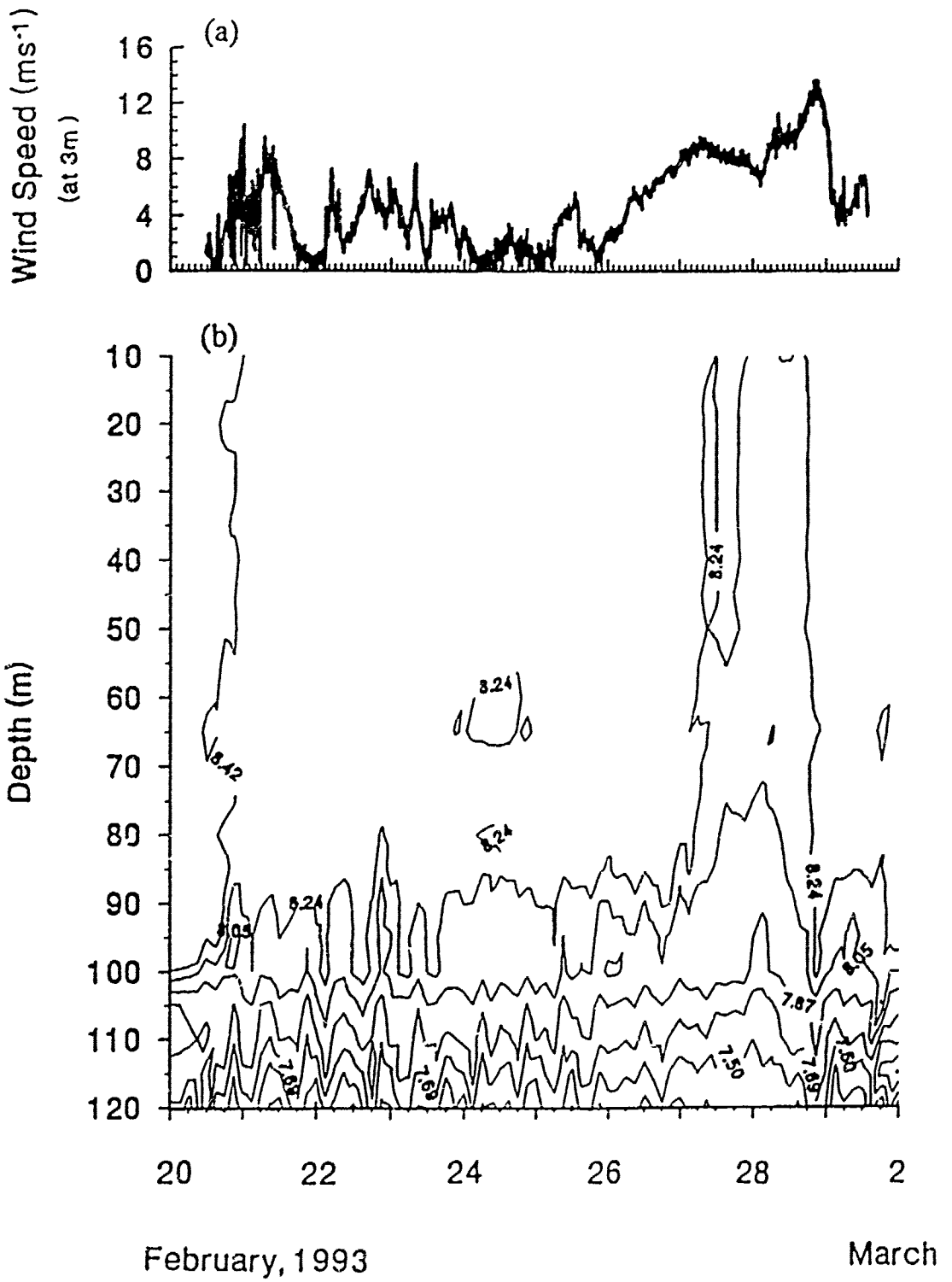

Figure 7.4 : Showing: (*a*) wind speed; (*b*) a contour plot of thermistor chain temperature (°C) data from 20 February to 2 March, 1993.

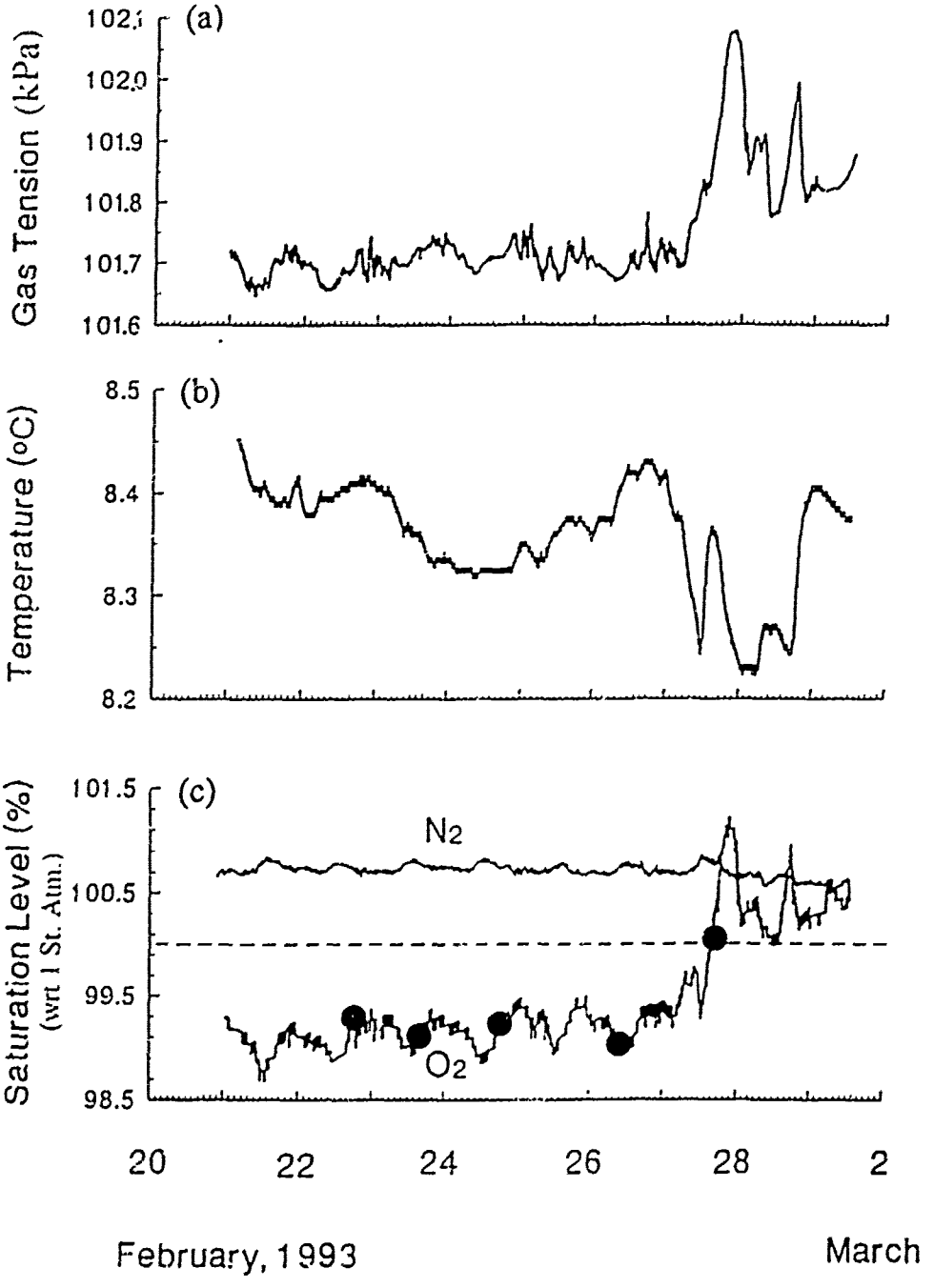

Figure 7.5 : Dissolved gas measurements, showing: (*a*) gas tension at 40 m depth; (*b*) water temperature as measured by the gas tension device in (*a*); (*c*) dissolved oxygen saturation level at 30 m, and the inferred dissolved nitrogen saturation level calculated using the oxygen at 30 m depth and the gas tension at 40 m depth. Saturation levels are expressed with respect to one standard atmosphere of moist air. Dissolved oxygen measurements from Winkler titrated bottle samples taken at 30 m depth (•) were used to calibrate the dissolved oxygen time series. Estimated accuracy of the Winklers is 0 8 % in units of saturation level.

percentage of saturation with respect to one standard atmosphere of moist air. The inferred nitrogen saturation level (Fig. 7.5*c*), calculated by the method discussed in Section 3.3.1., is also shown for comparison with the dissolved oxygen measurements. A mean mixed layer temperature and salinity of 8.35±0.1 °C and 32.37±0.02 ppt respectively were used to calculate dissolved argon concentration in the nitrogen calculation.

The noise level of the gas tension measurements at the Nyquist frequency of the data is ~5 μbar, which is equivalent to a hydrostatic pressure of 0.05 mm water. As the swell was typically 2-3 m during the deployment, this noise level confirms that the instrument operates with no significant hydrostatic effects.

7.3.3. Discussion

The data set divides into two very different weather regimes. During the 7 day period from 20-26 February, the weather was clear and sunny during the day time with colder night time air (Fig. 7.3). During the last two to three days a storm occurred (Fig. 7.3). Let us firstly consider the storm event.

The storm period has been investigated in detail, with the conclusion that the oceanographic changes that occurred were a result of advective effects (see the discussions in Sections 4.1. and 7.2.1.). The sudden rise in oxygen saturation level of nearly 2 % over the course of several hours strongly indicates that advection occurred Using Equations 5.1 and 2.5, with h = 60 m, Δt = 7 hr, $\Delta c/c^*$ = 2 % we obtain K_T (Sc=600) ~ 5000 cm.hr^{-1}, or two orders of magnitude larger than we would expect from Liss & Merlivat [1986]. Simultaneous mixed layer temperature decreases of ~ 0 15 °C occurred during the same period (see Figure 7.5*b*), again implying unrealistic surface heat fluxes of Q_h ~ -1500 Wm^{-2}, too large by a factor of 10 (estimates from J. Gemmrich using meteorological data). Satellite observations of sea-surface temperature during the storm

proved inconclusive in determining fronts or eddy structures due to dense cloud coverage over the area. As we have no measurements of horizontal variability of dissolved oxygen concentration over this time period we unfortunately cannot discuss gas budgets during the storm period. The relative stability in dissolved nitrogen saturation level during the storm is consistent with known patchiness in oceanic biological processes [Parsons *et al*, 1984]. Biological patchiness will not affect the dissolved nitrogen saturation level significantly but will, however, affect the dissolved oxygen saturation level. This interpretation provides confidence in the nitrogen measurements which will be used subsequently.

Let us now consider the fair weather regime of the data set (21-26 February). The oxygen signal (Fig. 7.5*c*) is clearly dominated by a diurnal cycle. Primary production and respiration are obvious candidates for explaining these variations. The maximum oxygen signal range is approximately 1% saturation. The oxygen is slightly (2.5%) undersaturated, which is common during winter time. The inferred nitrogen signal (Fig. 7.5*c*) is remarkably stable having a much smaller range of variation, of the order of 0 25% This result is consistent with nitrogen being biologically relatively inactive compared to oxygen as discussed in Section 2.4.2.. The nitrogen is slightly oversaturated by approximately 1.6%. This is again not uncommon during winter, when bubble dissolution tends to slightly supersaturate the water in nitrogen. Net biological respiration tends to offset this effect in the oxygen signal. The slight diurnal signal in the nitrogen is an artifact of the subtraction process due to the different depths of the oxygen and GTD sensors (this point will become self evident when we consider the diurnal variations in the dissolved oxygen concentrations with depth).

Thus far, the methodology of inferring dissolved nitrogen *in situ* from gas tension and dissolved oxygen (Section 3.3.1.) has now been developed and tested. When applied to

measurements obtained both in the open ocean and a fresh water lake (Section 3.4.), it has validated, at least provisionally in view of our understanding of biochemical processes, the methodology and provided some important insight to the relative magnitudes of biological cycling of each gas and indicates the potential of the system to further study processes like biological cycles and gas exchange [Farmer *et al.*, 1993].

7.4. Observations: Diurnal Variability

7.4.1. Introduction

Primary production in the ocean is forced at various time scales primarily by meteorological and oceanographic changes (including nutrient supply) Of particular interest is the coupling of these driving forces, and the subsequent feedback on primary productivity. It is commonly accepted that the depth of the mean seasonal thermocline increases during colder winter months and shallows during warmer summer months, aiding the development of spring phytoplankton blooms; additionally, depending on the location, zooplankton grazing effects also may play a significant role in the development of a spring phytoplankton bloom [Miller *et al.*, 1991; Frost, 1991]. Perhaps not fully appreciated however, is the often significant diurnal variability that can exist in oceanographic forcing of production. The depth of active mixing associated with nocturnal convection and day time solar heating, particularly during winter months, can deepen from the near surface to the base of the seasonal thermocline in a matter of hours [Shay & Gregg, 1986; Price & Weller, 1986; Lombardo & Gregg, 1989; Brainerd & Gregg, 1993]. Such rapid changes in the depth of active mixing above the seasonal thermocline and the vertical motions of

convecting water parcels within this layer have important implications for biological cycles and primary production.

Other investigators have studied the influence of diurnal convective mixing on, for example, timing of the spring phytoplankton bloom [*e.g.*, Wood & Onken, 1982; Taylor & Stephens, 1993; Townsend *et al.*, 1994]. Patterson [1991] modelled the effect of Langmuir circulation on the photosynthetic response of phytoplankton. However, simultaneous physical and biological measurements have been lacking The present study makes use of a comprehensive data set including observations of the key oceanographic and meteorological variables influencing production, simultaneously with measurements of dissolved oxygen and nitrogen. These data provide insight into the interaction between physical and biological oceanographic processes, from which emerge implications for the interpretation of *in situ* biological measurements at sea.

Measurements of primary productivity in the ocean are classified generally into either *in situ* or *in vitro* [Section 2.4.1.] (Note: some *in vitro* incubations are performed *in situ* however!). Isolation of the water mass during *in vitro* experiments introduces containment effects which may interfere with the measurement. Comparative studies have been performed to assess the importance of these effects [*e.g.*, Fahnenstiel & Carrick, 1988, Oudot, 1989] with the general conclusion that they can differ from each other by a factor of two or more. In addition to explanations offered by these authors, we suggest that there are other oceanographic processes like nocturnal convection that can lead to the observed disparity. Robertson *et al.* [1993] estimated *in situ* production from measurements of O_2 and pCO_2 from surface water obtained from a ship intake pump. However, an arbitrary definition of mixed layer depth (>20 m°C from the surface) was imposed when interpreting CTD observations. As will be evident from these observations, caution must be used when interpreting CTD observations to assess mixing layer depth,

particularly when the water column is close to being neutrally stable, as is often true during periods of strong diurnal convection.

We will now investigate in more detail diurnal variability in the data during the fair-weather period (21-26 February).

7.4.2. Oceanography

The physical oceanography during this period is dominated by a daily cycle of solar heating of a near surface layer during the day time and subsequent erosion of this layer during the evening by penetrative convection when the ocean surface cooled rapidly The consequences of this daily cycle are indicated in a sequence of temperature profiles (Fig 7.6) from a CTD for a representative day (24 February). There is considerable scatter in the data. This is due in part to the different locations of the casts and the changing meteorological conditions, however the daily convective signature is apparent. Thermistor chain data (Fig. 7.7) typically show the same signature though starting at 10 m depth.

The daily convective cycle is revealed most clearly by unique measurements made with Lagrangian mixed layer floats (Section 4.4.3.) as shown in Figure 7.8. The floats typically were deployed around noon time and recovered the following afternoon. The trajectories show trapping of the floats in the warm near surface during the day time, with the exception of the afternoon of 24 February, when one float penetrates to 30 m depth; this trajectory will be discussed subsequently. During the evening, convective plumes are observed to penetrate to the depth of the seasonal thermocline; this depth varies by internal wave motions by approximately 10 m throughout this period (Fig. 7.4*b*).

These observations are consistent with those of Brainerd & Gregg [1993] who observed increased levels of the rate of viscous dissipation of turbulent kinetic energy, ε, throughout the seasonal mixed layer during the evening and decaying levels of ε in water

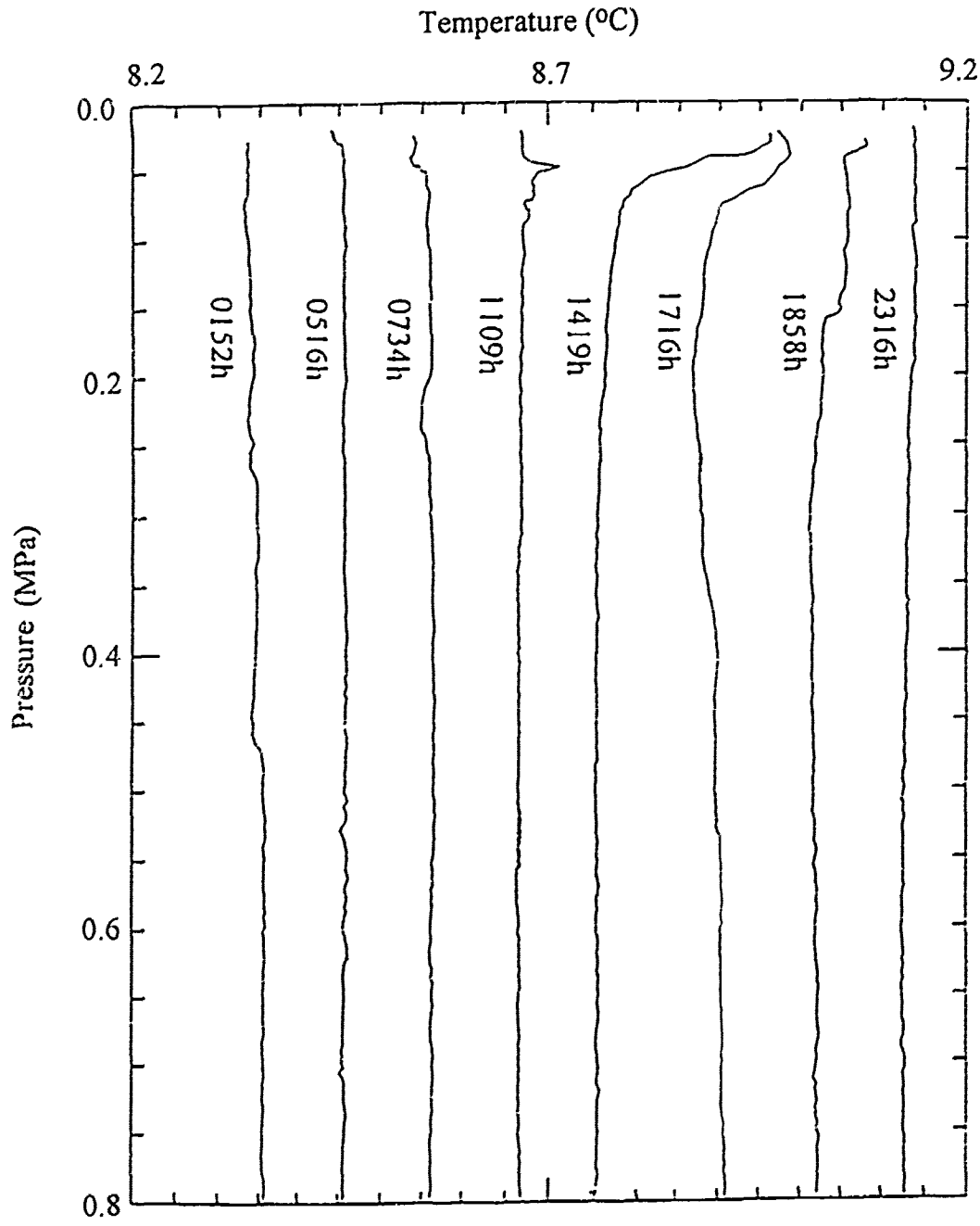

Figure 7.6 . A series of temperature profiles measured on 24 February, 1993 with a Sea-Bird Electronics CTD (temperature offset between each cast is 0.1 °C).

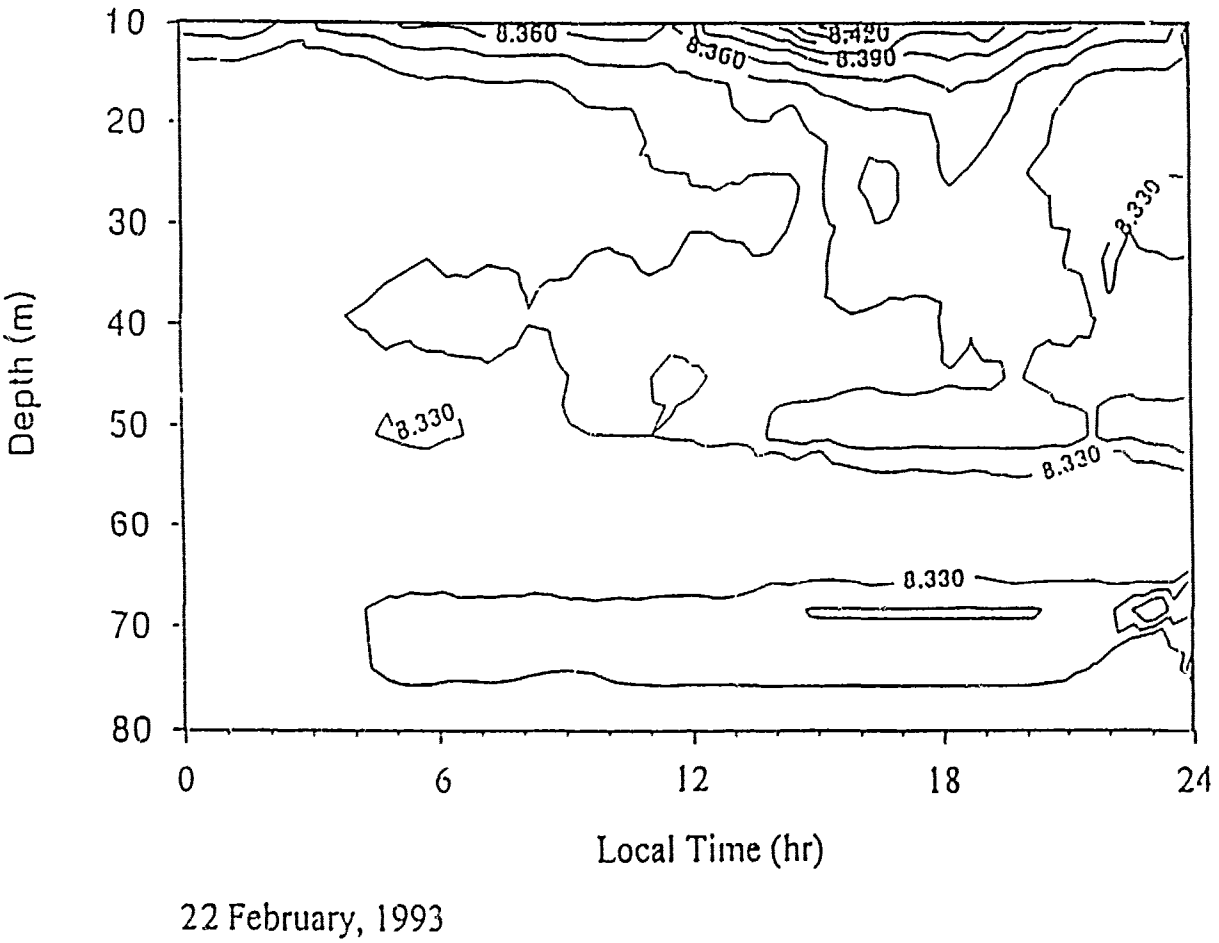

Figure 7.7 : A contour plot of thermistor chain temperature data (°C) on 22 February, 1993, showing the isolation of a thermally stratified near surface layer, which is mixed down in the early evening by penetrative convection.

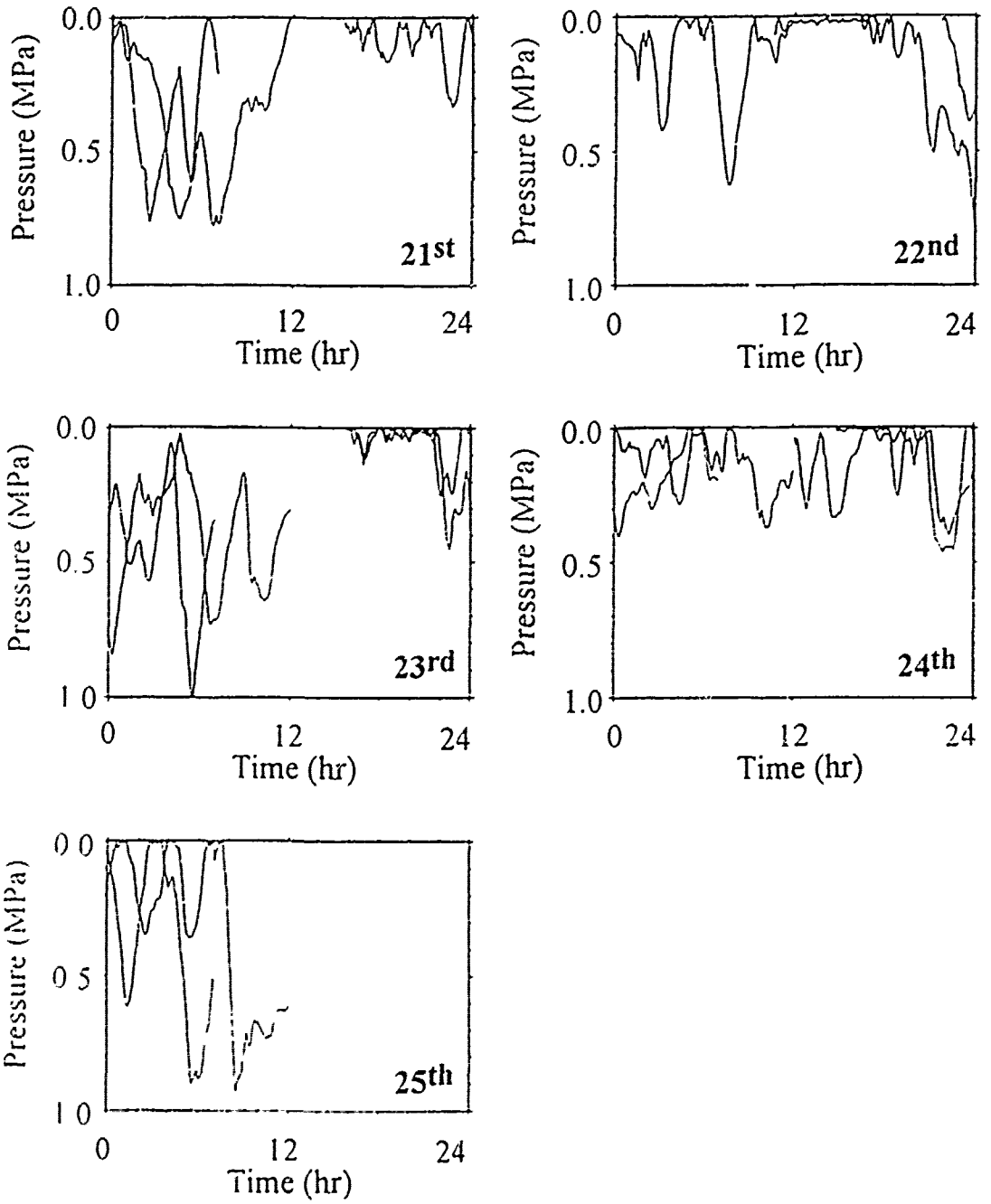

Figure 7.8 . Individual trajectories of hydrostatic pressure *versus* time recorded by the near neutrally buoyant floats for the days 21-25 February, 1993.

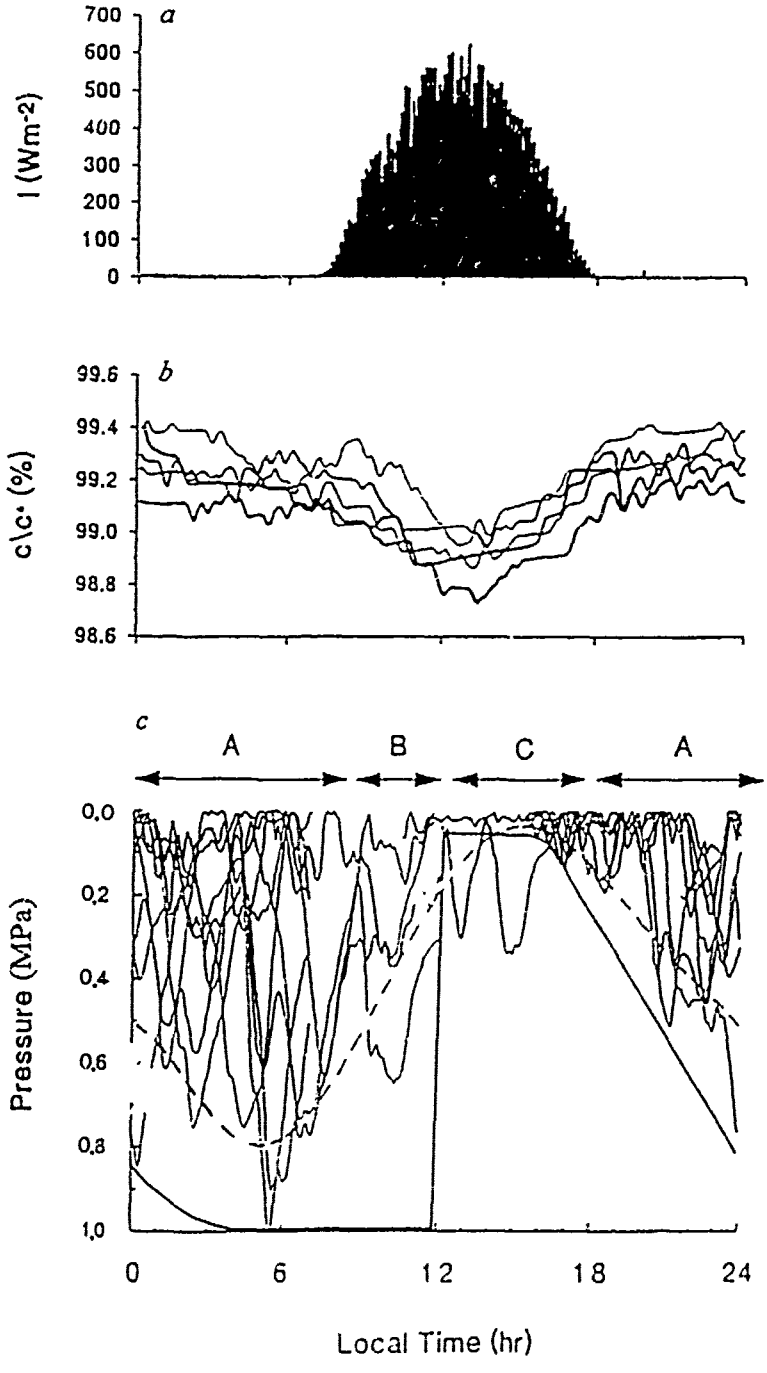

Figure 7.9 . A composite plot of daily observations between 21-25 February, 1993 of. (*a*) solar radiation intensity, (*b*) smoothed dissolved oxygen saturation level at 30 m depth, using a five point locally weighted filter, (*c*) neutrally buoyant mixed layer float observations (courtesy of E. D'Asaro and J. Dairiki, U. Washington, Seattle) Dominant oceanographic changes occurring during the labelled time periods are (A) penetrative convection towards the base of the seasonal thermocline, (B) inhibition of the mixing depth, subsequent restratification processes and residual convective motions, (C) isolation of a near surface layer by solar heating with decaying residual motions below The line fits in (*c*) are discussed in the text.

trapped beneath a shallow thermally stratified near surface layer during the day. The decay in ε below the near surface layer was observed to occur over a few hours The energy supply was attributed to residual motions of the convective plumes formed the previous evening. Unfortunately, our float data do not show this effect as clearly as the penetrative convection process. This is because the floats were released to the surface each day around noon; the time when this process is expected to occur. The exception is the float trajectory on 25 February between 0800 h and 1200 h, which does seem to indicate a rapid dampening in the plume energy around this time. It is possible that the float trajectory during the afternoon of day 24 February, previously discussed as being atypical in the context of the data set, resulted from the float becoming entrained into such residual motions.

Further insight into the statistical nature of the data set during the period 21-26 February is obtained by considering composite plots of the data. Shown in Figure 7 9*c* are composite plots of the float trajectories *versus* time; also shown are composite plots of solar radiation intensity (Fig. 7.9*a*) and dissolved oxygen saturation level at 30 m depth (Fig. 7.9*b*). Clearly, during this period, daily cycles in dissolved oxygen concentration are apparent also. Marked on Figure 7.9*c* are two lines. The solid line is a 'best guess' interpretation of the depth of active mixing above the seasonal thermocline for these data in the context of the slab layer model developed in Chapter 5. It encompasses the essential features of the physical processes discussed previously whilst being constrained by the float observations and those of Brainerd & Gregg [1993]. The dashed line marked on Figure 7.9*c* will be used to test the sensitivity of model results to the choice of line fit

7.4.3. Dissolved Oxygen

Figure 7.10 shows time series measurements of the raw and 1 hr filtered dissolved oxygen concentration at 21 m and 30 m depth during the fair-weather period of the experiment. The oxygen minimum at both depths occurs around noon and the oxygen maximum just before midnight. Oudot [1989] and Robertson *et al.* [1993] similarly observed an oxygen maximum late in the evening, but did not comment on its timing. We believe that the timing of the oxygen maximum and minimum observed in our data is a consequence of the interaction between mixing, photosynthetic activity and respiration as discussed subsequently. The fact that dissolved oxygen is undersaturated and dissolved nitrogen slightly oversaturated, indicates that net respiration of dissolved oxygen has occurred, presumably over the winter months. This is not atypical of open ocean water columns in late winter (Emerson [1987] reports a 0.5-3.0 % undersaturation of dissolved oxygen at Station Papa during the years 1969-1978). We have here no other supporting biological measurements to determine whether we observed an initial spring bloom, however a small net mixed layer dissolved oxygen concentration increase of ~0.025 $ml.l^{-1}$ was observed during this 5 day time period. Increases of oxygen saturation level due to increased mixed layer oxygen concentration are compensated by a mixed layer temperature decrease, thus maintaining a nearly constant oxygen saturation level (Fig. 7.5*c*). Horizontal gradients of oxygen were not measured, hence advective fluxes over the five day period are unknown, therefore the rise in oxygen concentration cannot be unambiguously attributed to net oxygen production alone. Figure 7.10*b* shows that oxygen changes at 30 m consistently lag the 21 m record by 1-2 hours. The amplitude of the diurnal variation at 21 m consistently exceeds that at 30 m. The phase lags are *not* a consequence of timing errors between the two instruments. This was verified by comparing water temperature records from the thermistor chains at the sensor depths and the water temperature recorded by the

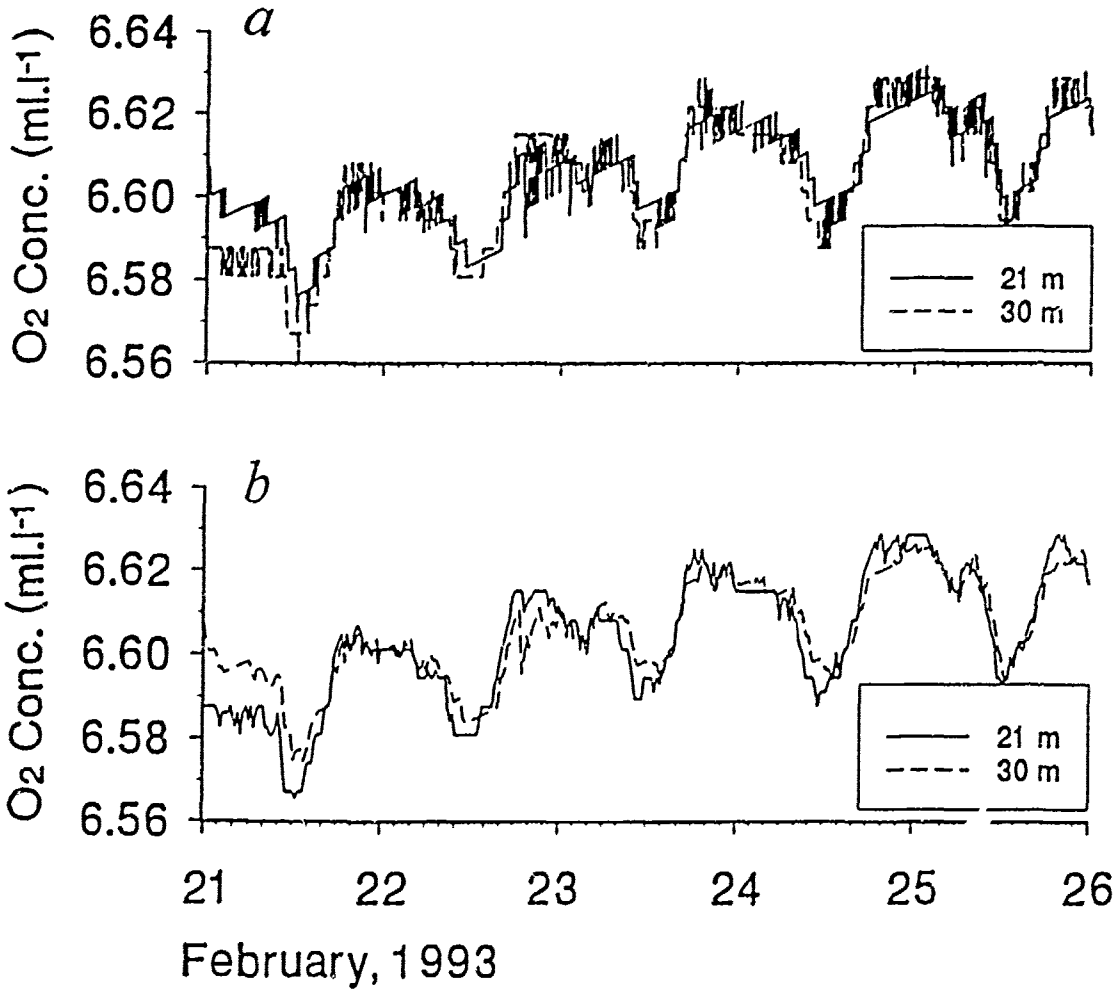

Figure 7.10 . Calibration corrected dissolved oxygen time series at 21 m and 30 m depth, showing: (*a*) the raw data; (*b*) the data filtered by a 1 hr average.

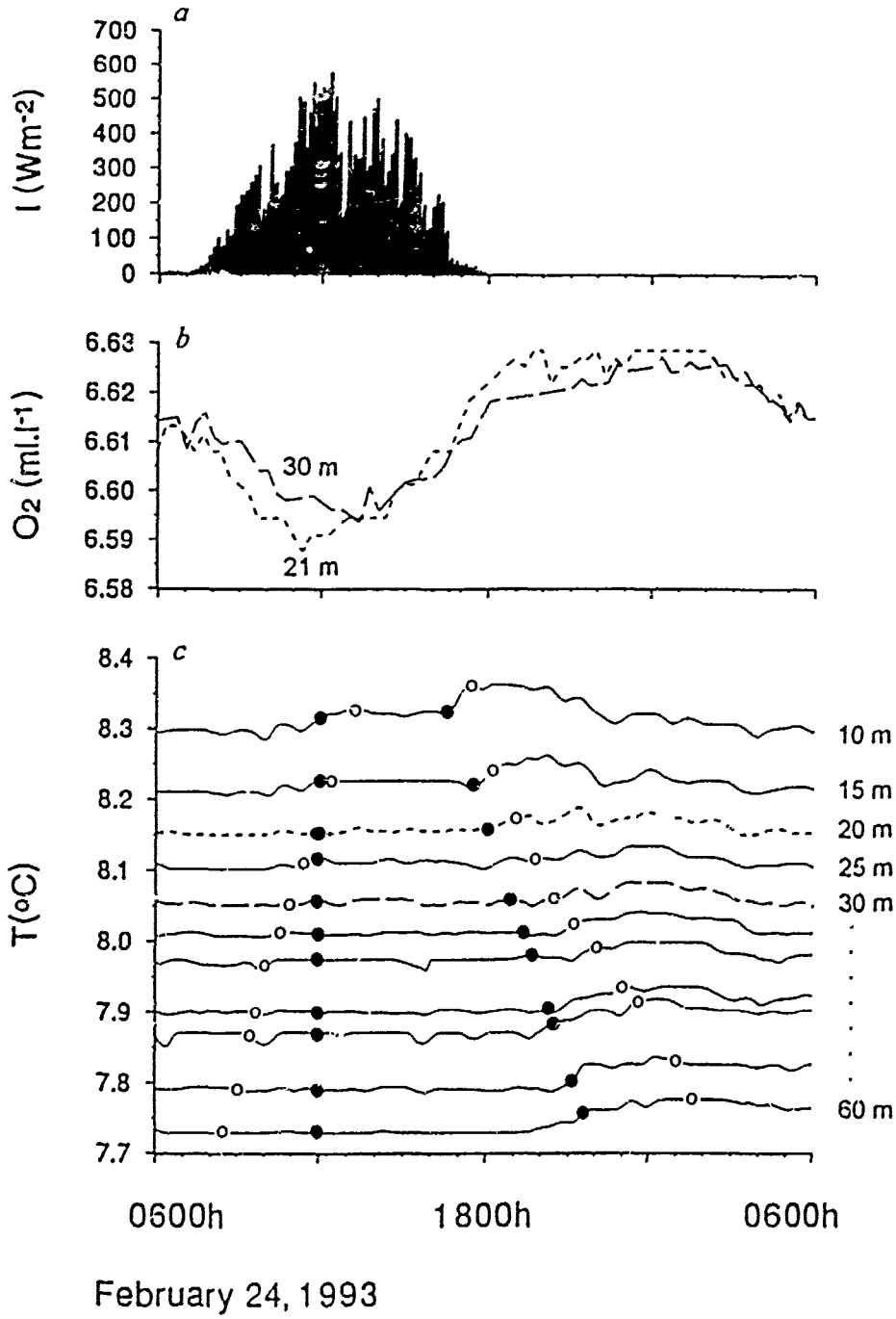

Figure 7.11 . Measurements made from sunrise on the 24 February to sunrise on the 25 February of. (*a*) solar radiation intensity recorded by a ship mounted weather station, (*b*) dissolved oxygen at 21 m (-----), 30 m (– – –), (*c*) water temperature recorded by the thermistor chain from 10 m to 60 m depth. Thermistors were separated by 5 m depth, and are shown with temperature offsets between adjacent thermistors of -0 05 °C The 20 m and 30 m records are highlighted in accordance with (*b*) above. The slight warming at depths > 40 m during the evening may be advective. The line fits to the float observations (Fig. 7.9*c*) are indicated for comparison: • - solid line, o - dashed line

dissolved oxygen sensors (being autonomous instruments), and by cross-checking with the deployment and recovery timing.

Figure 7.11 shows the effect of convection and restratification on the dissolved oxygen and temperature field. We will return to this figure when comparing model results with the observations.

7.4.4. Discussion

The uniqueness of the float measurements, as discussed in Section 4.4.3., perhaps are appreciated best by considering them as indicators of the depth of active mixing by convective plumes under their own negative buoyancy. This depth of mixing is very difficult to establish from more conventional measurements, such as CTD profiles and thermistor chain data, as indicated in Figures 7.6 and 7.7. The signature is of course apparent, however a rather large degree of subjectivity is required during interpretation. Commonly, an arbitrary criterion is imposed when defining the depth of active mixing from CTD data. Robertson *et al.* [1993] defined it as the depth at which the water temperature differed from the sea surface temperature by 20 m°C. As will be evident from our observations, caution must be used when interpreting CTD observations in this manner. This is particularly true when the water column is near neutral stability, as is the case for diurnally convecting water columns, where vertical gradients in density throughout the seasonal mixed layer are small. We observed warming of the near surface water by ~0.2 °C over 4 m depth during the day (see Fig. 7.6). Even in the absence of heat loss, the even distribution of this heat input over a 100 m mixed layer will increase the water temperature by only 8 m°C. This is a small signal for most CTD instruments and is undetectable by our thermistor chains having a resolution of 10 m°C. The interpretation of neutrally buoyant float data or dissipation profiles [*e.g.*, Brainerd & Gregg, 1993] can

provide a better indication of mixing layer depth, which is an essential measurement for these kind of budget studies.

7.5. Modelling the Diurnal Oxygen Variability

During the fair-weather period of these data, it will be shown that the dominant processes affecting diurnal variability in dissolved oxygen concentration within the seasonal mixed layer are biological production, respiration and redistribution associated with changes in mixing layer depth due to day time solar heating and nocturnal convection (this is in contrast to Chapter 6, where the dominant processes affecting dissolved gas concentrations were gas exchange across the air-sea interface, and entrainment associated with wind driven mixed layer deepening). We will use the modelling framework developed in Chapter 5 to investigate the interaction between these physical and biological processes.

7.5.1. Motivation

Our modelling efforts are motivated primarily by the observation of a periodic dissolved oxygen signal at 21 m and 30 m depth with a maximum late in the evening From our knowledge of primary production and respiration in the ocean, Section 2 4 1 , it may be expected that the dissolved oxygen would be maximum when the solar radiation is maximum near noon, or at least close to this time of the day as respiration occurs also, drawing down the oxygen content of the water. This feature of our observations provokes a more thorough investigation.

7.5.2. Model Development

After considering the supporting data, a simple one-dimensional, non-diffusive, mixed layer model coupled with net community production (*i.e.*, production minus respiration) was chosen. Since our goal is not to simulate the full complexity of the natural phenomenon, but rather to identify certain key features of the interactions, we have made use of the simplest possible representations of biological processes affecting dissolved oxygen concentration. It is considered that the solid line added to Figure 7.9*c* will indicate correctly the penetration depth of the larger scale convecting plumes, but will not be influenced significantly by mixing scales of the order of, or smaller than, the instrument dimensions (~1 m). We will use this depth in the model to indicate the depth of active mixing. It is a limitation of our model that we use a two-layer representation of a mixing process that is observed to have a diffuse property gradient at its lower boundary The simplicity of the model assumptions introduce certain limitations to the model. These limitations will be indicated and discussed further when comparing the model results with the data.

We shall suppose that the short wavelength component of the local solar radiation light intensity, $\Theta(t,z)$, is attenuated exponentially with depth according to Beer's law:

$$\Theta(t,z) = I(t)e^{-kz} \tag{7.1}$$

where k is the vertical diffuse attenuation coefficient. Here $I(t)$ is the time dependence of the solar radiation intensity at the water surface, which we approximate in accordance with Ikusima [1967] by:

$$I(t) = \begin{cases} 0 & \text{for } 0 \le \omega t < \theta \\ I_o \sin^n(\omega t - \theta) & \text{for } \theta \le \omega t \le \pi \end{cases} \tag{7.2}$$

where n and θ are chosen to match the observations (this approximation is better for large n and small θ, as observed).

We choose to make production, $P(t,z)$ in Equation 5.1, proportional to the local solar light intensity[1], or:

$$P(t,z) = \delta k \Theta(t,z) \tag{7.3}$$

where δ is the production efficiency, having dimensions mol $O_2.J^{-1}$. As δ is defined to be constant, this introduces the assumption that the phytoplankton concentration and nutrient concentration is independent of depth and time. Phytoplankton reproduction, mortality and grazing will allow some depth dependent phytoplankton stratification to build up during the day. However, vertical mixing each night will tend to reduce the importance of this effect. Both photo-inhibition and hysteresis in photosynthetic response are neglected for simplicity, although photoinhibition is most certainly a dominant process affecting the total oxygen production in the isolated surface layer (say <10 m depth). The Lagrangian measurements could in principle be used to study the effect of hysteresis, however, we are not attempting to model the dissolved oxygen concentration quantitatively at this stage The production rate of oxygen per unit volume, daily averaged and vertically integrated over the maximum mixed layer depth, P_{avg}, is found to be:

$$\begin{aligned} P_{avg} &= \frac{\omega}{h_{\max}\pi}\int_{z=0}^{h_{\max}}\int_{t=0}^{\pi/\omega} P(z,t)\,dt\,dz \\ &= \frac{I_o \delta \Gamma_n}{h_{\max}}\left(1 - e^{-kh_{\max}}\right) \end{aligned} \tag{7.4}$$

---

[1] The vertical length scale associated with the production at a depth z has to be k^{-1} due to the non-linearity of the attenuation with depth.

where $\Gamma_n = \frac{1}{\pi} \int_{\tau=0}^{\pi} \sin^n \tau \, d\tau$.

We have chosen to simplify respiration, R, in Equation 5.1 by expressing it as a depth and time independent fraction, F, of the average production of oxygen in the water column, or:

$$R = F P_{avg} \tag{7.5}$$

This simple representation of respiration does not include the processes described in Section 2.4.1., however, to first order it is a reasonable description.

7.5.3. Model Inputs

A composite plot of the observed surface solar radiation intensity for the period of interest is shown in Figure 7.9*a*. These data are used directly in the model with n = 9 (see Equation 7.2) and hence Γ_9 = 0.0825 [Abramowitz & Stegun, 1970]. Fluorometer measurements taken at the experiment site (C. Wirick, Brookhaven National Laboratory, personal communication) indicate a vertical diffuse attenuation coefficient for photosynthetically active radiation of $k \approx 0.1$ m^{-1}. For these parameters most of the oxygen production is confined to a relatively thin (~10 m) surface layer.

The surface gas flux, Q in Equation 5.1, is set to zero. This is justified as follows. Consider the terms in Equation 5.1 for the period 20-27 March. For an average wind speed of 6 ms^{-1}, the transfer velocity is K_T(Sc=600) = 8 cm.hr^{-1}, using Liss and Merlivat [1986]. Using the observed variation of oxygen, 0.6 % daily at a mean 1 % undersaturation, and an average mixed layer depth of 80 m, no entrainment terms or advection terms, Sc(oxygen) = 818, we find that the total of the Q terms (*i.e.*, surface + bubble) is at least five times less than the observed daily rate of change of dissolved

oxygen. This implies that during this period the oxygen signal is dominated on a daily basis by biological processes. This can also be seen from the time series of inferred dissolved gaseous nitrogen (Fig. 7.5*d*). On time scales of a day, elemental di-nitrogen is essentially biologically inert. Therefore, the dissolved nitrogen concentration can only change by entrainment across the seasonal thermocline, advection and surface gas exchange. The CTD and thermistor chain data show little evidence of advection or entrainment during this fair-weather period. Under this low wind speed regime, bubble mediated gas transfer is expected to be minimal. For thin film gas transfer, fluxes of oxygen and nitrogen are expected to be comparable in magnitude to within 20 % (estimated using a $Sc^{-2/3}$ ratio to compare K_T for both gases, implying a deviation of ~10 %, and the observed saturation level ratio between the gases of ~10 %). As the oxygen saturation level variations are more than five times those of the nitrogen, we conclude that the constant dissolved nitrogen concentration implies that surface gas transfer is a small effect, and of secondary importance in interpreting the oxygen time series.

As discussed previously, the solid line added to Figure 7.9*c* will be used as the mixed layer depth in the model and the dashed line will be used to test the sensitivity of the model results to the choice of line fit to the float data. We set $F = 1$ in Equation 7.5. This is seen from Figure 7.5*c* where respiration approximately balances production over a day (this is true to within ~13 %, given that we have no measurements of horizontal fluxes). Setting $F = 1$ also allows a check of the model results with the analytical solution for the average oxygen production given by Equation 7.4.

7.5.4. Model Results

Appropriate scales used for non-dimensionalisation of the model results are: h_{max} - the maximum depth of the line fit to the float data (Fig. 7.9*c*), which for the solid line equals

100 m and for the dashed line equals 80 m; c^* - the mean mixed layer equilibrium dissolved oxygen concentration in $molO_2.m^{-3}$; T - time scale in days.

Figure 7.12*a* compares the model mixed layer depth, chosen to be the solid line fit to the float data in Figure 7.9*c*, with the model results. Figure 7.12*b* shows the modelled solar radiation intensity as a function of depth, which is the solution of Equation 7 1, and Figure 7.12*c* shows the water column dissolved oxygen saturation levels derived from the model. The model has been initialised with the vertical dissolved oxygen structure set from the previous day. Figure 7.13 is similar to Figure 7.12 except the model mixed layer depth is chosen to be the dashed line fit to the float data in Figure 7.9*c*.

Both model runs predict a phase lag between the maximum in the near surface dissolved oxygen (approximately 1600h) and the local solar radiation maximum near noon Although we have no reliable time series of near surface dissolved oxygen measurements, this same signature was observed in the thermistor chain record (Fig. 7.7) where the isolated surface layer temperature has a maximum at 10 m depth at 1600h. This is a consequence of the heat content of the water being a time integral of the solar radiation absorbed during the day. As the short wavelength solar radiation drives oxygen production (see Figure 2.2), it is clear that this effect will be apparent in the modelled dissolved oxygen concentration. Local respiration exceeds production below the oxygen compensation depth, which varies throughout the day. In the model, vertical gradients of dissolved oxygen concentration develop throughout the day in the stratified waters below the mixed layer. The modelled dissolved oxygen profile depends on the choice of mixed layer depth, as seen by comparing Figures 7.12*c* and 7.13*c*.

At the onset of convection, the warmer and more oxygenated surface water is cooled by surface heat loss and mixed with the less oxygenated deeper water. With increasing sensor depth the oxygen maximum will occur at a later time as seen in the model results

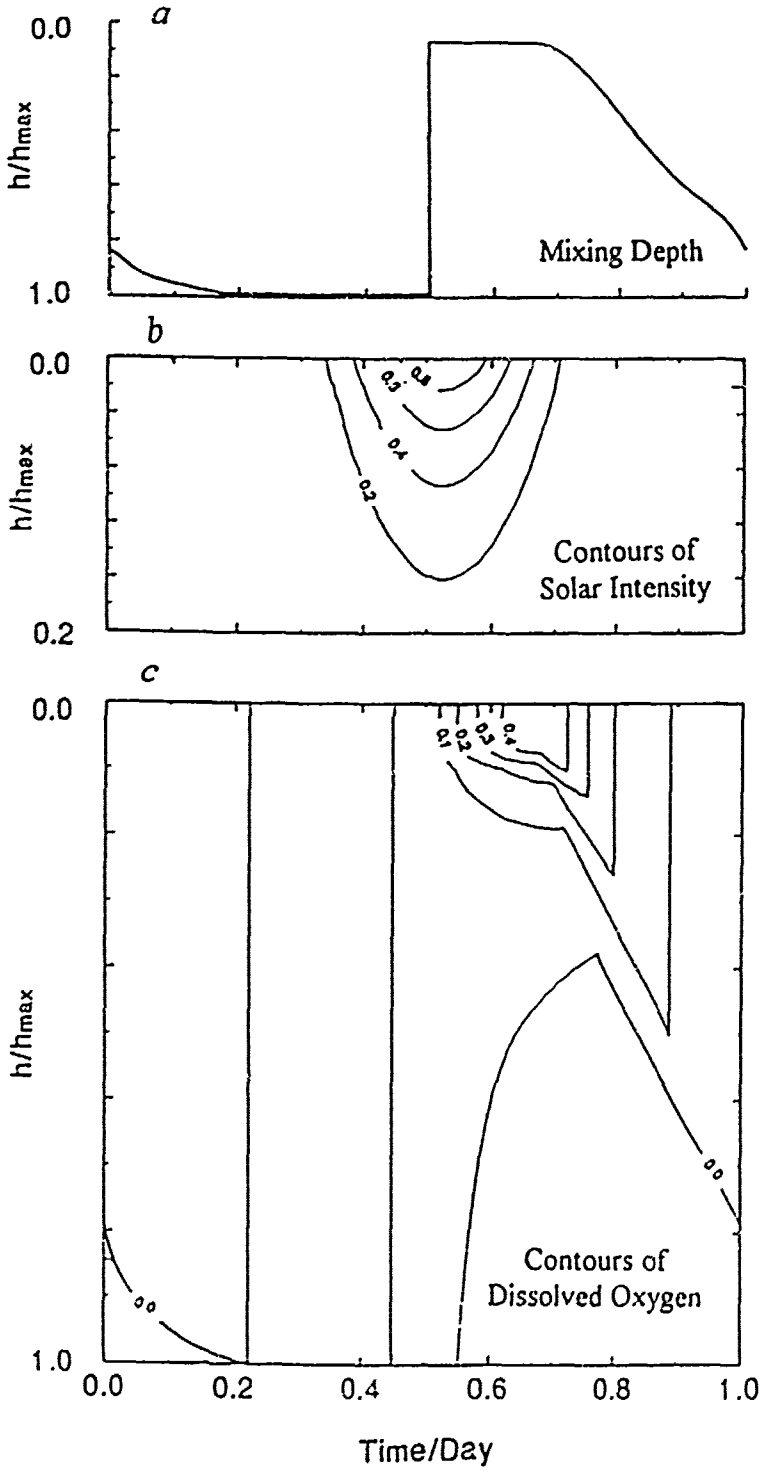

Figure 7.12 . Model inputs and results, showing: (*a*) normalised model mixed layer depth using the solid line fit to the neutrally buoyant float data shown in Figure 7 9*c* with h_{max} = 100 m, (*b*) contour plot of normalised modelled solar radiation intensity with time and depth (note the scale change on the depth axis); (*c*) contour plot of modelled dissolved oxygen percent saturation level for F=1 in Equation 7.5.

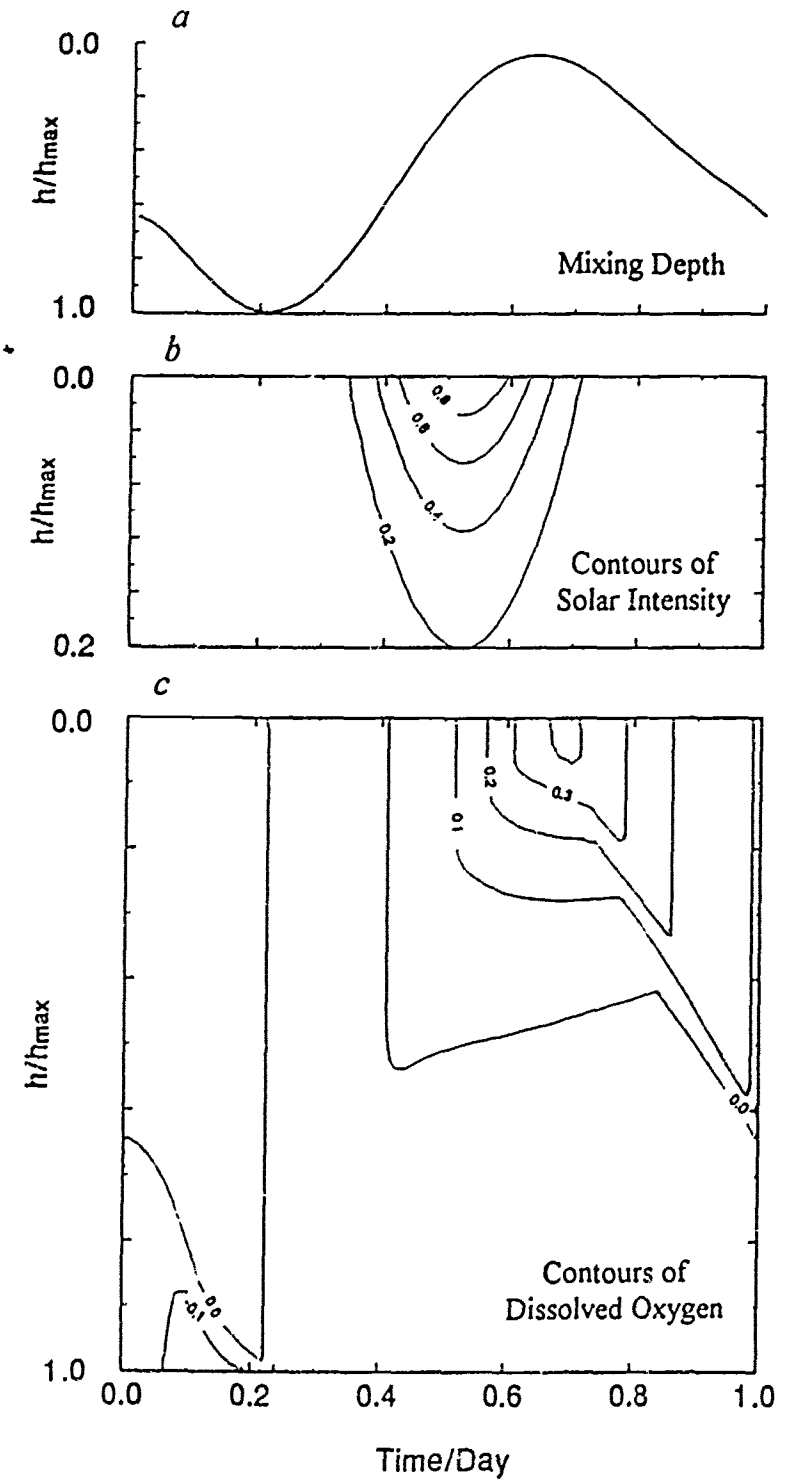

Figure 7.13 . Model inputs and results, showing: (*a*) normalised model mixed layer depth using the dashed line fit to the neutrally buoyant float data shown in Figure 7 9*c* with h_{max} = 80 m, (*b*) contour plot of normalised modelled solar radiation intensity with time and depth (note the scale change on the depth axis); (*c*) contour plot of modelled dissolved oxygen percent saturation level for F=1 in Equation 7.5.

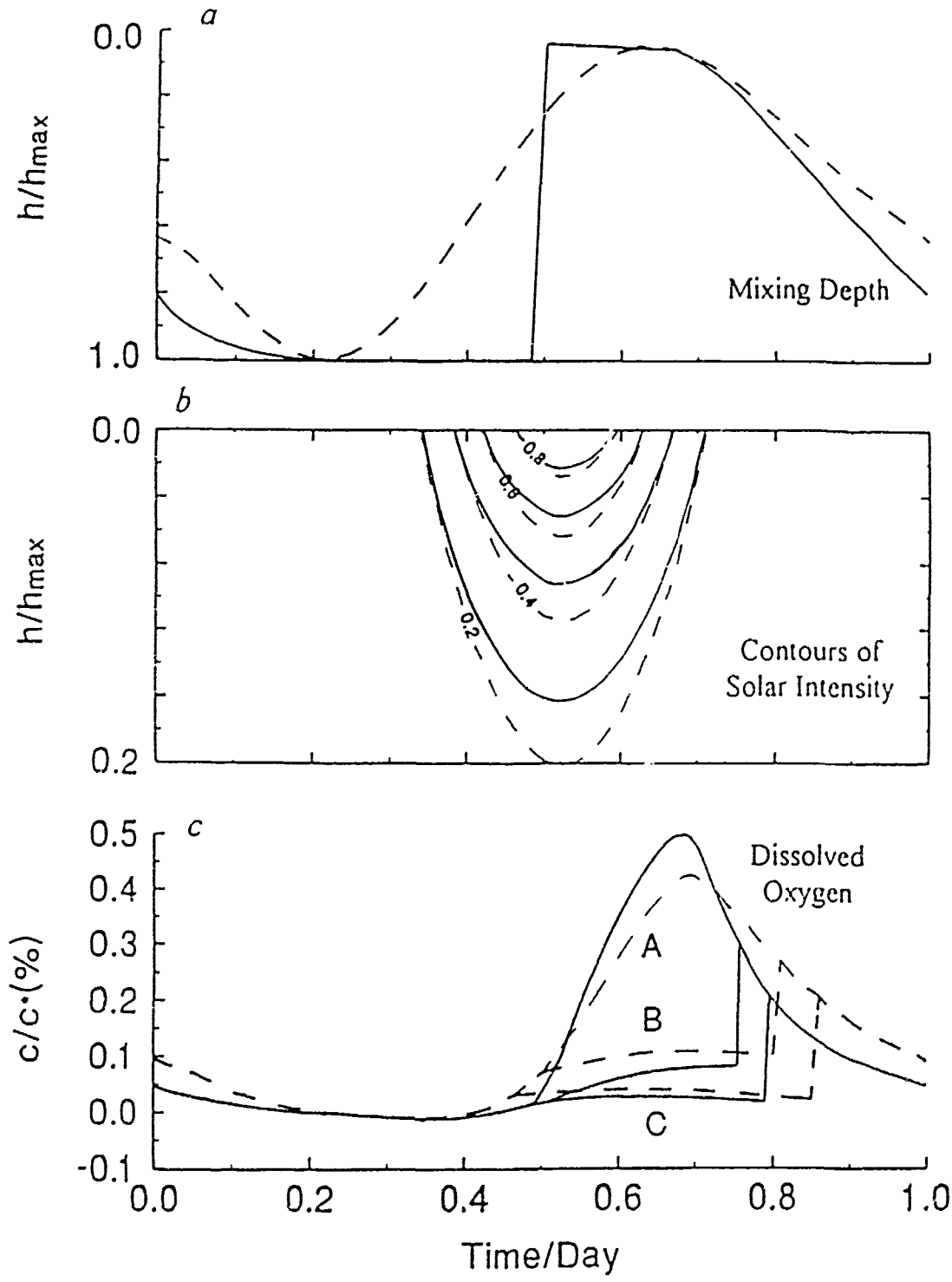

Figure 7.14 : Model inputs and results. The line type (solid and dashed) corresponds with the choice of line fit to the neutrally buoyant float data (Fig 7.9*c*) which is used in the model as mixed layer depth. Figures (*a*) and (*b*) are the same as those in Figures 7.12 and 7.13. The model results at three depths are shown in (*c*). A = surface, B = 20 m, C = 31 m.

(Figures 7.12*c* and 7.13*c*) and the data (Fig. 7.10). Thermistor chain data show this same effect for water temperature (Fig. 7.7)

Figures 7.14*a,b* are the same as those in Figures 7.12 and 7.13; the line type on these figures (solid and dashed) corresponds with the choice of line fit to the neutrally buoyant float data (Fig. 7.9*c*) which is used in the model as mixed layer depth. Figure 7.14*c* shows time series of the model results at the near surface and the two depths at which dissolved oxygen was measured. At a depth of 30 m, both model runs predict an oxygen maximum between 1900h and 2000h, in good agreement with the observations (Fig. 7.10*b*). Both model runs also predict a larger diurnal oxygen range for the deeper sensor than the shallower sensor and a time lag of one to two hours between the sensors reaching an oxygen maximum; these predictions are in accordance with the observations (Fig. 7.10*b*)

7.6. Comparison between Model Results and Observations

The model reproduces certain key features of the observations, particularly during periods of strong convection, and makes some predictions of the dissolved oxygen concentration in the rest of the water column throughout the day. Specifically, the model explains the diurnal oxygen variability as a consequence of the balance between surface production, convective mixing and respiration. The convective mixing is crucial to the redistribution of a thin surface production layer and explains the observed time delay in the oxygen maximum measured at progressively greater depths.

The simplifying assumptions used in the model development limit the extent to which quantitative predictions can be made. The most noticeable discrepancies between the model results and the data are the predicted instantaneous oxygen maximum at the depth

of the oxygen sensors during the evening (Figure 7.14*c*, lines B and C) coincident with the passage of the mixed layer past the sensor, and the timing of the oxygen minimum in the morning at the sensor depth which is several hours earlier than the observations These discrepancies can be explained by considering the effects, not included in the model, of smaller scale time and depth varying vertical mixing processes. Also, during the evening when the convective layer deepens beyond the measurement depth, the entraining dissolved oxygen concentration that has built up during the day will chiefly govern the oxygen time series recorded by a sensor. Oxygen stratification in the water column is determined primarily by biological processes, particularly respiration, and, as the model results show (Fig. 7.12 and 7.13), the depth of active mixing. An inadequate description of these effects will be apparent in model and data comparisons.

The larger scale convective motions, which result from surface cooling, store kinetic energy that continues to be available for further mixing several hours after the buoyancy flux changes sign [Brainerd & Gregg, 1993]. This can result in residual mixing below the shallow surface layer and above the seasonal thermocline. As convection proceeds in the evening, energy is fed back into the larger scale motions, providing more energy for mixing and redistribution of the shallow surface layer temperature and dissolved oxygen anomaly. Thus a time and depth dependent vertical mixing would be expected, with decreasing vertical gradients in temperature and dissolved oxygen as convection homogenises the water column. The turnover time scale for the larger convective motions is observed from the float observations to be approximately two to four hours Thus, we do not expect, at least initially, complete vertical homogenisation of the water column particularly in the presence of penetrative convection. We shall now discuss what effects these processes would have in modifying the model results if they were included in a more comprehensive model, firstly for the restratification period then for the deepening period

During the restratification period, at any depth the dissolved oxygen concentration represents a consequence of the competing effects of both oxygen sources and sinks, the minimum occurring when they are equal in magnitude. The oxygen sources include local production, which is concentrated near the surface, and turbulent mixing down from the near surface layer to the sensor depth. This vertical mixing is inhibited as the near surface warms. The oxygen sinks include local respiration and the mixing of the oxygen deficit resulting from respiration elsewhere in the water column. Our observations (Fig. 7.11*b*) show an oxygen minimum at 21 m occurring before the minimum at 30 m. This implies that the oxygen sources at 21 m at 1100h exceed the oxygen sinks, whereas this balance does not occur at 30 m until about 1300h. The timing of the minimum is not accurately predictable in our model, because the model does not include time and depth dependent variations in the turbulent processes within the mixing layer.

During the evening a similar process occurs in reverse, except the surface buoyancy flux which previously restratified the surface water now has changed sign resulting in convective instability due to cooling. The dissolved oxygen concentration at any given depth now is determined by respiration, vertical mixing from above and entrainment from below. Again, the intensity of mixing is neither uniform over the mixing layer nor time invariant, and vertical gradients will develop allowing continual supply of warmer and more oxygenated water to greater depths for an extended period. The model reproduces the progressive delay with respect to depth of the measured dissolved oxygen maximum However, since the representation is strictly two-layer, a sudden change occurs as the mixed layer advances past any given depth. The observations show a continuous increase in temperature and oxygen over several hours (Fig. 7.11) as oxygen is continually mixed down from above. As the near surface gradients diminish, respiration and entrainment dominate the oxygen balance and the concentration decreases.

The observations show a continuously increasing dissolved oxygen level at 21 m from approximately mid-day until 2400h (Fig. 7.11). This continuous increase represents a smooth transition between the two distinct regimes discussed above. By mid-day the oxygen sources at this depth are dominated by primary production, although there may be a weak and decaying residual turbulent exchange. As evening approaches, primary production ceases and convective mixing of oxygen rich water from the surface becomes the only source. The persistent, but diminishing vertical dissolved oxygen gradient, which together with the depth dependent mixing maintains the source term at intermediate depth, is not represented in the model. This explains the difference between the predicted discontinuity and the smooth transition that is observed.

7.7. Implications for In Situ Primary Production Measurements

Diurnal oxygen variations have previously been used to calculate productivity [*e.g.*, Oudot, 1989]. The clear diurnal convection signal presented here motivates an analysis of its implications for similar productivity calculations based on the diurnal oxygen cycle. If we first neglect the cycle of convective mixing and assume instead that mixing is continuous and extends to a fixed depth, productivity is estimated as $Q = h\beta\Delta s/\Delta t$. Parameters appropriate for the present study are Δs = 0.6% (Fig. 7.5*c*), h = 80 m, β = 293 mmol.m^{-3} [Weiss, 1970] leading to Q = 140 mmolO_2.m^{-2}.(½ day)$^{-1}$. These results may be translated to units of mmol.C by using an appropriate 'PQ' ratio, as discussed in Section 2.4.1. Using a PQ ratio of 1.1-1.3 (Section 2.4.) results in Q = 1.8-2.2 gC.m^{-2}.day^{-1}. We anticipate that this production rate is too large by at least a factor of 2.5-4.0, as will be discussed subsequently, placing upper bounds on our production estimate of between 0.4-

0.9 $gC.m^{-2}.day^{-1}$. Annual average total production rates of 0.5 $gC.m^{-2}.day^{-1}$ have been reported at Station Papa (50° N, 145° W) with maximum production rates in excess of 1.0 $gC.m^{-2}.day^{-1}$ [Welschmeyer *et al.*, 1993]. Primary production estimates at Station Papa are not comparable directly with these results due to our site being closer to coastal waters. In fact, this being so, primary production at Station Papa may be expected to be slightly lower (to what degree is uncertain) than our experiment location. Notwithstanding this point, and the fact that our estimate is an upper bound, the comparison between the estimates is good.

Consider now the effects of diurnal convection on an oxygen measurement made at half the maximum depth to which mixing extends. When the surface waters containing most of the photosynthetically produced oxygen at the end of the day mix to the instrument depth, the signal recorded by the instrument will show a daily oxygen peak to trough excursion that is twice that observed if the layer was thoroughly mixed all day In fact, the enhancement by convection of the diurnal oxygen variation observed at a particular depth depends primarily on the ratio of maximum mixed layer depth to instrument depth. This enhancement is 2.5-4.0 for our data. These effects may well be important in explaining the discrepancy between *in situ* and *in vitro* measurements discussed in Section 2.4.1. This simple enhancement will not be the only determining factor as production and respiration will vary with depth and time. The entrainment term in Equation 5.1 will play a major role in determining the observed oxygen time series at a particular depth. Neglect of this effect will again overestimate the daily production rate

7.8. Summary

In this chapter, we have investigated bio-physical interactions in a convecting water column using a unique set of observations and simplified models. From this study, we can conclude that interpretation of dissolved oxygen measurements at specified depths made under convectively driven conditions requires knowledge of the changing oceanographic conditions. In particular, we have seen that use of oxygen time series measurements to estimate primary production can be seriously in error if no correction is made for a changing mixing layer depth due to nocturnal convection and day time solar heating

Our conclusions, however, are not limited only to dissolved oxygen measurements, but are applicable to measurements of any biologically relevant scalar, like phytoplankton concentration [Gardner *et al.*, 1993] and organic/inorganic concentrations of photosynthetic products. The nocturnal convection and day time restratification described here provides an example of the role played by quite subtle physical processes which need to be considered in the design of chemical and biological studies of the upper ocean In these kind of studies, it may be necessary to use more sophisticated oceanographic instrumentation such as turbulence probes or, as used in this study, neutrally buoyant floats.

CHAPTER 8.

SUMMARY AND DISCUSSION

8.1. Oxygen and Nitrogen Fluxes in the Upper Ocean

We have endeavored through this research to gain insight into the processes controlling fluxes of oxygen and nitrogen into and out of the oceanic mixed layer through a programme of direct measurements and investigative modelling. As a result of this endeavour, some general lessons have been learnt. Interpretation of data from many previous experiments at higher wind speeds have not recognised fully the often significant oceanographic changes that can occur simultaneously. In particular, no publications previous to Farmer *et al.* [1993] had solved a coupled oceanographic gas exchange model (to the author's knowledge). We have learnt from our modelling efforts on the coastal experiment (Chapter 6) that the oceanographic changes can be the chief contributor to measured mixed layer dissolved gas changes. In fact, we observed the extreme example of gas invasion into the water yet a simultaneous mixed layer dissolved gas concentration decrease due to entrainment from below.

Through a combination of the literature review presented in Section 2.4. and our experimental results, it became clear that the chief difference between dissolved oxygen

and nitrogen is their response to biological processes, which only significantly affects dissolved oxygen. This basic result can be utilised to provide a rather simplified differential measurement of biological activity. Changes in saturation level anomaly between the two gases can be interpreted in terms of net biological production and can provide, subject to certain limitations, a means of separating, *via* a budget model, surface fluxes of oxygen from the oxygen budget. Alternatively, if good estimates of primary production are available from independent measurements, surface gas fluxes for both oxygen and nitrogen can be compared.

8.2. Specific Findings and Developments from this Research

Identified below are three significant contributions of this research to the oceanographic community.

8.2.1. Unique *In Situ* Dissolved Nitrogen Measurements

The most important technological development that has resulted from this thesis work is the capability of measuring dissolved nitrogen gas *in situ*. Previous to this development, dissolved nitrogen was measurable only by gas chromatography of an equilibrated water sample. The development of a sensor with an equilibration time of tens of minutes and accuracy in dissolved nitrogen concentration of 0.7 % has opened new and exciting possibilities for gas exchange measurements at sea. The long term stability of the pressure sensor (0.01 % over 3 years) used in the primary measurement of gas tension (Section 3.3.2.) yields an instrument package suitable for mooring at specified depths for extended periods. The integration of the GTD onto the Seabird Electronics CTDO (Section 3.2.)

has, we believe, concluded this part of the technological developments, providing a robust and reliable system that is easy to use.

8.2.2. Gas Transfer Velocities During A Storm Using Gas Tension Measurements

Measurements of dissolved gas concentrations, meteorological conditions and oceanographic variations made during a storm in a coastal environment (Chapter 6) indicate that bubble mediated gas transfer associated with bubble dissolution in Langmuir cells is an important process in controlling gas transfer of weakly soluble gases such as oxygen and nitrogen into the ocean. A significant enhancement of previously published gas exchange coefficients was found, the enhancement being up to a factor of four The enhancement was found to be correlated with bubble cloud penetration depth. These findings indicate that local, smaller temporal and spatial scale processes, such as Langmuir circulation and wave breaking, play an important role in controlling the magnitude of oceanic fluxes of dissolved oxygen and nitrogen. At higher wind speeds (>12 ms^{-1}) these processes can become dominant and surface gas fluxes may be between 10 and 100 times those at lower wind speeds (< 7 ms^{-1}). The findings also provoke a more insightful parameterisation of gas exchange processes in terms of these controlling processes rather than the generally accepted wind speed parameterisation of Liss & Merlivat [1986] The role played by Langmuir circulation in deepening the mixed layer and eroding near surface stratification was apparent in the observations. Particularly intriguing was the observation of bubble penetration depth following (for a limited period) the mixed layer depth, indicating Langmuir circulation reached to the base of the mixed layer, limited only by deeper stratification. This may be more typical of a coastal environment, but seems to identify the fact that gas exchange can be controlled by local oceanographic changes which

occur on short temporal and spatial scales. To properly measure these changes one has to develop new instrumentation capable of measuring dissolved gases *in situ* on time scales of minutes.

8.2.3. Implications of Diurnal Convection for *In Situ* Measurements and Primary Production Estimates

Analysis of measurements obtained in the open ocean during early spring (Chapter 7) provided a detailed description of the coupling between oxygen production by solar radiation forcing and the diurnal response of the ocean mixed layer to solar heating and nocturnal cooling. The observations obtained are certainly the most comprehensive available in the literature. The data show a diurnal cycle of solar heating during the day time associated with primary production of oxygen and water column restratification. Cooling of the surface waters after sunset was associated with mixed layer deepening by convection and subsequent mixing down of warmer more oxygenated water from the near surface. This water is then diluted by less oxygenated water from below. This daily cycle results in a sub-surface dissolved oxygen maximum during the late evening and a delayed oxygen minimum near noon. The interpretation of the measurements requires a knowledge of the coupling of physical and biological oceanographic processes occurring in the water column throughout the day. It was concluded that neglect of these interactions in the interpretation of oxygen time series at specified depths would result in an overestimation of primary production from the oxygen measurements by a factor depending primarily on the ratio of the maximum mixed layer depth to the instrument depth (typically a factor of more than two).

8.3. Broader Implications of this Research

The conclusions developed from Chapter 7 are not limited to *in situ* measurements of dissolved oxygen concentration alone, but are applicable to any biologically relevant scalar, like phytoplankton concentration [Gardner *et al.*, 1993] and organic/inorganic concentrations of photosynthetic products. This has implications, for example, for time and depth dependent respiration in the water column. Higher phytoplankton concentrations trapped at the near surface during the later part of the solar day may develop as phytoplankton cell doubling can occur on time scales of days [Parsons *et al.*, 1984]. This in turn may enhance grazing rates by zooplankton, as zooplankton are known to migrate towards the surface around dusk [Frost, 1991]. The importance of this effect will depend critically on the timing of the onset of convection *versus* the timing of the zooplankton vertical migration. The possibility also exists for a transition period, whereby increased phytoplankton concentrations at the surface are mixed down past the vertically migrating zooplankton. A better knowledge or measurement of vertical migration of zooplankton would be necessary to estimate the importance of these effects for these data Recent work on this subject is becoming available in the literature [Taylor & Stephens, 1993].

The persistence of an isolated shallow and warmer surface layer during the day time will have implications for gas transfer when the dissolved gas concentrations are close to their equilibrium concentrations. If in this layer, significant changes in chlorophyll concentration and photosynthetic product concentrations occur, satellite measurements of sea surface colour, which are used to estimate chlorophyll concentrations and thence primary productivity, would have to be interpreted depending on the time of day the measurements are made. Temporal variability in ocean colour over time scales of a day

should be interpreted, when and where convection is deemed important, in view of the processes described in this chapter.

The role of the ocean in producing, absorbing, recycling and redistributing atmospheric pollutants and naturally occurring organic/inorganic compounds is a current research topic. Particularly important to global radiative budgets and ozone budgets [Najjar *et al.*, 1993] are carbonyl sulphide, carbon monoxide and non-methane hydrocarbons which are produced by photolysis of dissolved organic matter in sea water by UV radiation (UV radiation is ~2 % of solar radiation and has a typical e-folding attenuation depth in sea water of 5-10 m) [Kantha & Clayson, 1993]. Exposure time, radiation intensity and energy, and possible hysterisis effects in the photoresponse of such compounds depend on the depth and vertical displacements of these compounds within the photic zone during the day time. Air-sea gas exchange of trace gases such as methane [Lammers *et al.*, 1994] and dimethyl sulphide (DMS), which is produced by phytoplankton, have important considerations for global biogeochemical cycles [Liss *et al.*, 1993]. Outgassing to the atmosphere of DMS is linked to the production of sulphate aerosols, an important cloud condensation nuclei, and subsequent effects on the acidity of rain [Malin *et al.*, 1992]. The modelling efforts and insights gained from analysis of the dissolved oxygen data in Chapter 7 are particularly applicable to address questions related to the role of the oceanic mixed layer in the production, recycling and air-sea gas fluxes of such compounds.

8.4. Future Work

8.4.1. Technological Developments

In circumstances where dissolved nitrogen concentration is expected to vary on time scales much shorter than dissolved oxygen concentration, Equation 3.4 provides a means of correcting the oxygen measurement to better resolve short time scale oxygen fluctuations. This would be true in, for example, a primary production incubating chamber, which is sealed to prevent dissolved gases escaping. Changes in the dissolved oxygen concentration could then be measured by the gas tension device. The maximum resolution of a Paroscientific pressure sensor is 0.000001 kPa, giving increased oxygen resolution over a standard oxygen probe by a factor of approximately twenty thousand! In this particular application gas tension fluctuations will be due primarily to dissolved oxygen production and to a lesser extent carbon-dioxide removal. This potential application has not yet been investigated fully, but may be a future application of the gas tension device either at sea or in the laboratory.

The above idea can be taken one step further by using an instrument that makes a differential measurement between total gas tension and a measurement of gas tension with a particular gas removed. The differential measurement yields the partial pressure of that gas. Chemical removal of oxygen can be achieved by various compounds. Thus in principle, two gas tension devices, one with an oxygen absorbent behind the membrane, will measure the partial pressure of oxygen to the resolution of the pressure sensor, as discussed above, by a factor of 20,000 better resolution than commercially available probes. Furthermore, the use of gas tension as the primary measurement will allow an oxygen sensor to be designed with the long term stability of the pressure sensor (0.01 % over 3 years). When achieved, this will most certainly be a technological breakthrough

with wide reaching possibilities for stable long term dissolved oxygen measurements in the ocean (see Section 4.2. for a discussion of present dissolved oxygen probe technology and problems associated with lack of long term stability). As the response time for the GTD system is much slower than commercially available dissolved oxygen probes (tens of minutes rather than seconds), this new instrument would serve well as a long term *in situ* calibration measurement for faster response probes, if faster response was indeed a concern for that particular application. Biofouling of the GTD membranes would only limit the response time (as yet unquantified) of the GTDs, leaving the precision of the oxygen measurement uncompromised. Through our continued collaboration with Bruce Johnson we are at present making such instrumentation.

8.4.2. Continued Scientific Research

The chief limitation of the modelling efforts developed in Section 7.5 is that no smaller scale diffusive processes were included in the model. It is suggested that this may be overcome by using an oceanographic model that explicitly contains representations of small scale diffusive processes (see discussions and references in the review paper by Garrett [1994] and Thomas *et al.*, [1993]), coupled with a biological model that includes photoinhibition and the full photosynthetic response of phytoplankton [*e.g.*, Denman & Marra, 1986]. The observed time scales for overturning of the convective plumes and their penetration depth throughout the day as observed by the floats would be the key measurements incorporated into the model. Phytoplankton concentration could be modelled by having simple representations of growth, mortality and grazing. The uniqueness of the data with simultaneous measurements of dissolved oxygen and chlorophyll concentration (C. Wirick, Brookhaven National Laboratories, N.Y.) provides

a truly novel opportunity to investigate this bio-physical interaction and its implications for primary production in the ocean.

A gas tension-dissolved oxygen system of the type used in Section 3.4. was moored in the Labrador Sea during May 1994 It is expected to be recovered sometime in May-July 1995. In this deep water convection region, oxygen, carbon-dioxide and other atmospheric gases are removed from the atmosphere and transferred to the deeper ocean It is expected that such experiments, which require the kind of *in situ* dissolved gas instrumentation developed in this thesis work, can address key scientific questions relating to the role of the world's oceans in transferring gases between the atmosphere and ocean

BIBLIOGRAPHY

Abramowitz, M. and Stegun, *Handbook of Mathematical Functions.*, Dover Public., Inc., N.Y., 1046 pp. (1970).

Anderson, M.L. and B.D. Johnson, "Gas transfer. a gas tension method for studying equilibration across a gas water interface", *Journal of Geophysical Research*, 97(C11):17899-17904 (1992).

Asher, W.E., E.C. Monahan, R. Wanninkhof and T.S. Bates, "Correlation of gas transfer velocities with fractional whitecap coverage", *Air-Water Mass Transfer*, Selected Papers from the Second International Symposium on Gas Transfer at Water Surfaces (1990).

Bernstein, R.L. and J.H. Morris, "Tropical and mid-latitude North Pacific sea surface temperature variability from the SEASAT SMMR", *Journal of Geophysical Research*, 88(C3):1877-1891 (1983).

Brainerd, K.F. and M.C. Gregg. "Diurnal restratification and turbulence in the oceanic surface mixed layer - part 1 : Observations". In press in *Journal of Geophysical Research* (1993).

Broecker, H.C., J. Petermann, and W. Siems, "The influence of wind on CO_2-exchange in a wind-wave tunnel, including the effects of monolayers", *Journal of Marine Research*, 36:595-610 (1978).

Broecker, H.C., and W. Siems, "The role of bubbles for gas transfer from water to air at higher wind speeds, Experiments in the wind-wave facility in Hamburg". In Brutsaert, W. and G.H. Jirka (eds.), *Gas Transfer at Water Surfaces*. pp. 228-238, Reidel, Hingham, Massachusetts (1984).

Brumley, B.B. and G.H. Jirka, "Air-water transfer of slightly soluble gases Turbulence, interfacial processes and conceptual models", *Physicochemical Hydrodynamics*, 10:295-319 (1988).

Carpenter, E.J., "Nitrogen fixation by marine *Oscillatori. Trichodesmium* in the world's oceans". In Carpenter, E.J. and D.G. Capone (eds.), *Nitrogen in the Environment*, pp. 65-103, Academic Press Inc., London, 900 pp. (1983)

CJGOFS-93, "Eddy Correlation Technique: a Re-Evaluation", collective oral presentation at the Canadian JGOFS Annual Meeting, Halifax, N.S., Canada (1993).

Clift, R., J.R. Grace and M.E. Weber, *Bubbles, Drops and Particles*, Academic Press Inc., N.Y., USA, 379 pp. (1978).

Craig, H. and T. Hayward, "Oxygen supersaturation in the ocean. Biological versus physical contributions", *Science*, **235**:199-202 (1987).

Crean, P.B. and A.B. Ages, *Oceanographic Records from Twelve Cruises in the Strait of Georgia and Juan de Fuca Strait*, Vol. 1, Department of Energy, Mines and Resources, Marine Sciences Branch Victoria, B.C. (1968).

Csanady, G.T., "The role of breaking wavelets in air-sea gas transfer", *Journal of Geophysical Research*, **95**(C1):749-759 (1990).

Dankwerts, P.V., "Significance of liquid-film coefficients in gas adsorption", *Industrial and Engineering Chemistry*, **43**(6):1460-1467 (1951).

D'Aoust, B.G., H. Siebold and R. White, "Direct measurements of total dissolved gas pressure", *Undersea Biomedical Research*, **2**:141-149 (1975).

D'Aoust, B.G. and M.J.R. Clark, "Analysis of supersaturated air in natural waters and reservoirs", *Transactions of the American Fisheries Society*, **109**:708-724 (1980).

Deacon, W.L, "Gas transfer to and across an air-water interface", *Tellus*, **29**:363-374 (1977).

Denman, K.L., "Scale-determining biological-physical interactions in oceanic food webs" In Giller, P.S., A.G. Hildrew and D.G. Raffaelli (eds.), *Aquatic Ecology: Scale, Pattern and Process*, pp. 377-402, Blackwell Scientific Publications, Oxford, U.K., (1992).

Denman, K.L. and A.E. Gargett, "Biological/physical interactions in the upper ocean: The role of vertical and small scale transport processes", submitted to *Annual Review of Fluid Mechanics* (1994).

Denman, K.L. and J. Marra, "Modelling the time dependent photoadaptation of phytoplankton to fluctuating light", *Marine Interfaces Ecohydrodynamics*, **42**:341-360, Elsevier Oceanography, (1986).

Dobbins, W.E., "The nature of oxygen transfer coefficient in aeration systems". In McCabe, J. and W.W. Eckenfelder, (eds.), *Biological Treatment of Sewage and Industrial Wastes*, Vol. I, Reinhold Book Corporation, N.J. (1956).

Emerson, S., "Seasonal oxygen cycles and the biological new production in surface waters of the subarctic Pacific Ocean", *Journal of Geophysical Research*, **92**(C6). 6535-6544 (1987).

Emerson, S., P. Quay, C. Stump, D. Wilbur and M. Knox, "O_2, Ar, N_2 and ^{222}Rn in surface waters of the subarctic Pacific Ocean: Net biological O_2 production", *Global Biogeochemical Cycles*, 5:49-69 (1991).

Emerson, S., P. Quay and P. A. Wheeler, "Biological productivity determined from oxygen mass balance and incubation experiments", *Deep-Sea Research*, **40**.2351-2358 (1993).

Erickson III, D.J., "A stability dependent theory for air-sea gas transfer", *Journal of Geophysical Research*, **98**(C5):8471-8488 (1993).

Farmer, D.M. (Chief Scientist on *C.S.S. John P. Tully*), *CST-7 Cruise Report*, Institute of Ocean Sciences, Sidney, B.C. (1992).

Farmer, D.M. and M. Li, "Patterns of bubble clouds organised by Langmuir circulation", Submitted to *Journal of Physical Oceanography* (1994).

Farmer, D.M., C.L. McNeil and B.D. Johnson, "Evidence for the importance of bubbles in increasing air-sea gas flux", *Nature* **361**:620-623 (1993).

Farmer, D.M. and Vagle, S., "Waveguide propagation of ambient sound in the ocean-surface bubble layer", *The Journal of the Acoustical Society of America*, **86**(5):1897-1908 (1989).

Fahnenstiel, G.L. and H.J. Carrick, "Primary production in Lakes Huron and Michigan: *in vitro* and *in situ* comparisons", *Journal of Plankton Research*, **10**(6).1273-1283 (1988).

Fickeisen, D.H. and M.J. Schneider. *Gas bubble disease*, in CONF-741033, Technical Information Center, Energy Research and Development Administration, Oak Ridge, Tennessee, USA (1976).

Fluxes, Newsletter of the Canadian JGOFS (Joint Global Ocean Flux) Experiment, Volume 1, JGOFS Canada Secretariat, Dalhousie University (1993).

Freeland, H.J., W.R. Crawford and R.E. Thompson, "Currents along the Pacific Coast of Canada", *Atmosphere-Ocean*, **22**:151-172 (1984).

Frost, B.W., "The role of grazing in nutrient-rich areas of the open sea", *Limnology and Oceanography*, **36**(8):1616-1630 (1991).

Gardner, W.D., I.D. Walsh and M.J. Richardson. "Biophysical forcing of particle production and distribution during a spring bloom in the North Atlantic", *Deep-Sea Research II*, **40**(1/2):171-195 (1993).

Garrett, C., "Processes in the surface mixed layer of the ocean", in *Proceedings of the 4th International Symposium on Stratified Flows*, Grenoble, France (1994).

Garrettson G.A., "Bubble transport theory with application to the upper ocean", *Journal of Fluid Mechanics*, **59**:187-206 (1973).

Gemmrich, J., T.D. Mudge and V.D. Polonichko, "On the energy input from wind to surface waves", *Journal of Physical Oceanography*, **24**(11):2413-2417 (1994).

Goering, J.J., Dugdale, R.C., and Menzel, D.W., "Estimates of in situ rates of nitrogen uptake by Trichodesmium spp in the tropical Atlantic Ocean", *Limnology and Oceanography*, **11**:614-620 (1966).

Halldal, P., "Solar energy capturing by marine plants". In Shibata, K., A. Imamura and A. Ikegami (eds.), *Biological and Chemical Utilisation of Solar Energy*, pp. 48-58 Japan Scientific Societies Press, London, in Japanese (1981).

Hasse, L., "Gas exchange across the air-sea interface", *Tellus*, **32**:470-481 (1980).

Hasse, L., "On the mechanism of gas exchange at the air-sea interface", *Tellus*, **42B**:250-253 (1990).

Hasselmann, K., T.P. Barnett, E. Bouws, H. Carlson, D.E. Cartwright, K. Ende, J.A. Ewing, H. Gienapp, D.E. Hasselmann, P. Kruseman, A. Meerburg, P. Muller, D.J. Olbers, K. Richter, W. Sell and H. Wladen, "Measurements of wind wave growth and swell decay during the joint north sea wave project (JONSWAP)", *Deutsche Hydrographische Zeitung, Ergänzungsheft* **A8**(12) (1973).

Higbe, R., "On the adsorption of a pure gas into a still liquid during short period of exposure", *Transactions of the American Institute of Chemical Engineers*, **31**:365-390, (1935).

Hutchinson, E., *Chemistry: the Elements and their Reactions*, 2nd Edition, W.B. Saunders Company, Philadelphia, USA, pp. 693 (1962).

Ikusima, I. "Ecological studies on the productivity of aquatic plant communities III Effect of depth on daily photosynthesis in submerged macrophytes". *Botanical Magazine, Tokyo*, **80**:57-67 (1967).

Jähne, B., T. Wais, L. Memery, G. Caulliez, L. Merlivat, K. O. Munnich, and M. Coantic, "He and Rn gas exchange experiments in the large wind-wave facility of IMST", *Journal of Geophysical Research*, **90**:11989-11997 (1985).

Johnson, B.D., *Calibration Procedures and Evaluation of Performance for the Model 1 GTD Field Instrument*, Technical Report, Department of Oceanography, Dalhousie University, N.S., December (1992).

Johnson, B.D. and R.C. Cooke, "Bubble populations and spectra in coastal waters: a photographic approach", *Journal of Geophysical Research* **84**(C7):3761-3766 (1979).

Johnson, B.D. and R.C. Cooke, "Organic particle and aggregate formation resulting from dissolution of bubbles in sea water", *Limnology and Oceanography*. **25**:653-661 (1980).

Kantha, L.H and C.A. Clayson, "An improved nixed layer model for geophysical applications", submitted to *Journal of Geophysical Research* (1993).

Keeling, R.F., "On the role of large bubbles in air-sea gas exchange and supersaturation in the ocean", *Journal of Marine Research*, **51**:237-271 (1993).

Keeling, R.F. and S.R. Shertz, "Seasonal and interannual variations in atmospheric oxygen and implications for the global carbon cycle", *Nature*, **358**:723-727 (1992)

Kennish, M.J., ed., *Practical Handbook of Marine Sciences*, CRC Press Inc., Boca Raton, Florida, 710 pp. (1989).

Kinsman, B., *Wind Waves: Their Generation and Propagation on the Ocean Surface*, Prentice-Hall Inc., Englewood Cliffs, N.J. (1965).

Lamarre, E. and W.K. Melville, "Instrumentation for measurement of void fraction in breaking waves: Laboratory and field results", *IEEE Journal of Oceanic Engineering*, **17**:204-215 (1992).

Lammers, S., E. Suess, M. Mantsurov and V. Anikiev, "Variations of atmospheric methane supply from the Sea of Okhotsk induced by the seasonal ice cover", to appear in *Global Biogeochemical Cycles* (1994).

LeBlond, P.H., "Gas diffusion from ascending gas bubbles", *Journal of Fluid Mechanics*, 35(4):711-719 (1969).

Levich, V.G., *Physicochemical Hydrodynamics*, Prentice-Hall, Englewood Cliffs, N.J, (1962).

Li, M. and C. Garrett, "Cell merging and the jet/downwelling ratio in Langmuir circulation", *Journal of Marine Research*, 51:737-769 (1993).

Lighthill, J., *Waves in Fluids*, Cambridge Uni. Press, Cambridge, 504 pp. (1978).

Liss, P.S., "Processes of gas exchange across an air-water interface", *Deep-Sea Research*, 20:221-238 (1973).

Liss, P.S., "Tracers of air-sea gas exchange", *Philosophical Transactions of the Royal Society of London*, A325:93-103 (1988).

Liss, P.S. and L. Merlivat, "Air-sea gas exchange rates. Introduction and synthesis" In Buat-Menard, P. (ed.), *The Role of Air-Sea Exchange in Geochemical Cycling*, pp. 113-127, D. Reidel Pub. Co., Dordrecht, Holland, (1986).

Liss, P.S., A.J. Watson, M.I. Liddicoat, G. Malin, P.D. Nightingale, S.M. Turner and R.C. Upstill-Goddard, "Trace gases and air-sea exchanges", *Philosophical Transactions of the Royal Society of London*, A304:532-541 (1993).

Lombardo, C.P. and M.C. Gregg, "Similarity scaling of viscous and thermal dissipation in a convecting surface boundary layer", *Journal of Geophysical Research*, 94(C5):6273-6284 (1989).

Longuet-Higgins, M.S., "On the statistical distribution of the heights of sea waves". *Journal of Marine Research*, 11:245-266 (1952).

Mague, T.H., Weare, M.M., and Holm-Hansen, O., "Nitrogen fixation in the North Pacific Ocean", *Marine Biology*, 41:213-227 (1974).

Mackas, D.L., H. Sefton, C.H. Miller and A. Raich, "Vertical habitat partitioning by large calanoid copepods in the oceanic subarctic Pacific during Spring", *Progress in Oceanography*, 32:259-294 (1993).

Malin, G., S.M. Turner, and P. Liss, "Sulphur: The plankton/climate connection", *Journal of Phycology*, **28**:590-597 (1992).

Martin, J.H. and S.E. Fitzwater, "Iron deficiency limits phytoplankton growth in the north-east Pacific subarctic", *Nature*, **331**:341-342 (1988).

McNeil, C.L., "Calibration of dissolved oxygen data for the Lake Biwa Experiment", Technical report for *Ocean Acoustics*, Institute of Ocean Sciences, Sidney. B C , Canada (1994).

McNeil, C.L. and D.M. Farmer. "Observations of the influence of diurnal convection on upper ocean dissolved gas measurements", *Journal of Marine Research*, **53**(1):151-169 (1995).

McNeil, C.L., B.D. Johnson and D.M. Farmer. "In situ measurement of dissolved nitrogen and oxygen in the ocean", accepted for publication in *Deep-Sea Research* (1994).

Merlivat, L. and L. Memery, "Gas exchange across an air-water interface: Experimental results and modeling of bubble contribution to transfer", *Journal of Geophysical Research*, **88**(C1):707-724 (1983).

Miller, C.B., B.W. Frost, P.A. Wheeler, M.R. Landry, N. Welschmeyer and T.M. Powell, "Grazing control: Ecological dynamics in the subarctic Pacific, a possibly iron-limited ecosystem", *Limnology and Oceanography*, **36**(8):1600-1615 (1991)

Minneart, M., "On musical air bubbles and the sounds of running water", *Philosophical Magazine*, **16**:235-248 (1933).

Monahan, E.C., I.A. Leykin. L.Li, Y.Liu, R. Marks, I.G. O Muircheartaigh, J.W. Steele, G.Wang, Q. Wang, W. Wang, X. Wang, and M.B. Wilson, *Oceanic Whitecaps and Associated, Bubble-Mediated, Air-Sea Exchange Processes*, Whitecap report No. 12, Marine Sciences Institute, University of Connecticut at Avery Point, Connecticut, October (1992).

Najjar, R.G., D.J. Erickson III and S. Madronich, "Modeling the air-sea fluxes of carbonyl sulphide and carbon monoxide", in *The Role of Non-Living Organic Matter in the Earth's Carbon Cycle*, in preparation (1993).

Nernst, W. "Theorie der Reaktionsgeschwindigkeit in heterogenen Systemen", *Zeitschrift für Physikalische Chemie*, **47**:52-55 (1904).

Niiler, P.P and E.B. Kraus, *One-Dimensional Models of the Upper Ocean. Modelling and Prediction of the Upper Layers of the Ocean.*, Pergamon Press, pp. 143-172, Oxford (1977).

Odum, E.P., *Fundamentals of Ecology*, 3rd ed., W.B. Saunders, Philadelphia (1971).

Olbers, D.J., "Models of the oceanic internal wave field", *Review of Geophysical Space Physics*, **21**(7):1567-1606 (1985).

Oudot, C., "O_2 and CO_2 balances approach for estimating biological production in the mixed layer of the tropical Atlantic Ocean (Guinea Dome area)", *Journal of Marine Research*, **47**:385-409 (1989).

Parsons, T.R., M. Takahashi and B. Hargrave, *Biological Oceanographic Processes*, 3rd Edition, Pergamon Press, Exeter England (1984).

Patterson, J.C. "Modelling the effects of motion on primary production in the mixed layer of lakes", *Aquatic Sciences*, **53**:218-238 (1991).

Platt, T. and W.G. Harrison, "Reconciliation of carbon and oxygen fluxes in the upper ocean", *Deep-Sea Research*, **33**(2):273-276 (1986).

Pollard, R.T., P.B. Rhines and R.O.R.Y. Thompson, "The deepening of the wind mixed layer", *Geophysical Fluid Dynamics*, **3**:381-404 (1973).

Press, H.W., Teukolsky S.A., Vetterling W.T. and B.P. Flannery, *Numerical Recipes in C*, Cambridge University Press, Cambridge, U.K. (1988).

Price, J.F, R.A. Weller and R. Pinkel, "Diurnal cycling: Observations and models of the upper ocean response to diurnal heating, cooling and wind mixing", *Journal of Geophysical Research*, **91**(C7):8411-8427 (1986).

Robertson, J.E. and A.J. Watson, "Thermal skin effect of the surface ocean and its implications for CO_2 uptake", *Nature*, **358**:738-740 (1992).

Robertson, J.E., A.J. Watson, C. Langdon, R.D. Ling and J.W. Wood, "Diurnal variation in surface pCO_2 and O_2 at 60°N, 20°W in the North Atlantic", *Deep-Sea Research II*, **40**(1/2):409-422 (1993).

Shay, T.J. and M.C. Gregg, "Convectively driven turbulent mixing in the upper ocean", *Journal of Physical Oceanography*, **16**:1777-1798 (1986).

Smith, S.D., *Factors for adjustment of wind speed over water to a 10-meter height*, Report series / BI-R-81-3 / December, Bedford Institute of Oceanography, Dartmouth, N.S., (1981*a*).

Smith, S.D., *Coefficients for Sea Surface Wind Stress, Heat Flux, and Wind Profiles as a Function of Wind Speed and Temperature*, Report series / BI-R-81-19 / December, Bedford Institute of Oceanography, Dartmouth, N.S., (1981*b*).

Smith, S.D. and E.P. Jones, "Evidence for wind-pumping of air-sea gas exchange based on direct measurements of CO_2 fluxes", *Journal of Geophysical Research*, 88:707-724 (1983).

Smethie, W.M., T.T. Takahashi, D.W. Chipman, and J.R. Ledwell, "Gas exchange and CO_2 flux in the tropical Atlantic Ocean determined from ^{222}Rn and pCO_2 measurements", *Journal of Geophysical Research*, 90:7005-7022 (1985).

Spitzer, W.S. and W.J. Jenkins, "Rates of vertical mixing, gas exchange and new production. estimates from seasonal gas cycles in the upper ocean near Bermuda", *Journal of Marine Research*, 47:169-196 (1989).

Stewart, R.W., "Understanding fluxes to and within the ocean. a key to understanding climate", *Journal of Oceanography*, 48:5 -12 (1992).

Taylor, A.H. and J.A. Stephens, "Diurnal variations of convective mixing and the spring bloom of phytoplankton", *Deep-Sea Research II*, 40:389-408 (1993).

Thomas, F., Minster J.F., Gaspar P. and Y. Gregoris, "Comparing the behaviour of two ocean surface models in simulating dissolved O_2 concentration at O.W S P ", *Deep-Sea Research I*, 40(2):395-408 (1993).

Thorpe, S.A.,"On the clouds of bubbles formed by breaking wind-waves in deep water, and their role in air-sea gas transfer", *Philosophical Transactions of the Royal Society of London*, A304:155-210 (1982).

Thorpe, S.A., "The effect of Langmuir circulation on the distribution of submerged bubbles caused by breaking wind waves", *Journal of Fluid Mechanics*, 142 151-170 (1984*a*).

Thorpe, S.A., "The role of bubbles produced by breaking waves in super-saturating the near-surface ocean mixing layer with oxygen", *Annual Reviews in Geophysics* 2(1):53-56 (1984*b*).

Thorpe, S.A., "A model of the turbulent diffusion of bubbles below the sea surface", *Journal of Physical Oceanography*, **14**:841-854 (1984*c*).

Thorpe, S.A., "On the determination of K_v in the near-surface ocean from acoustic measurements of bubbles", *Journal of Physical Oceanography*, **14**:855-863 (1984*d*).

Thorpe, S.A, "Bubble clouds. a review of their detection by sonar, of related models, and of how K_V may be determined". In Monahan, E.C. and G. Mac Niocaill (eds.), *Oceanic Whitecaps*, pp. 57-68, D. Reidel Pub. (1986*a*).

Thorpe, S.A, "Measurements with an automatically recording inverted echo sounder; ARIES and the bubble clouds", *Journal of Physical Oceanography*, **16**:1462-1478 (1986*b*).

Thorpe, S.A. and A.J. Hall, "Bubbles in a freshwater lake", *Nature*, **279**:403-405 (1979).

Thorpe, S.A. and P. N. Humphries, "Bubbles and breaking waves", *Nature*, **283**:463-465 (1980).

Townsend, D.W., L.M. Cammen, P.M. Holligan, D.E. Cambell and N.R. Pettigrew, "Causes and consequences of variability in the timing of the spring phytoplankton blooms", *Deep-Sea Research*, **41**(5/6):747-765 (1994).

UNESCO, *The Practical Salinity Scale 1978 and the International Equation of State of Seawater 1980*, UNESCO Division of Marine Sciences, #36, Paris, 25 pp. (1981)

Upstill-Goddard, R.C., A.J. Watson, P.S. Liss and M.L. Liddicoat, "Gas transfer velocities in lakes measured with SF_6", *Tellus*, **42B**:364-377 (1990).

Vagle, S. and D.M. Farmer, "The measurement of bubble size distributions by acoustical backscatter", *Journal of Atmospheric and Oceanic Technology*, 9(5):630-644 (1992).

Wallace, D.W.R. and C.D. Wirick, "Large air-sea fluxes associated with breaking waves", *Nature*, **356**:694-696 (1992).

Wanninkhof, R., "Relationship between wind speed and gas exchange over the ocean", *Journal of Geophysical Research*, 97(C5):7373-7382 (1992).

Wanninkhof, R., W. E. Asher, R. Weppernig, H. Chen, P. Schlosser, C. Langdon and R. Sambrotto, "Gas transfer emperiment on Georges Bank using two volatile deliberate tracers", *Journal of Geophysical Research*, **98**(C11):20,237-20,248 (1993).

Wanninkhof, R. and L. Bliven, "Relationship between gas exchange, wind speed and radiation backscatter in a large wind-wave tank", *Journal of Geophysical Research*, **96**:2785-2796 (1991).

Wanninkhof, R., J.R. Ledwell and W.S. Broecker, "Gas exchange - wind speed relationship measured with sulfur hexaflouride on a lake", *Science*, **227**.1224-1226 (1985).

Watson, A.J., R.C. Upstill-Goddard and P.S. Liss, "Air-sea gas exchange in rough and storm seas measured by a dual-tracer technique", *Nature*, **349**:145-147 (1991).

Weast, R.C. and M.A. Astle, *Handbook of Chemistry and Physics*, 62nd Edition, CRC Press, Inc., Boca Raton, Florida, USA, (1981).

Weiss, R.F., "On the solubility of nitrogen, oxygen and argon in water and seawater", *Deep-Sea Research*, **17**:721-735 (1970).

Welschmeyer, N.A., S. Strom, R. Goericke, G. DiTullio, M. Belvin and W. Petersen, "Primary production in the subarctic Pacific Ocean: Project SUPER", *Progress in Oceanography*, **32**:101-135 (1993).

Whitman, W.G., "The two-film theory of gas absorption", *Chemical Metallurgy Engineering*, **29**:146-148 (1923).

Wilhelms, S.C. and Gulliver, J.S., (eds.) *Air-Water Mass Transfer, Selected Papers from the Second International Symposium on Gas Transfer at Water Surfaces* (1990).

Wood, J.D. and R. Onken, "Diurnal variation and primary production in the ocean - preliminary results of a Lagrangian ensemble model", *Journal of Plankton Research*, **4**(3):735-756 (1982).

Woolf, D.K., "Bubbles and the air-sea transfer velocity of gases", *Atmosphere-Ocean*, **31**(4):517-540 (1993).

Woolf, D.K. and S.A. Thorpe, "Bubbles and the air-sea exchange of gases in near-saturation conditions", *Journal of Marine Research* **49**:435-466 (1991)

Wu, J., "Bubbles populations and spectra in the near-surface ocean: Summary and review of field measurements", *Journal of Geophysical Research*, **86**:457-463 (1981).

Zedel, L. and D.M. Farmer, "Organised structures in subsurface bubble clouds: Langmuir circulation in the open ocean", *Journal of Geophysical Research*, **96**(C5):8889-8900 (1991).

APPENDIX A

Bubble Dynamics and Gas Flux

Single bubbles, a description

Given a bubble of volume b and radius r, containing a fluid of density ρ, with bubble velocity v and transporting fluid velocity V in the same reference frame, the equation of motion can be written as:

$$b\rho\frac{dv}{dt} = b\rho g + F_P + F_D + F_M \qquad (A.1)$$

where the right hand terms are respectively the forces on the bubble due to buoyancy, pressure gradient, $F_P = -b\nabla P$, drag, in the case of viscous interaction between the fluid and the bubble which behaves like a solid sphere, $F_D = -6\pi\rho_w\nu(v - V)$, *added mass effect.* As the bubble moves relative to the transporting fluid it 'drags' with it an amount of fluid having a volume equal to some fraction β of the bubble volume. By Newton's third law, this adhering mass provides a supplementary reaction term given by:

$$F_M = -\beta b\rho_f\frac{du}{dt} \qquad (A.2)$$

in which u is the relative velocity of the bubble, $u = v - V$, and β is the additional mass factor. This force acts to increase the bubble's effective inertial mass, hence the *added mass effect.*

Turbulence will affect the movement of a bubble. The scale of smallest eddies is given in a turbulent fluid to be $L_v=(\nu^3/\varepsilon)^{1/4}$, typically 1-6 mm. As the smallest eddies are much larger than the Kolmogorov length scale L_v, the bubble essentially rises in a reference

frame moving with the bubble at its terminal velocity. Turbulence will not increase the gas flux or dissolution rate of small bubbles.

Internal pressure

The pressure inside a bubble is increased above atmospheric pressure, P_o, by hydrostatic pressure and surface tension effects:

$$P = P_o + \rho g h + 2\gamma / r \tag{A.3}$$

where γ is the surface tension coefficient

Rise Velocity.

The Rybezynski-Hadamard formula [Levich, 1962] gives the terminal velocity of a gas sphere in a liquid:

$$u_c(r) = \frac{1}{3}\left(\frac{gr^2}{\nu}\right) \tag{A.4}$$

where the subscript denotes a 'clean' bubble surface (*i.e.*, a free slip boundary condition on the bubble's surface). Bubbles adsorb quickly particles and surface active material on their surface. The terminal rise velocity of a so called 'dirty' bubble is given by:

$$u_d(r) = \frac{2}{9}\left(\frac{gr^2}{\nu}\right) \tag{A.5}$$

These formula are restricted to nearly spherical bubbles (< 5% distortion of the bubble diameter). For thin liquids (*e.g.*, water) this degree of distortion is reached at Re =

$O(10^2)$. For thicker liquids (*e.g.*, oils) such distortion is present at $Re = O(10^2)$ [LeBlond, 1969].

Gas Transfer

Gas transfer from a single gas bubble can be written as:

$$\frac{dn}{dt} = -A.Q = -4\pi r^2.\frac{NuD}{r}\nabla c = -4\pi rNuD[c^* - c^n] \qquad (A.6)$$

where n is the number of moles of gas inside the bubble. In this expression, K_T, the transfer velocity is equal to NuD/r. This is seen to be correct by dimensional analysis Note that $Nu=Nu(Pe)$. For small bubbles:

$$Nu \propto Pe^{1/3}, \qquad (A.7)$$

thus, dirty bubbles have an effective piston velocity that has a $Sc^{-2/3}$ dependence (Equation 2.4.) - analogous to gas transfer at a rigid surface.

Note that the scaling of the diffusion equation for gas transfer from a bubble is given in terms of Pe. For bubbles with large Pe and small Re, gas transfer can be considered to occur through a thin diffusion boundary layer around the bubble of width $\delta^2 \approx Dr/U$ As D is typically three orders of magnitude less than ν, this holds for a wide range of bubble radii.

Bubbles Plumes, a Description

If bubble coalescence is neglected, and bubble interaction occurs on a time scale short compared to changes in the bubble size distribution, $N(x,v,r,t)$, then N satisfies a Boltzman type transport equation whose solution describes the ensemble-average behaviour of the

bubble population in terms of single bubble dynamics. The equation governing N can be derived by recognizing that vN, aN and $(dr/dt)N$ are the fluxes of bubbles in position space, velocity space and radius space respectively. The net flux of bubbles into the elemental space $d^7v = d^3x d^3v dt$ by virtue of streaming is:

$$F = -[\nabla_x.(\mathbf{v}N) + \nabla_v.(\mathbf{a}N) + \frac{\partial}{\partial r}(N\frac{dr}{dt})] \tag{A.8}$$

where the subscripts on the gradient operators signify the gradient in that particular space By conservation of bubbles:

$$\frac{\partial N}{\partial t} = F + S \tag{A.9}$$

where S represents distributed sources and sinks. Expanding the operators and using the fact that x and v are independent variables ($\nabla_x.v = 0$), we obtain the *Bubble Transport Equation*:

$$\frac{\partial N}{\partial t} + v.\nabla_x N + \mathbf{a}.\nabla_v N + \frac{dr}{dt}\frac{\partial N}{\partial r} = \mathrm{S} - N(\nabla_v.\mathbf{a} + \frac{\partial}{\partial r}\frac{dr}{dt}) \tag{A.10}$$

describing the average bubble density within a bubble cloud [Garrettson, 1973]

For most applications of this equation, the acceleration terms are neglected; this assumption is reasonable as bubbles approach very quickly their terminal rise velocity in a fluid (for small bubbles, within a few bubble radii).

Gas Transfer

There are two approaches to calculating the gas transfer associated with bubble clouds, classified into Eulerian and Lagrangian representations:

Lagrangian

This method requires the specification of a source distribution, following the solution by characteristics described in Garrettson [1973]. Using this representation, a bubble cloud will be in steady state when advective and diffusive processes, which re-distributing bubbles in r,x space, balance distributed sources of bubbles which are envisioned as releasing bubbles at position x_0 with radius r_0. A particular bubble will transfer a total amount of gas, $q(r_0,z_0)$, to the fluid, found by integrating its instantaneous gas flux over the lifetime of the bubble. This formulation has a problem in that it assumes that bubbles are instantaneously injected at depth with the same gas composition as the atmosphere, or some pre-described ratio. This is unrealistic.

The gas flux associated with bubble cloud would be approximately:

$$Q_b = \int_r \int_z \Omega(r_o,z_o) q(r_o,z_o) dr_o dz_o \qquad \text{(A.11)}$$

where $\Omega(r_0,z_0)$ is the source function for the observed bubble distribution $\Phi(r_0,z_0)$

Merlivat and Memery [1983] simplified the source function by neglecting the terms representing the flux in radius space to:

$$\Omega = \frac{\partial z}{\partial t}\frac{\partial \Phi}{\partial z} = \frac{2gr^2}{9\nu}\frac{\partial \Phi}{\partial z} \qquad \text{(A.12)}$$

When turbulence and Langmuir circulation effects are included in the calculations, q would be an average value over many bubbles with the same initial conditions Some of

the bubbles may completely dissolve, some may rise and escape from the surface, either loosing or gaining gas from the water. The observed functional form of Φ is:

$$\Phi(r,z) \propto U^a r^{-b} e^{-kz} \tag{A.13}$$

where $a = 4.0 \rightarrow 5.0$, $b = 3.5 \rightarrow 5.0$, $k = 0.25 \rightarrow 1.0$ [Wu, 1981].

Eulerian

This method was presented by Thorpe [1982*a*] as:

$$Q_b = \int_r \int_z \frac{dn}{dt} N(r,z) dr dz. \tag{A.14}$$

This is the total gas flux associated with the bubble cloud, being an integral over the bubble distribution of the instantaneous gas flux associated with a particular bubble The formulation also requires specification of the fractional gas composition of bubbles at depth z when calculating nitrogen and oxygen fluxes separately.

APPENDIX B

Calculations

The following calculations derive Equation 5.6.

We choose to re-write Equation 5.5 as:

$$h(t) = h_o t^{\frac{1}{3}} \tag{B.1}$$

where $h_o = U_*(12m)^{1/3}N^{-2/3}$. Substitution of Equations B.1 into Equation 5.1, with $P = R = 0$ and Q specified by 2.7, we obtain as our starting equation:

$$\frac{dc}{dt} = At^{-\frac{1}{3}} - Dct^{-\frac{1}{3}} - Ect^{-1} + Bt^{-1} \tag{B.2}$$

where:

$$A \equiv K_T.c^*(1+\Delta)/h_o,\ D \equiv K_T/h_o,\ E \equiv 1/3,\ B \equiv c_d/3. \tag{B.3}$$

We shall solve Equation B.2 by using the integrating factor method, which can be derived as follows:

Let y=y(x), f=f(x) and f'=df/dx, then:

$$\begin{aligned} \frac{d}{dx}(ye^{f(x)}) &= yf'e^{f(x)} + e^{f(x)}\frac{dy}{dx} \\ &= e^{f(x)}[yf' + \frac{dy}{dx}] \\ \Rightarrow \frac{dy}{dx} + yf'(x) &= e^{-f(x)}\frac{d}{dx}(ye^{f(x)}) \end{aligned} \tag{B.4}$$

We recast Equation B.2 in this solvable form by writing f(x)=($3Dt^{2/3}$)/2 + Ξ.ln(t), with solution:

$$c(t) = e^{-f(t)} \int e^{f(t)} [At^{-\frac{1}{3}} + Bt^{-1}] dt \tag{B.5}$$

or:

$$c(t) = t^{-\frac{1}{3}} . \exp\left(-\frac{3Dt^{\frac{2}{3}}}{2} \right) . [AI + BII]$$

$$\text{where: } I = \int_0^T \exp\left(\frac{3Dt^{\frac{2}{3}}}{2} \right) dt, \quad II = \int_0^T t^{-\frac{2}{3}} . \exp\left(\frac{3Dt^{\frac{2}{3}}}{2} \right) dt \tag{B.6}$$

We shall solve for the integrals I and II separately.

Integral I

By making the following substitution

$$\xi^2 = \left(\tfrac{3D}{2}\right) t^{\frac{2}{3}} \tag{B.7}$$

and using the following identity:

$$ierf(iz) = \frac{-2}{\sqrt{\pi}} \int_0^z e^{t^2} dt \tag{B.8}$$

we can calculate integral I by parts to obtain:

$$I = t^{\frac{1}{3}} \left[\frac{e^{\xi}}{D} + \frac{i}{D} \left(\tfrac{\pi}{4}\right)^{\frac{1}{2}} \xi^{-\frac{1}{2}} erf(i\xi^{\frac{1}{2}}) \right]. \tag{B.9}$$

Integral II

Similarly, substituting Equation B.7 into integral II, and using the identity B.8, we obtain.

$$II = t^{\frac{1}{3}}\left[-3\xi^{-\frac{1}{2}}\left(\tfrac{\pi}{4}\right)^{\frac{1}{2}}.ierf\left(i\xi^{\frac{1}{2}}\right)\right]. \tag{B.10}$$

We substitute now integrals I and II back into Equation B.6. Rearranging and grouping common terms, we obtain:

$$c(t) = \left[\frac{A}{D}\right] + i\left(\tfrac{\pi}{4}\right)^{\frac{1}{4}}.erf(i\xi^{\frac{1}{2}}).\xi^{-\frac{1}{2}}e^{-\xi}\left[\frac{A}{D} - 3B\right]. \tag{B.11}$$

Substituting the definitions in Equation B.3 into Equation B.11, we obtain finally.

$$c(\xi) = c_s + i(\frac{\pi}{4})^{1/4}(c_s - c_d)\xi^{-1/2}erf(i\xi^{1/2})e^{-\xi} \tag{B.12}$$

where $c_S = c^*(1+\Delta_i)$, $\xi = (t/\tau)^{2/3}$ and $\tau = (32m/9)^{1/2}(U*/K_T)^{3/2}N^{-1}$.

CURRICULUM VITAE

Surname: McNeil
Given Name: Craig Logan
Place of Birth: Belfast, N. Ireland
Date of Birth: September 18, 1967

Educational Institutions Attended:

University of Victoria	1990-1995

Degrees Awarded:

Ph.D.	University of Victoria	expected 1995
B.Sc. (Honours)	Heriot-Watt University, Scotland	1989

Honours and Awards:

John Moyes Lessells Fellowship 1991-1992
(The *Royal Society of Edinburgh*)

NSERC Fellowship 1992-1993
(*Joint Global Ocean Flux Study*)

Fessenden Student Prize in Underwater Acoustics 1994
(The *Canadian Acoustical Association*)

Publications:

"Evidence for the importance of bubbles in increasing air-sea gas flux", D.M Farmer, C.L McNeil and B.D. Johnson, *Nature*, **361**:620-623 (1993).

"Observations of the influence of diurnal convection on upper ocean dissolved gas measurements", C.L. McNeil and D.M. Farmer, *Journal of Marine Research*, **53**:151-169 (1995).

"*In situ* measurement of dissolved nitrogen and oxygen in the ocean", C.L. McNeil, B.D. Johnson and D.M. Farmer, *Deep-Sea Research*, in press (1995).

Title of Thesis/Dissertation:

A Study of Dissolved Gaseous Oxygen and Nitrogen Fluxes in the Upper Ocean.

Author:

CRAIG LOGAN MCNEIL
March 6, 1995